

Inorganic carbon dynamics in coastal marine systems

Peter Andrew Faber

Bachelor of Advanced Science (Hons)

A thesis submitted in total fulfilment of the requirements for the degree of
Doctor of Philosophy

Water Studies Centre, School of Chemistry, Faculty of Science



MONASH University

April 2014

Under the Australian Copyright Act 1968, this thesis must be used only under the normal conditions of scholarly fair dealing. In particular no results or conclusions should be extracted from it, nor should it be copied or closely paraphrased in whole or in part without the written consent of the author. Proper written acknowledgement should be made for any assistance obtained from this thesis

I certify that I have made all reasonable efforts to secure copyright permissions for third-party content included in this thesis and have not knowingly added copyright content to my work without the owner's permission.

Table of Contents

PART A: General Declaration	12
Abstract.....	15
Acknowledgements	19
List of figures.....	21
List of tables:	24
1. Introduction.....	25
1.1 Dissolved inorganic carbon speciation in natural waters	25
1.2 Partial pressure of CO ₂	27
1.3 Anaerobic alkalinity generation	31
1.4 Carbonate dissolution.....	33
1.5 DIC dynamics in estuaries	34
1.6 DIC dynamics and benthic metabolism in intertidal sediments	36
1.7 Factors influencing sedimentation and Fe input	39
1.8 Global relevance of carbonate system studies	40
1.9 Knowledge gaps	41
1.10 Project aims, hypotheses and thesis structure	42
1.11 References.....	44

2. The role of alkalinity generation in controlling the fluxes of CO₂ during exposure and inundation on tidal flats	58
2.1 Declaration for Thesis Chapter two.....	59
2.2 Abstract.....	60
2.3 Introduction.....	61
2.4 Materials and methods	63
2.4.1 Experimental	63
2.4.2 Model formulation	65
2.4.3 pH model.....	68
2.4.4 Boundary conditions and initial state	69
2.4.5 Numerical model solution.....	70
2.4.6 Description of model runs	71
2.4.7 Sensitivity model runs.....	72
2.5 Results	73
2.5.1 Experimental	73
2.5.2 Model simulations	76
2.5.3 Simulation profiles	80
2.6 Discussion.....	81
2.6.1 Alkalinity producing reactions	81
2.6.2 Model sensitivity towards piston velocity	82

2.6.3	Agreement of simulations with experimental data	84
2.6.4	Model sensitivity towards sedimentary iron.....	85
2.7	Conclusions.....	88
2.8	Acknowledgements	88
2.9	References.....	89
3.	Porewater exchange driven by tidal pumping causes alkalinity export in two intertidal inlets	96
3.1	Declaration for Thesis Chapter Three.....	97
3.2	Abstract	99
3.3	Introduction.....	100
3.4	Methods	103
3.4.1	Field sites.....	103
3.4.2	In situ monitoring of water parameters and sampling.....	105
3.4.3	Nutrient Analysis	106
3.4.4	Estimation of carbonate dissolution.....	107
3.4.5	TA measurement and calculation of DIC and PCO ₂	107
3.4.6	δ ¹³ C of dissolved inorganic carbon.....	108
3.4.7	CO ₂ flux calculations	108
3.4.8	Seagrass export measurements.....	109
3.4.9	Porewater input and residence time.....	110

3.4.10	Core extractions and incubation.....	112
3.5	Results	113
3.5.1	Time series	113
3.5.2	Porewater	115
3.5.3	Advective carbon fluxes.....	118
3.5.4	Carbon isotope signatures	120
3.6	Discussion.....	122
3.6.1	Alkalinity export	123
3.6.2	Porewater exchange	126
3.6.3	Carbon budget.....	129
3.6.4	DIC sources.....	132
3.7	References.....	135
4.	Trends in alkalinity and inorganic carbon fluxes from estuaries across a land use gradient in South Eastern Australia	142
4.1	Declaration for Thesis Chapter Four.....	143
4.2	Abstract.....	144
4.3	Introduction.....	145
4.3.1	Anaerobic alkalinity production.....	145
4.3.2	Fe input to estuaries.....	147

4.3.3	Determination of how catchment land use affects inorganic carbon and alkalinity export.....	147
4.4	Methods	148
4.4.1	Sites.....	148
4.4.2	Sampling	151
4.4.3	$\delta^{13}\text{C}$ of dissolved inorganic carbon.....	152
4.4.4	Determination of DIC, pCO_2 and TA.....	152
4.4.5	CO_2 flux calculations	153
4.4.6	Dissolved inorganic carbon and alkalinity budgets	154
4.4.7	DIC sources.....	157
4.4.8	Calculation of TP loading.....	158
4.5	Results.....	158
4.5.1	Fluvial inputs.....	158
4.5.2	Carbon budget.....	160
4.5.3	Mixing plots	164
4.5.4	Estuarine changes in DIC and $\delta^{13}\text{C}_{\text{DIC}}$	165
4.6	Discussion	167
4.6.1	Fluvial inputs of inorganic carbon	167
4.6.2	Estuarine fluxes of CO_2	168
4.6.3	Non-conservative behaviour in DIC, TA and $\delta^{13}\text{C}_{\text{DIC}}$	170
4.6.4	Carbon budget components comparison	181

4.6.5	The effect of catchment impact on carbon dynamics and alkalinity export	182
4.6.6	Future avenues of research	185
4.7	Conclusion	186
4.8	Acknowledgements	187
4.9	References.....	188
4.10	Appendices.....	195
4.10.1	Appendix 4A Estuary selection.....	195
4.10.2	Appendix 4B: Mixing plots	201
5.	Discussion and concluding remarks	204
5.1	Research questions.....	204
5.2	Chapter summaries.....	205
5.2.1	Chapter 2 summary	205
5.2.2	Chapter 3 summary	206
5.2.3	Chapter 4 summary	209
5.3	Implications of present research	210
5.4	Future research	212
5.5	References.....	214

PART A: General Declaration

Monash University

Declaration for thesis based or partially based on conjointly published or unpublished work

General Declaration

In accordance with Monash University Doctorate Regulation 17.2 Doctor of Philosophy and Research Master's regulations the following declarations are made:

I hereby declare that this thesis contains no material which has been accepted for the award of any other degree or diploma at any university or equivalent institution and that, to the best of my knowledge and belief, this thesis contains no material previously published or written by another person, except where due reference is made in the text of the thesis.

This thesis includes one original paper published in peer reviewed journals, one paper which has been submitted, and one unpublished publication. The core theme of the thesis is Inorganic carbon and alkalinity fluxes from coastal marine sediments. The ideas, development and writing up of all the papers in the thesis were the principal responsibility of myself, the candidate, working within the School of Chemistry under the supervision of Dr. Perran Cook

The inclusion of co-authors reflects the fact that the work came from active collaboration between researchers and acknowledges input into team-based research.

In the case of chapters 2, 3 and 4 my contribution to the work involved the following:

Thesis chapter	Publication title	Publication status*	Nature and extent of candidate's contribution
2	The role of alkalinity generation in controlling the fluxes of CO ₂ during exposure and inundation on tidal flats	Published	Running the computer model which produced results, analysis of samples, data analysis, literature review, formulation of paper, key ideas.
3	Porewater exchange driven by tidal pumping causes alkalinity export in two intertidal inlets	Published	Sampling and data collection, laboratory analysis of samples, literature review, data analysis, key ideas, formulation of paper.
4	Trends in inorganic carbon fluxes from estuaries across a land use gradient in South Eastern Australia	In prep.	Sampling and data collection, laboratory analysis of samples, literature review, data analysis, key ideas, formulation of paper.

I have / have not (circle that which applies) renumbered sections of submitted or published papers in order to generate a consistent presentation within the thesis.

Signed:

Date:

Abstract

Carbon dioxide (CO₂) plays a central role in the Earth's climate and there is presently a great deal of interest in the exchange of this compound between atmospheric, terrestrial and marine realms. The terrestrial-marine interface is particularly dynamic and is attracting increasing interest because there is significant material deposition and recycling at this point. While there have been many studies of carbon cycling and CO₂ emissions in this environment, there have been few specific studies on how anthropogenic activities affect carbon emissions and how this affects the balance between export as carbon dioxide and dissolved inorganic carbon (DIC), or carbonate alkalinity. Unlike CO₂, DIC in the form of carbonate alkalinity cannot diffuse into the atmosphere, so remains dissolved. For this reason, the production of alkalinity may control the balance of inorganic carbon export to the atmosphere and to the ocean. One major source of alkalinity production in coastal systems is sulfate reduction. In order for a net alkalinity flux to occur, the product of sulfate reduction, sulfide, must be buried as iron sulfide (FeS) so that it is not reoxidised, consuming alkalinity. I therefore expect the burial of reduced solutes to play a key control over the release of inorganic carbon as CO₂ (to the atmosphere) and alkalinity (exported to the ocean). This thesis examines the following 3 questions, each of which is on a different spatial scale:

1. Does alkalinity generation within tidal flat sediments control the relative export of inorganic carbon to the atmosphere and to coastal waters?
2. Do differing degrees of terrestrial inputs influence the dominant modes of carbon export from tidal flats?
3. Do differing regimes of anthropogenic land use in river catchments control inorganic carbon and alkalinity production in estuaries?

In chapter 2, I investigated dissolved inorganic carbon (DIC), gaseous CO₂ and total alkalinity (TA) fluxes from intertidal mudflats during periods of exposure and inundation, using laboratory core incubations, field data and reactive transport model simulations. During periods of alkalinity production, the flux of DIC out of the sediment was 1.8 times greater during inundation than exposure. The observed alkalinity production was attributed to the accumulation of reduced sulfur species within the sediment. This finding was supported by the reactive transport simulations, which showed that large amounts of sulfate reduction and subsequent reduced sulfur burial, as FeS, induced an alkalinity flux from the sediment during high tide conditions. Model simulations also found that the amount of oxidised Fe in the sediment influences the extent of net alkalinity production. Our finding, that CO₂ fluxes can be significantly lower than total metabolism during exposure, has implications for studies that aim to measure metabolism on tidal flats.

In chapter 3, carbon and TA export from two adjacent intertidal inlets with different terrestrial inputs were investigated. One inlet receives water from a small creek from a highly impacted, agriculturally dominated catchment, leading to the input of terrestrially sourced material; whereas, the other is relatively isolated from terrestrial inputs. The inlet with the greater amount of terrestrial inputs exported much more TA (310 vs. 46 mmol m⁻² d⁻¹), indicating that the extent of land-to-sea connectivity influences how carbon is exported from this interface. I hypothesize this is due to the increased input of iron from terrestrial sources, which fosters net TA production through the burial of reduced sulfur species as iron sulfides as found by the previous chapter. A simple mass balance showed the TA fluxes observed over 24 h were higher than could be sustained continuously with iron input from the catchment (0.49 mmol Fe m⁻² d⁻¹), indicating that the observed TA fluxes could not be sustained on long times scales by this mechanism. It

is likely that there are periods of net reduction and net oxidation in response to wave action and calm conditions, highlighting the importance of long term monitoring over different seasons and weather patterns to obtain representative budgets. Keeling plots of $\delta^{13}\text{C}_{\text{DIC}}$ measurements over the sampling period suggested the source of DIC was from mineralisation of seagrass/microphytobenthos and mangrove organic matter. The carbon budget I produced showed that DIC was the dominant mode of carbon export from mangroves, which is relevant to recent investigations on the missing mangrove carbon sink. The ^{222}Rn data collected during the time series measurements indicated that porewater exchange played an important part in controlling carbon export from the sediment and the residence time of porewater within both inlets was $\sim 6.6\text{--}7.4$ h, indicating that porewater exchange was driven by tidal pumping.

In chapter 4, I used $\delta^{13}\text{C}_{\text{DIC}}$, DIC, TA and partial pressure of carbon dioxide (pCO_2) measurements to determine the dominant carbon cycling processes; aerobic respiration, anaerobic respiration (alkalinity generation) and photosynthesis in eight Southern Australian temperate estuaries. For each estuary, I calculated inorganic carbon and alkalinity budgets, and using $\delta^{13}\text{C}_{\text{DIC}}$ measurements, I employed a mass balance approach to determine the drivers of DIC production or consumption in the estuaries. By comparing the export of carbonate alkalinity from estuaries with varying catchment land uses, I was able to determine the differences in carbon dynamics under different levels of land use impact within the catchment. All but the least impacted estuaries showed clear non-conservative mixing behaviour of DIC, TA and $\delta^{13}\text{C}_{\text{DIC}}$. The estuaries ranged between large sources and large sinks of atmospheric CO_2 , with fluxes from $-17 - 502$ $\text{mmol m}^{-2} \text{d}^{-1}$, and were highly dependent on the sampling period. It was found that in highly impacted estuaries, there were often high rates of DIC production within the estuary (up to $510 \text{ mmol m}^{-2} \text{d}^{-1}$) and this coincided with a high production of alkalinity

(up to $273 \text{ mmol m}^{-2} \text{ d}^{-1}$). As more impacted catchments will tend to export more organic carbon and Fe, the higher rates of DIC and alkalinity production are expected owing to the burial of reduced solutes as discussed previously. Likewise, in some estuaries, high rates of photosynthesis reflect the higher loadings of inorganic nutrients from more impacted catchments. The export of alkalinity from highly impacted estuaries was highly variable between seasons. I hypothesise this is due to a higher amount of FeS being buried within sediments, which is easily oxidised when conditions permit.

Acknowledgements

The completion of my doctoral research and this thesis would not have been as enjoyable without assistance and support from a number of people.

Firstly, I acknowledge my supervisor Perran Cook, who provided me with guidance throughout my project. I've been lucky to have a supervisor with such a contagious enthusiasm for science and really appreciate the broad knowledge he has of his research interests, his good character and his sense of humour.

I also thank Ian McKelvie who provided guidance through the first year or so of my PhD, and Peter Ellis to whom I am grateful for an immeasurable amount of education... not always directly related to my project, but skills I will have for a lifetime.

Also, I am grateful for the assistance and friendship of past and present members of the Water Studies Centre. In particular I would like to thank Ryan Woodland, Victor Evrard, Adam Kessler, Todd Scicluna, Erinn Richmond, Yafei Zhu, Wei Wen Wong, Ian Cartwright, Tina Hines and Kerrie Browne for their help in field work, lab analysis and other activities.

Also, thanks to Mum and Dad, and Melissa for providing moral support and relationships which have nurtured my work in the last few years.

If I had known at the start of my PhD what I know now, it probably would have taken half as long. I've found for myself, that the best path forward in scientific inquiry is to: 1. look around, including backwards to absorb as much information and available knowledge as possible. 2. Consider all paths forward –exhaust all options intellectually first, and then figure out the best way to approach the line of inquiry, and 3. Challenge all assumptions that act as obstacles to true inquiry –including beliefs, biases and dogma –

personal, and that of others. Sometimes all that a hard problem needs is a rapid shift of attitude, and it seems to me that this is the essence of creative problem solving. The greatest education of the last 4 years has been the integration of some of that way of thinking into my work, and more importantly, into my character.

List of figures

Figure 1.1: Speciation diagram for $[\text{CO}_2]$, $[\text{HCO}_3^-]$ and $[\text{CO}_3^{2-}]$ in a closed, seawater system at 20 °C.	26
Figure 1.2: Diagram of estuarine carbon cycling in estuaries.	35
Figure 1.3: pCO_2 and pH in surface waters, along a salinity gradient in the Elbe estuary.	36
Figure 2.1: Diagram of the experimental setup, showing the conditions of simulated tides.	65
Figure 2.2: Simulated mean fluxes of CO_2 during exposure (CO_2), dissolved inorganic carbon (DIC) and alkalinity during inundation in the computer simulation with 95 and 19 $\mu\text{mol Fe/g}$ sediment (d/w) and laboratory core incubation fluxes with (+OM) and without (-OM) added organic matter.	75
Figure 2.3: Fluxes of dissolved inorganic carbon (DIC) versus exposed CO_2 fluxes for two experimental data sets, and a model simulation.....	77
Figure 2.4: Fluxes of dissolved inorganic carbon (DIC), exposed CO_2 and alkalinity fluxes for a simulation of a 50 day period with an imposed profile of 7.6, 19 and 95 $\mu\text{mol g}^{-1}$ sediment (d/w) FeOOH.....	79
Figure 2.5: A simulation showing the FeOOH concentration before and after an organic matter pulse with initial FeOOH concentration of 19 $\mu\text{mol g}^{-1}$ sediment (d/w).	80
Figure 2.6: Exposed flux of CO_2 with varying piston velocity and respiration rate.....	83
Figure 2.7: Profiles of pH, CO_2 , DIC, TA, FeOOH and HS^- and O_2 from two simulations	86
Figure 3.1: (A) Map of Australia, adapted from (Evrard et al. 2013) with approximate location of Western Port. (B) Map of Watson Inlet (WI), Watson Creek (WC), and Chinaman Inlet (CI) in the north-eastern corner of Western Port (WP).	104

Figure 3.2: Time series measurements of mean flow, tide height, salinity, pH, DO, PCO ₂ , TA, DIC, Excess Ca ²⁺ , $\delta^{13}\text{C}$, ²²² Rn, NH ⁴⁺ , NO _x and FRP	114
Figure 3.3: Export of water, CO ₂ , DIC, and TA from the inlets to WP during the time series campaigns for Watson Inlet (left) and Chinaman Inlet (right).	119
Figure 3.4: Keeling plots of time series measurements (top) and porewater samples (bottom) for Watson Inlet (WI) and Chinaman Inlet (CI).	121
Figure 3.5: Conceptual diagram of the components of carbon export from the intertidal zones of the inlets.....	122
Figure 4.1: Estuary field sites in Victoria, SE Australia.....	149
Figure 4.2: Diagram indicating fluxes within an open-mouth estuary, including fluvial input of DIC (FI _{DIC}), estuarine flux of DIC (EF _{DIC}), CO ₂ flux across the water-atmosphere interface (F _{CO2}) and total export of DIC (TE _{DIC}).	154
Figure 4.3: Plots of calculated ΔDIC (deviation from conservative mixing) and $\delta^{13}\text{C}_{\text{Est}}$ vs. salinity for sites with sufficient mixing data.....	166
Figure 4.4: Plots of calculated ΔDIC and $\delta^{13}\text{C}_{\text{Est}}$ vs. time for sites where diurnal effects were the dominant factors affecting carbon dynamics.	167
Figure 4.5: Schematic diagram of the dominant modes of carbon transformation occurring in estuaries	172
Figure 4.6: Estuary fluxes of TA vs. catchment impact level and the ranges of long term TP loading from 1990-2013.....	184
Figure A1: Ordination of 27 estuaries in Victoria, Australia based on principal components analysis of catchment land use (n = 7) and population (n = 1) characteristics.	199
Figure A2: Mixing plots of TA, DIC and $\delta^{13}\text{C}_{\text{DIC}}$ for field sites from campaign 1 (top), 2 (middle) and 3 (bottom)	203

Figure 5.1: Fluxes of dissolved inorganic carbon (DIC) versus exposed CO ₂ fluxes for two experimental data sets, and a model simulation.....	206
Figure 5.2: Conceptual diagram of the components of carbon export from the intertidal zones of the Watson Inlet (WI) and Chinaman Inlet (CI).....	207
Figure 5.3: Estuary fluxes of TA vs. catchment impact level and the ranges of long term TP loading from 1990-2013.....	210

List of tables:

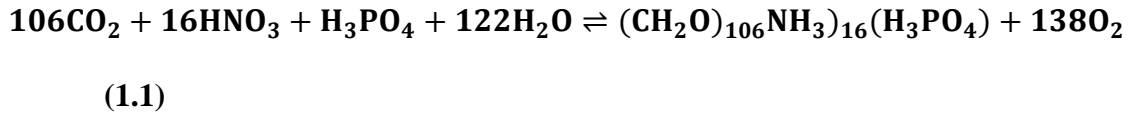
Table 2.1: Kinetic reactions included in the reaction set	66
Table 2.2: Kinetic rate expressions for the reactions included in the reaction set	67
Table 2.3: Overview of model parameter values	72
Table 3.1: Coverage of different habitat at Watson Inlet (WI) and Chinaman Inlet (CI) as areas and percentage of total areas.....	105
Table 3.2: Porewater analysis of carbon species and nutrients, including relevant ^{222}Rn measurements and the total volume of exported porewater for Watson Inlet (WI), Chinaman Inlet (CI), and Western Port (WP).....	117
Table 3.3: Carbon budget of Watson Inlet and Chinaman Inlet as a total export, an area integrated flux and as a percentage of total C export.....	119
Table 3.4: Keeling plot y-intercepts for the time series and porewater samples at Watson Inlet (WI) and Chinaman Inlet (CI).	121
Table 4.1: Site abbreviation, total estuary surface area, catchment impact and catchment land use	150
Table 4.2: Riverine DIC concentrations, TA concentrations and average river flow at the field sites during each campaign.....	159
Table 4.3: Carbon budget of the eight estuaries.....	160
Table 4.4: Alkalinity budget of the eight estuaries. Included is fluvial TA input (FI_{TA}), total ocean export of TA (TE_{TA}) and estuarine flux of TA (EF_{TA}).	163
Table 4.5: Estuarine carbon transformations in each estuary, during each campaign. ...	176
Table A1. Table of river catchment land use and population characteristics considered in multivariate analysis of 27 estuaries in Victoria, Australia.	198

1. Introduction

1.1 Dissolved inorganic carbon speciation in natural waters

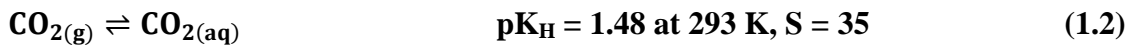
The breakdown and production of organic matter dominates the global carbon cycle and is intimately linked to the uptake and release of the nutrients nitrogen and phosphorus through the ‘Redfield’ equation (**Eq. 1.1**) which describes the stoichiometry of the production and breakdown of phytoplankton (Sarmiento and Gruber 2006).

Dissolved inorganic carbon (DIC) (also referred to in the literature as total carbonate, TCO_2 or $\sum \text{CO}_2$) is a product of organic carbon breakdown.



DIC is comprised mostly of three chemical species: dissolved carbon dioxide ($\text{CO}_{2(\text{aq})}$), bicarbonate (HCO_3^-) and carbonate (CO_3^{2-}). Carbonic acid (H_2CO_3) is also present, but its concentration is generally less than 0.3% of $[\text{CO}_{2(\text{aq})}]$ (Zeebe and Wolf-Gladrow 2001). For simplicity $[\text{CO}_{2(\text{aq})}] + [\text{H}_2\text{CO}_3]$ is written as $[\text{CO}_2]$. In some papers, the combination of dissolved CO_2 and H_2CO_3 is also denoted as $[\text{H}_2\text{CO}_3^*]$. **Figure 1.1** shows the speciation of DIC in seawater with varying pH. The pKa values of these equilibria are strongly dependent on temperature and salinity.

The equations governing these equilibria are (**Eq. 1.2-1.4**; Roy et al. 1993; Stumm and Morgan 1996; Zeebe and Wolf-Gladrow 2001; Millero et al. 2006):



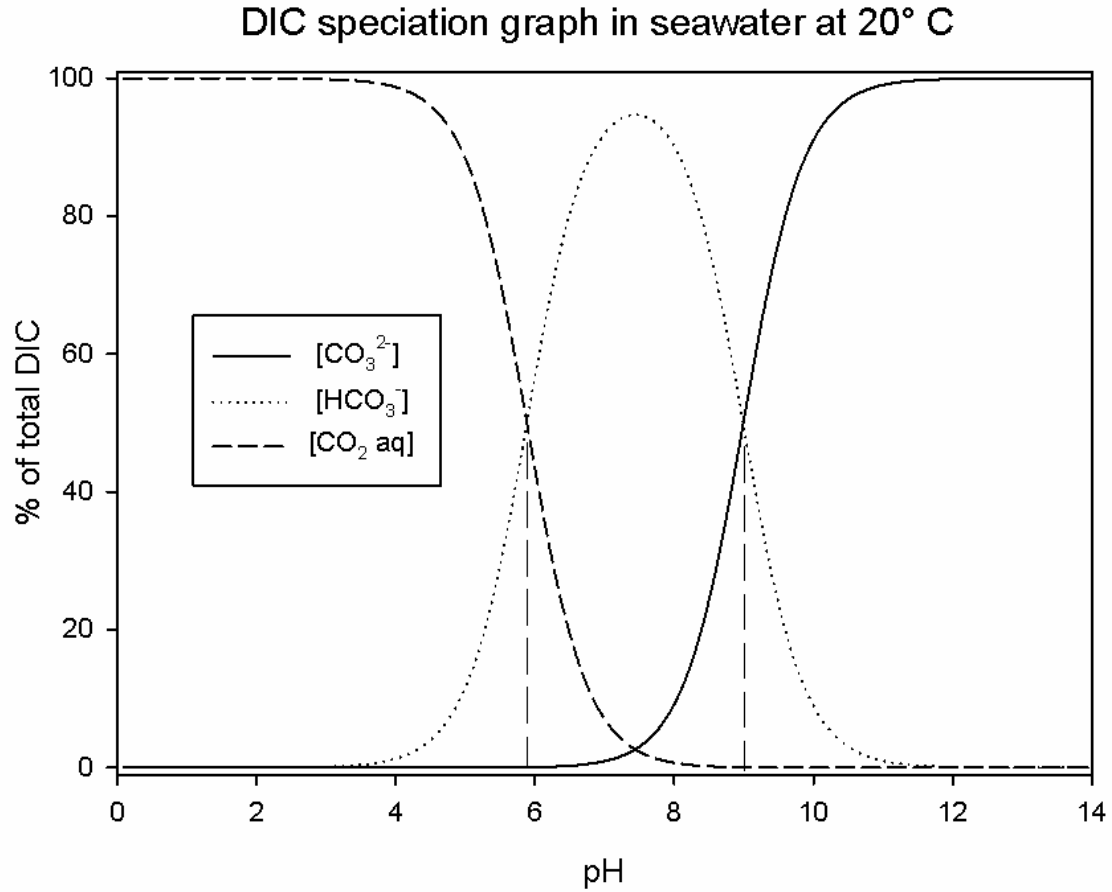


Figure 1.1: Speciation diagram for $[\text{CO}_2]$, $[\text{HCO}_3^-]$ and $[\text{CO}_3^{2-}]$ in a closed, seawater system at 20 °C. The vertical dashed lines represent the pKa values of the equilibrium equations, and are at approximately 5.89 and 8.99 at this salinity and temperature.

Total alkalinity (TA) in an aqueous solution is defined as the sum of all bases with $\text{pK}_a \geq 4.5$, minus the acids with $\text{pK}_a < 4.5$ present (Dickson 1981). The units of alkalinity are mM. This is represented in seawater by the following equation (**Eq. 1.5**) (Dickson 1981; Zeebe and Wolf-Gladrow 2001):

$$\text{TA} = [\text{HCO}_3^-] + 2[\text{CO}_3^{2-}] + [\text{B}(\text{OH})_4^-] + [\text{OH}^-] + [\text{HPO}_4^{2-}] + 2[\text{PO}_4^{3-}] + [\text{H}_3\text{SiO}_4^-] + [\text{NH}_3] + [\text{HS}^-] - [\text{H}^+] - [\text{HSO}_4^-] - [\text{HF}] - [\text{H}_3\text{PO}_4] \quad (1.5)$$

Of these, $[\text{HCO}_3^-]$, $[\text{CO}_3^{2-}]$, $[\text{B}(\text{OH})_4^-]$, $[\text{OH}^-]$ and $[\text{H}^+]$ are high, while the concentrations of the other components are considered negligible for most applications.

The carbonate alkalinity (A_c) is defined as (**Eq. 1.6**):

$$A_c = [\text{HCO}_3^-] + 2[\text{CO}_3^{2-}] \quad (1.6)$$

In many natural, freshwater systems $[\text{HCO}_3^-]$ and $[\text{CO}_3^{2-}]$ make up much of the TA, meaning that A_c often provides a good estimate of TA. In seawater, TA (generally around 2.4 mM (Millero 1995)) can be calculated from A_c by considering the relatively stable and conservative concentration of the other major species such as $[\text{B(OH)}_4^-]$. TA measurements are important in understanding large scale phenomena such as the environmental impacts of increasing CO_2 concentrations in oceans as it acts as a buffer for the dissolution of CO_2 (Zeebe and Wolf-Gladrow 2001).

Using any two of the carbonate system parameters (A_c , H^+ , DIC, $[\text{CO}_2]$, $[\text{HCO}_3^-]$, $[\text{CO}_3^{2-}]$) all of the others can be calculated (Zeebe and Wolf-Gladrow 2001), although certain combinations of the two magnify the error associated with measurements and in practice are never used. In general, the use of TA or DIC coupled with pH to calculate $[\text{CO}_2]$ results in values with modest uncertainties, and is commonly used (Millero 1995; Boehme et al. 1998).

1.2 Partial pressure of CO_2

The partial pressure of CO_2 ($p\text{CO}_2$) in an aqueous or gaseous phase is related to $[\text{CO}_{2(\text{aq})}]$ by K_H (**Eq. 1.7**):

$$p\text{CO}_2 = [\text{CO}_2]/K_H \quad (1.7)$$

The fugacity of CO_2 ($f\text{CO}_2$) accounts for CO_2 being a real gas, rather than an ideal gas. In general, $p\text{CO}_2$ values are commonly used in the literature, in the place of $f\text{CO}_2$, as

fCO₂ is only about 0.3-0.4% lower than pCO₂, between 0 and 30°C (Zeebe and Wolf-Gladrow 2001) and thus is a close approximation.

As the partial pressure is equal between aqueous and gaseous phases in equilibrium, pCO₂ measurements are useful in estimating fluxes across the water-air interface, which may form a significant part of the system's carbon budget, depending on the speciation of DIC (Frankignoulle 1988; Frankignoulle et al. 1996; Raymond et al. 1997; Cai and Wang 1998; Frankignoulle et al. 1998; Abril et al. 2000; Raymond et al. 2000; Raymond and Cole 2001; Borges et al. 2004a; Zappa et al. 2007). Measurements of pCO₂ in estuaries provide an indicator whether the system is acting as a net source or sink of atmospheric CO₂. For instance, many European and North American estuaries documented in the literature are heterotrophic, exhibiting supersaturated pCO₂ relative to the atmosphere as a result of intense aerobic degradation of organic matter, and are net sources of CO₂ to the atmosphere (Cai and Wang 1998; Frankignoulle et al. 1998; Raymond et al. 2000; Abril et al. 2002; Borges et al. 2006).

CO₂ flux (F) across the water atmosphere interface can be calculated using **Eq.**

1.8

$$F = k([CO_2]_{\text{water}} - [CO_2]_{\text{air}}) \quad (1.8)$$

where k is the gas transfer velocity, [CO₂]_{water} is the concentration of measured CO₂ in water and [CO₂]_{air} is the concentration of CO₂ in water at equilibrium with the atmosphere.

The terms [CO₂]_{water} and [CO₂]_{air} are calculated from pCO₂ using **Eq. 1.9**

$$[CO_2] = K_H \times pCO_2 \quad (1.9)$$

where K_H is the Henry's constant for the in situ temperature and salinity of the sample.

(K_H is strongly affected by temperature and salinity, so these should be considered when

assuming an equilibrium between $p\text{CO}_2$ and $[\text{CO}_{2(\text{aq})}]$, such as when calculating $p\text{CO}_2$ from $[\text{CO}_2]$ or vice versa.) Although $p\text{CO}_2$ measurements are generally easy to obtain, either through direct measurements (Frankignoulle 1988; Goyet et al. 1992; Walt and Goyet 1993; Degrandpre et al. 1995; Feely et al. 1998; Körtzinger et al. 2000; Raymond et al. 2000; Frankignoulle and Borges 2001; Wang et al. 2002; Wang et al. 2003; Gazeau et al. 2005b; Borges et al. 2008; Faber et al. 2011) or by calculation using DIC/TA and pH (Millero 1995; Frankignoulle et al. 1996; Cai and Wang 1998; Frankignoulle et al. 1998; Abril et al. 2000; Borges et al. 2004a; Ortega et al. 2005; Koné and Borges 2008; Miyajima et al. 2009; Maher and Eyre 2012; Maher et al. 2013) (see (Boehme et al. 1998) for a comparison of direct $p\text{CO}_2$ measurements and calculated $p\text{CO}_2$). The gas transfer velocity presents more of a challenge. The value of k is influenced by turbulent mixing in the mass boundary layer which is controlled by numerous processes including wind speed, tidal currents and microscale breaking waves (Zappa et al. 2003; Borges et al. 2004a; Zappa et al. 2007; Vachon et al. 2010). Typically, wind speed is the simplest and easiest to measure proxy for turbulence at the mass boundary layer and is very commonly used to empirically estimate k in systems which are not subject to strong tidal currents, riverine flow, or waves. Several relationships between wind speed and k have been established and are commonly used (Wanninkhof 1992; Wanninkhof and McGillis 1999; Raymond and Cole 2001). These include estimates based on gas fluxes across the water-atmosphere interface within a floating dome (e.g. Marino and Howarth 1993) or water-atmosphere fluxes obtained from purposeful or natural gas tracer studies (e.g. Elsinger and Moore 1983; Clark et al. 1992; Clark et al. 1994). Estimates of k between estuarine and freshwater studies vary considerably (between 1 and 26 cm h^{-1}) indicating that this value is difficult to compare between sites and measurement methods (Raymond and Cole 2001). Unlike earlier studies that estimated k on either oceans (Wanninkhof 1992) or

lakes (Cole and Caraco 1998), Raymond and Cole (2001) estimate k from studies in rivers and estuaries, and show that the value of k in these systems may be higher at average wind speeds. To calculate k from wind speed, the relationship (**Eq. 1.10**) of Raymond and Cole (2001) can be used:

$$k = 1.58e^{0.3u} \quad (1.10)$$

where u is wind speed in m/s. This relationship excludes data from floating chamber studies as they have been shown to overestimate k values due to their effect on near surface turbulence, which is accepted to be a major driver of gas transfer (Matthews et al. 2003; Vachon et al. 2010). The k value must be normalised to a Schmidt number of 660 (Sc_{CO_2} ; the Schmidt number of CO_2 at 20 °C in seawater (Wanninkhof 1992)). As the Schmidt number is highly sensitive to temperature, k should be corrected for temperature by calculating the Schmidt number using the equations in Wanninkhof (1992). The adjusted k (k_{CO_2}) was calculated using **Eq. 1.11**.

$$\frac{k_{660}}{k_{CO_2}} = \left(\frac{660}{Sc_{CO_2}}\right)^n \quad (1.11)$$

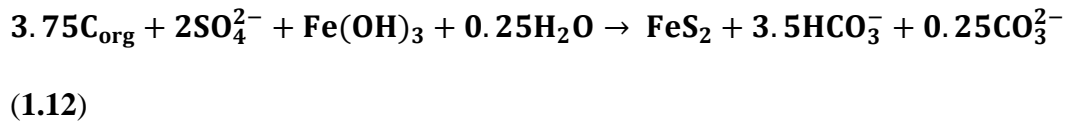
The value of n depends on the process that dominates diffusion. A value of -0.5 is commonly used and is based on an estimate of best fit made by Jähne et al (Jähne et al. 1987) and used by others e.g. (Wanninkhof 1992; Raymond et al. 2000; Borges et al. 2004a). In high flow environments, when flow data is present (see chapter 3), k can be estimated by inclusion of terms for flow and water depth (Borges et al. 2004a, Borges et al. 2004b)

1.3 Anaerobic alkalinity generation

Biogeochemical processes in sediments are fuelled by the bacterial breakdown of organic matter, deposited from the water column (Burdige 2006). Under oxic conditions, degradation of organic matter uses oxygen as an electron acceptor and results in the production of CO₂. Within sediments, oxygen concentrations decrease with depth as a result of aerobic respiration by the microbial community. In anoxic layers of sediment, the degradation of organic matter progresses via other biogeochemical pathways following a redox cascade where electron acceptors (oxidants) are sequentially used in organic matter respiration (Reeburgh 1983).

Within anoxic marine sediments, denitrification and sulfate reduction occur, utilising NO₃⁻ and SO₄²⁻ respectively as electron acceptors. In contrast to earlier views, that carbonate dissolution and precipitation were the only processes of controlling alkalinity in oceans, net denitrification and sulfate reduction in oceanic margins produce alkalinity in quantities significant to global alkalinity budgets (Chen 2002; Thomas et al. 2009; Hu and Cai 2011b). Several conditions exist with these two processes, for net alkalinity production to occur. Although the process of denitrification produces alkalinity, in a natural setting the cycling of nitrogen between ‘fixed’ forms and the atmosphere often consists of coupled nitrification and denitrification. In this instance, net alkalinity production is nil, due to the fact that nitrification is an alkalinity consuming process. Therefore, consideration must be given to the source of nitrate if alkalinity production is being investigated (Hu and Cai 2011b). In the literature, the distinction is made by referring to alkalinity producing denitrification of external sources as ‘net denitrification.’ As N₂ is the terminal product of denitrification, loss of N₂ to the atmosphere effectively removes N from the system permanently meaning that this process is irreversible. If net alkalinity production is to occur from sulfate reduction, then oxidised Fe needs to be

present so that iron sulfides (FeS and FeS₂) can be formed. Equation (**Eq. 1.12**) indicates the possible stoichiometry for sulfate reduction and coupled pyrite (FeS₂) burial (Hammond et al. 1999).



In this process, HS⁻, the product of sulfate production is prone to reoxidation upon diffusion into oxygen containing sediment or the water column. The reoxidation of HS⁻ consumes alkalinity meaning that no net alkalinity production occurs. Only through the permanent burial of reduced sulfur species can sulfate reduction result in net alkalinity production. Iron sulfides (FeS/FeS₂) are insoluble and relatively resistant to oxidation. This means that the formation and burial of FeS/FeS₂ leads to a net alkalinity production (Berner et al. 1970; Berner 1982; Hammond et al. 1999). For simplification, FeS and FeS₂ can be considered terminal species for reduced sulfate. This is probably not the case in highly dynamic systems such as estuaries and intertidal zones owing to the fact that FeS is much more readily oxidisable than FeS₂. For instance, periods of sulfate reduction and reduced sulfur oxidation are controlled by organic matter supply, with a high supply leading to an accumulation of reduced sulfur (as FeS), followed by reoxidation as the organic matter supply is diminished (Ferguson et al. 2003a). In the event of resuspension of sediment, FeS will be oxidised leading to alkalinity consumption. In contrast, FeS₂ is much more resilient to oxidation, but is formed on much longer time scales than FeS. Cycles of FeS oxidation may be responsible for seasonal or sporadic changes in alkalinity production due to the sudden availability of freshly oxidised Fe. Periodic resuspension of sediments due to increased wave energy or changes in current induced scouring (Wolanski et al. 1980; Jickells and Rae 2005) and subsequent FeS oxidation may provide

a source of oxidised Fe which allows periods of high alkalinity production. This may explain why high rates of instantaneous anaerobic alkalinity production can be observed despite inadequate inputs of terrestrial Fe. Due to the unpredictability of storm events and their likely effect on sediment resuspension, deposition and transport, Jickells and Rae (2005) emphasise that caution must be taken when extrapolating data from coastal systems during low energy periods. This is a knowledge gap that so far has proved difficult to fill due to difficulties and the absence of effective sampling techniques during these events.

1.4 Carbonate dissolution

Carbonate dissolution and precipitation are processes which control the majority of alkalinity production and removal in the world's oceans. Carbonate dissolution can be simplified by **Eq. 1.13** where solid CaCO_3 in the sediment dissolves:



This process produces 1 mol of DIC and 2 mol of TA for every mol of CaCO_3 dissolved. The production of dissolved $[\text{Ca}^{2+}]$ provides a means of quantifying carbonate dissolution, as it can be compared with a conservative ion such as $[\text{Na}^+]$ to determine if $[\text{Ca}^{2+}]$ is elevated. Carbonate dissolution can only occur when there is an undersaturation of CaCO_3 minerals within the water and this typically occurs when there is sufficient acid in the water to shift the equilibrium of DIC. In coastal sediments and estuaries, most alkalinity production is due to anaerobic processes such as denitrification and sulfate reduction (Berner et al. 1970; Hu and Cai 2011b), however, carbonate dissolution may still be a relevant part of the carbon budget of individual estuaries or coastal embayments. Miyajima et al. (2009) assumed that carbonate dissolution would be negligible in many

estuaries as the process would occur slowly relative to water exchange. In estuaries with low water exchange, for instance in lagoon systems, or in areas with low Fe inputs, carbonate dissolution may be a non-negligible DIC and TA source. Carbonate dissolution in shallow marine sediments was once thought to be negligible due to the fact that carbonate minerals are typically saturated in the water column. If this saturation does not continue below the sediment surface, then carbonate dissolution may be an important alkalinity and DIC producing process. In fact, carbonate dissolution has been shown to occur in shallow marine sediments where it is most extensive under conditions of high irrigation and the reoxidation of reduced iron sulfides (Aller 1982; Green et al. 1993). Acid produced as a result of aerobic carbon mineralisation and H₂S mineralisation may promote carbonate dissolution within the surface layers of the sediment (Aller 1982; Walter and Burton 1990; Walter et al. 1993).

1.5 DIC dynamics in estuaries

Estuaries are highly active coastal areas owing to the fact that they form an interface between land and ocean. Rivers transport substances such as dissolved organic carbon (DOC), particulate organic carbon (POC), nutrients and sediment from catchments, all of which play an important part in estuarine functioning (**Fig. 1.2**). High rates of deposition in estuaries means that substances can undergo transformation before export to the ocean. Due to the high availability of organic carbon, estuaries are typically zones of intense respiration, which can cause CO₂ production as well as anaerobic alkalinity production. Likewise, an abundant supply of nutrients may cause intense photosynthesis in some estuaries.

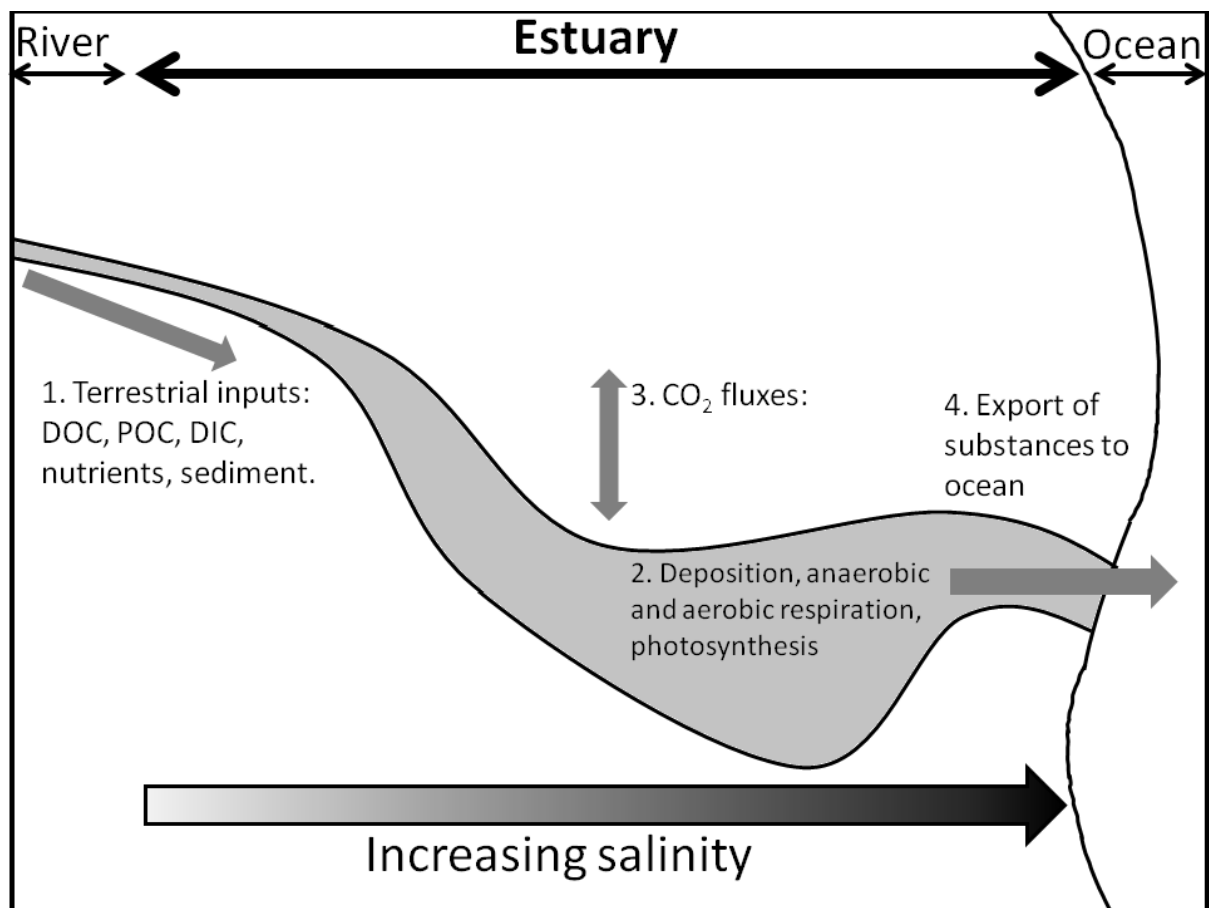


Figure 1.2: Diagram of estuarine carbon cycling in estuaries. 1. Terrestrial inputs which includes organic sources of carbon and inorganic carbon as well as inorganic nutrients. 2. Important processes occurring within the estuary; Deposition of organic matter, anaerobic and aerobic respiration and photosynthesis. 3. Fluxes of CO₂ into or out of the estuary. 4. Export of substances to the ocean.

Brasse et al. (2002) observed a pCO₂ profile down the North European, Elbe estuary which illustrated how parts of estuaries can act as sources and sinks of atmospheric CO₂ (**Fig. 1.3**). This pattern of pCO₂ saturation has been observed in highly impacted estuaries in North America (Raymond et al. 2000) and Europe (Frankignoulle et al. 1998; Brasse et al. 2002). The line at ~380 µatm pCO₂ indicates pCO₂ at atmospheric saturation. As salinity increases, pCO₂ decreases and the system begins to act as a sink of atmospheric carbon. This is due to an increase in primary production within the estuary,

due to decreased turbidity as a result of flocculation and settling of particles as they are destabilised by the increasing ionic strength of the water. This profile can be a result of high allochthonous inputs of organic carbon and inorganic nutrients. Upstream, where the water is turbid, organic carbon is mineralised producing CO_2 , whereas downstream, with lower turbidity (increased sunlight penetration into the water column) inorganic nutrients fuel the growth of algae, which causes an uptake of CO_2 . The spatial complexity of this profile can be increased by the fact that estuarine systems can be stratified.

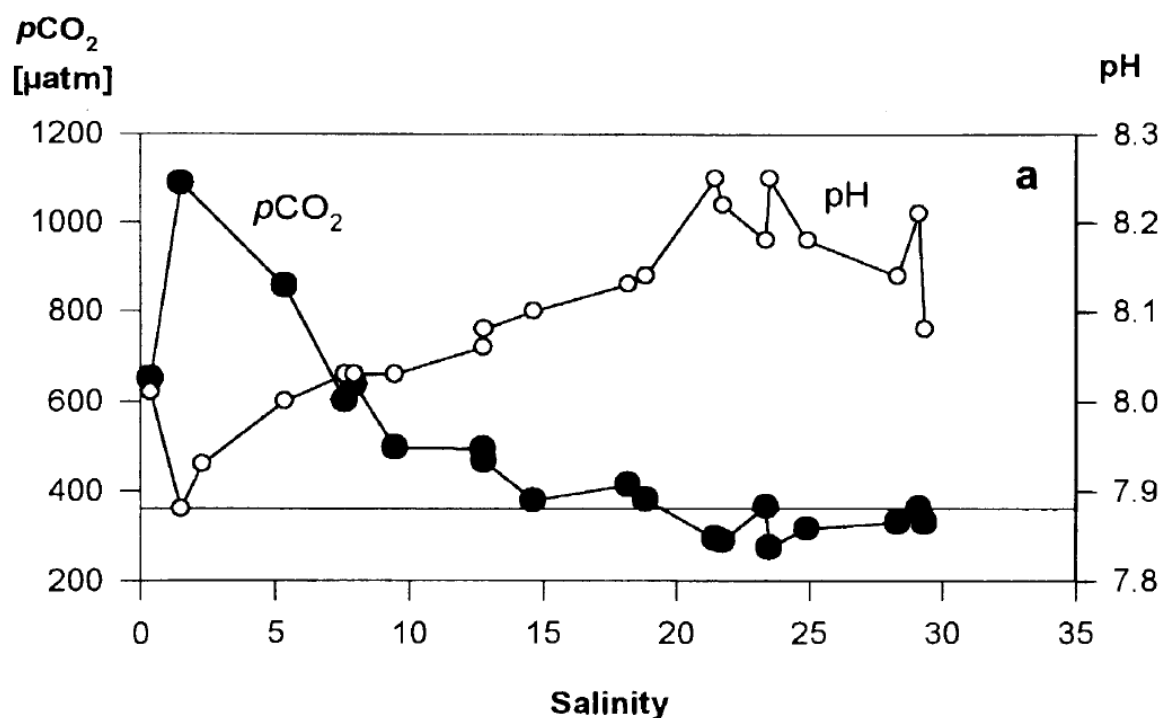


Figure 1.3: pCO₂ and pH in surface waters, along a salinity gradient in the Elbe estuary.

Source: (Brasse et al. 2002).

1.6 DIC dynamics and benthic metabolism in intertidal sediments

Intertidal sediments are important and dynamic places for the mineralisation of organic matter due to their high supply rates and high temporal and spatial variability.

Likewise, they are important for other processes such as primary production and nitrogen cycling. Coastal embayments, especially intertidal zones are areas of low wave and current energy and for this reason are areas of high deposition (Jickells and Rae 2005). Physically and chemically, they are an important interface between land sourced allochthonous material and the sea, due to their location and involvement in the transformation of materials. In early studies of estuarine benthic metabolism, consideration of intertidal sediments has been limited, despite their likely significance in organic carbon mineralisation (Middelburg et al. 1996). Measurements of benthic organic carbon mineralisation have traditionally been through oxygen flux measurements. It has been realised that this method does not consider anaerobic carbon mineralisation, which consumes oxidants other than oxygen, and which can be reoxidised at a later time, giving a misrepresentation of the actual rates (Hargrave and Phillips 1981; Anderson et al. 1986; Therkildsen and Lomstein 1993). Using this reasoning, researchers have used DIC fluxes, coupled with O₂ fluxes to determine benthic metabolism accounting for net anaerobic respiration processes such as sulfate reduction (Hopkinson 1985; Therkildsen and Lomstein 1993; Eyre and Ferguson 2002; Cook et al. 2004; Forja et al. 2004). The community respiration quotient (CRQ, DIC:O₂ ratio) can give information about the discrepancies between metabolism measured using O₂ and DIC fluxes. For instance, a CRQ value >1 indicates anaerobic respiration without the reoxidation of reduced species. A low value indicates aerobic respiration or processes such as the consumption of oxygen through reoxidation of reduced species such as S²⁻, or the loss of DIC through precipitation of CaCO₃ (Andersen and Kristensen 1988; Therkildsen and Lomstein 1993).

Unlike O₂ measurements, using DIC as a measurement of net metabolism accounts for both aerobic and anaerobic respiration, which may produce CO₂ or A_c. As

anaerobic respiration produces A_c , quantifying this is of interest in determining the relative rates of aerobic and anaerobic respiration.

Many studies of intertidal sediments focus on CO_2 during low tide exposure (Middelburg et al. 1996; Migné et al. 2002; Migné et al. 2005), or DIC fluxes during inundation (Cai et al. 1999). Studies measuring inorganic carbon fluxes on intertidal sediments during both inundation and exposure are rare. Alongi et al. (1999) measured inorganic carbon fluxes from mudflats during both inundation and exposure and found that these fluxes were similar. This contrasts with other studies which indicate that inorganic carbon fluxes during exposure and inundation differ considerably, with inundated fluxes of DIC being 2.5-5 times higher than CO_2 fluxes during exposure (Gribsholt and Kristensen 2003; Cook et al. 2004). The production of alkalinity in the sediment can titrate CO_2 produced by shifting the equilibrium of the carbonate system in the opposite direction, effectively turning CO_2 into its conjugate bases HCO_3^- and CO_3^{2-} . This may lead to large discrepancies between fluxes from inundated and exposed sediment, as alkalinity can only have a flux out of the sediment during inundation. There is a lack of understanding in the literature regarding this effect in intertidal sediments, but it is an important step in understand their role in carbon cycling, and the extent of mineralisation that is exported as alkalinity.

In intertidal sediments, the application of computer models in understanding these dynamics is a useful tool. Matching observations of laboratory experiments with computer models provides a way to predict carbon dynamics on a larger scale, provide insight into our mechanistic understanding of the mechanisms controlling carbon dynamics and to determine the effects of factors such as changes in organic carbon loading and sedimentation rates (increasing Fe) without *in situ* manipulation.

1.7 Factors influencing sedimentation and Fe input

Fe is transported in rivers where it exists nearly entirely as Fe-organic matter colloids (Boyle et al. 1977; Martin and Meybeck 1979; Haese 2000). This form of Fe is important when considering input to estuarine and coastal sediments as it undergoes highly non-conservative mixing behaviour. Due to the increases in dissolved ion concentrations, the colloids become unstable so that flocculation and settling occurs as salinity increases. This process causes the removal of ~90% of the Fe from the river water before entering the ocean (Boyle et al. 1977). Due to flocculation and deposition, estuaries have a high rate of sedimentation compared to typical ocean sediments, and the sediment in these systems is particularly rich in freshly delivered Fe. Anthropogenic changes in river catchments may change the amount of sediment transported meaning that estuaries are therefore particularly influenced. Increasing sediment supply to estuaries due to anthropogenic influences in river catchments is well known (Dunne 1979; Howarth et al. 1991; Hopkinson and Vallino 1995; Allan et al. 1997; Dauer et al. 2000; Neil et al. 2002; Alongi and Mckinnon 2005). Increases of fourfold in sediment delivery to the Great Barrier Reef lagoon of Australia since European settlement have been observed, and indicate that the main drivers of increased sedimentation loads are the increase in urbanisation and agriculture in river catchments (Alongi and Mckinnon 2005). The studies of increased sediment loadings have generally focused on the effect of sediment supply on coral reef communities and the influence of sedimentation rates on carbon mineralisation modes and rates (Canfield 1994; Alongi and Mckinnon 2005) but little research has involved determining the influence of sediment supply on net alkalinity production, via sulfate reduction and reduced sulfide burial, in estuaries.

1.8 Global relevance of carbonate system studies

In studies of European, Asian and North American estuaries, some of which are extremely affected by urbanisation and intensive agriculture, high organic carbon loading leads to high respiration and production of high concentrations of CO_2 , which escapes to the atmosphere (Frankignoulle et al. 1996; Raymond et al. 1997; Frankignoulle et al. 1998; Cai et al. 1999; Abril et al. 2000; Raymond et al. 2000; Frankignoulle and Borges 2001; Borges et al. 2004a; Zhai et al. 2005) and contributes a significant proportion of anthropogenic carbon budget (5-10% in Western Europe; Frankignoulle et al. 1998). Interest in the CO_2 fluxes of water bodies is increasing, due to the rising levels of atmospheric CO_2 on Earth. It is recognized that water bodies play an important part in global carbon budgets as they have a large potential to act both as major carbon dioxide producers, and as carbon sinks for anthropogenic CO_2 (Smith and Hollibaugh 1993; Frankignoulle et al. 1996; Raymond et al. 1997; Frankignoulle et al. 1998; Abril et al. 2000; Raymond et al. 2000; Terner et al. 2000). Because of the importance of Earth's water bodies in the global carbon budget, there is a considerable interest in monitoring these systems.

Changes in pCO_2 in marine systems have direct consequences because the speciation of inorganic carbon changes, resulting in a decreased pH and lower concentration of CO_3^{2-} . This is particularly relevant for marine life, as many organisms rely on the precipitation of CaCO_3 to form their shells. If a system becomes undersaturated with regard to CaCO_3 then there will be dire consequences for these organisms, including coral reef systems (Sabine et al. 2004). An increase in pCO_2 has been shown to reduce shell growth rate, and even lead to shell dissolution in laboratory experiments (Gattuso et al. 1998; Gazeau et al. 2007).

1.9 Knowledge gaps

Although there are several recent studies investigating carbon dynamics in Australian estuaries (e.g. Maher and Eyre 2012), most studies on carbon dynamics have been carried out in systems in the Northern hemisphere. This research aims to close a knowledge gap in Australian systems, which behave very differently to Northern hemisphere systems, as they are typically more episodic due to high variability in rainfall (Eyre 1998), and often have high amounts of suspended solids. With high organic carbon and sediment loading, sulfate reduction accounts for a large proportion of respiration (Canfield et al. 2005), leading to FeS_2 burial and alkalinity production when sufficient Fe is present. In Australian estuaries, these processes have not been studied in detail.

Although there are many studies looking at pCO_2 and DIC in estuaries, these haven't investigated the relationship between various modes of carbon cycling and catchment land use. The driving force behind changing carbon cycling in these systems is related to catchment land use, due to increases in carbon matter, nutrient and sediment loads (Bianchi 2007). Studying this link will be useful in understanding how these factors interact to change DIC dynamics. For instance, increased organic carbon input from catchments may lead to increased pCO_2 in the upper estuary, but increased inorganic nutrient inputs may lead to lower pCO_2 in the lower estuarine surface waters due to photosynthesis. Increased organic matter and sediment (and associated Fe) loading to the sediment will change the dynamics of carbon due to influences on alkalinity.

Another knowledge gap exists in the carbon fluxes from mangrove systems. Studies on DIC dynamics in mangrove systems are of considerable interest because of the high rates of processes such as sedimentation, photosynthesis and respiration occurring in these systems, their ability to recycle inputs of terrestrially sourced nutrients and their ability to export substances such as DOC and DIC to coastal oceans. Currently, a

knowledge gap in carbon export from mangrove systems exists, with several studies suggesting that DIC export from mangroves may account for this “missing sink” (Bouillon et al. 2008a; Maher et al. 2013). Contributions to this field of knowledge are especially important and may aid in determination of carbon budgets for coastal oceans in general. Similarly, mangroves can export alkalinity which may be relevant to oceanic budgets of alkalinity.

1.10 Project aims, hypotheses and thesis structure

The aims of this thesis can be summarised using several general research questions which investigate DIC export on three spatial scales:

1. Does alkalinity generation within tidal flat sediments control the relative export of inorganic carbon to the atmosphere and to coastal waters?
2. Do differing degrees of terrestrial inputs influence the dominant modes of carbon export from tidal flats?
3. Do differing regimes of anthropogenic land use in river catchments control inorganic carbon and alkalinity production in estuaries?

Chapter 2 investigates carbon dynamics on intertidal mudflats. This follows on from the observation that DIC fluxes from the sediment may be different between inundated and exposed phases (Cook et al. 2004) and addresses research question 1 by conducting laboratory core incubations and computer simulations of an intertidal system. This chapter also investigates the drivers of this discrepancy by investigating the effect Fe has on DIC export from intertidal sediments using computer simulations. This is based on the hypotheses that the discrepancy between exposed and inundated DIC fluxes is a result of

alkalinity production, and the knowledge that Fe is a driver of net alkalinity flux via the burial of the reduced sulfur products of sulfate reduction within the sediment.

In light of this study, and investigation of the influence of Fe on alkalinity production, chapter three investigates the differences in carbon export between two intertidal systems which are subject to differing degrees of terrestrial inputs (research question 2). One site, Chinaman Inlet has no significant input of terrestrial matter, whereas the other, Watson Inlet has a small creek with an impacted catchment. The observable differences between the terrestrial inputs creates the hypothesis that Watson Inlet will export more alkalinity than Chinaman inlet due to a greater input of terrestrially sourced Fe which will allow burial of reduced sulfur. Time series sampling allows data to be obtained over the full tidal cycle to determine how fluxes change as porewater drainage occurs. Sampling is conducted within the inlet channels so that convective fluxes can be observed. As these inlets contain considerable areas of mangrove forest, our observations may aid in understanding of how carbon is exported from mangroves.

The study presented in chapter four investigates anthropogenic impacts on inorganic carbon export from eight estuaries across Victoria, Australia, which have catchments with differing levels of catchment impact (question 3). These impacts are due to anthropogenic activities such as agriculture and urbanisation, and increase as the extent of these activities increases. The more impacted catchments are hypothesised to export more Fe, as suspended sediment, and organic carbon and this may change the way inorganic carbon is exported. Although chapter 2 investigates the importance of Fe in controlling the export of inorganic carbon, it doesn't investigate the relationship between inorganic carbon export and catchment impact within actual systems. Chapter 4 aims to quantify and determine dominant modes of inorganic carbon export in several temperate Australian estuaries and attempts to relate this to the influence of catchment impact.

1.11 References

- Abril, G., H. Etcheber, A. Borges, and M. Frankignoulle. 2000. Excess atmospheric carbon dioxide transported by rivers into the Scheldt estuary. *Comptes Rendus de l'Academie des Sciences-Series IIA-Earth and Planetary Science* **330**: 761-768.
- Abril, G., M. Nogueira, H. Etcheber, G. Cabecadas, E. Lemaire, and M. Brogueira. 2002. Behaviour of organic carbon in nine contrasting European estuaries. *Estuarine, Coastal and Shelf Science* **54**: 241-262.
- Allan, D., D. Erickson, and J. Fay. 1997. The influence of catchment land use on stream integrity across multiple spatial scales. *Freshwater Biology* **37**: 149-161.
- Aller, R. C. 1982. Carbonate dissolution in nearshore terrigenous muds: the role of physical and biological reworking. *The Journal of Geology*: 79-95.
- Alongi, D., and A. Mckinnon. 2005. The cycling and fate of terrestrially-derived sediments and nutrients in the coastal zone of the Great Barrier Reef shelf. *Marine Pollution Bulletin* **51**: 239-252.
- Alongi, D., F. Tirendi, P. Dixon, L. Trott, and G. Brunskill. 1999. Mineralization of organic matter in intertidal sediments of a tropical semi-enclosed delta. *Estuarine, Coastal and Shelf Science* **48**: 451-467.
- Andersen, F., and E. Kristensen. 1988. The influence of macrofauna on estuarine benthic community metabolism: a microcosm study. *Marine Biology* **99**: 591-603.
- Anderson, L. and others 1986. Benthic respiration measured by total carbonate production. *Limnology and Oceanography* **31**: 319-329.

- Berner, R. A. 1982. Burial of organic carbon and pyrite sulfur in the modern ocean: its geochemical and environmental significance. *Am. J. Sci* **282**: 451-473.
- Berner, R. A., M. R. Scott, and C. Thomlinson. 1970. Carbonate alkalinity in the pore waters of anoxic marine sediments. *Limnology and Oceanography*: 544-549.
- Bianchi, T. S. 2007. *Biogeochemistry of estuaries*. Oxford University Press, USA.
- Boehme, S., C. Sabine, and C. Reimers. 1998. CO₂ fluxes from a coastal transect: a time-series approach. *Marine Chemistry* **63**: 49-67.
- Borges, A., B. Delille, L. Schiettecatte, F. Gazeau, G. Abril, and M. Frankignoulle. 2004. Gas transfer velocities of CO₂ in three European estuaries (Randers Fjord, Scheldt, and Thames). *Limnology and Oceanography*: 1630-1641.
- Borges, A., L. S. Schiettecatte, G. Abril, B. Delille, and F. Gazeau. 2006. Carbon dioxide in European coastal waters. *Estuarine, Coastal and Shelf Science* **70**: 375-387.
- Borges, A. V., K. Ruddick, L.-S. Schiettecatte, and B. Delille. 2008. Net ecosystem production and carbon dioxide fluxes in the Scheldt estuarine plume. *BMC ecology* **8**: 15.
- Bouillon, S. and others 2008. Mangrove production and carbon sinks: a revision of global budget estimates. *Global Biogeochemical Cycles* **22**: GB2013.
- Boyle, E., J. Edmond, and E. Sholkovitz. 1977. The mechanism of iron removal in estuaries. *Geochimica et Cosmochimica Acta* **41**: 1313-1324.
- Brasse, S., M. Nellen, R. Seifert, and W. Michaelis. 2002. The carbon dioxide system in the Elbe estuary. *Biogeochemistry* **59**: 25-40.

- Burdige, D. J. 2006. Geochemistry of marine sediments, Chapter. Princeton University Press Princeton.
- Cai, W., L. Pomeroy, M. Moran, and Y. Wang. 1999. Oxygen and carbon dioxide mass balance for the estuarine-intertidal marsh complex of five rivers in the southeastern US. *Limnology and Oceanography* **44**: 639-649.
- Cai, W., and Y. Wang. 1998. The chemistry, fluxes, and sources of carbon dioxide in the estuarine waters of the Satilla and Altamaha Rivers, Georgia. *Limnology and Oceanography*: 657-668.
- Canfield, D., E. Kristensen, and B. Thamdrup. 2005. Aquatic geomicrobiology, vol. 48. *Advances in Marine Biology*. Elsevier, Oxford, United Kingdom.
- Canfield, D. E. 1994. Factors influencing organic carbon preservation in marine sediments. *Chemical Geology* **114**: 315-329.
- Chen, C.-T. A. 2002. Shelf-vs. dissolution-generated alkalinity above the chemical lysocline. *Deep Sea Research Part II: Topical Studies in Oceanography* **49**: 5365-5375.
- Clark, J. F., H. J. Simpson, W. M. Smethie, and C. Toles. 1992. Gas exchange in a contaminated estuary inferred from chlorofluorocarbons. *Geophysical Research Letters* **19**: 1133-1136.
- Clark, J. F., R. Wanninkhof, P. Schlosser, and H. J. Simpson. 1994. Gas exchange rates in the tidal Hudson River using a dual tracer technique. *Tellus B* **46**: 274-285.
- Cole, J., and N. Caraco. 1998. Atmospheric exchange of carbon dioxide in a low-wind oligotrophic lake measured by the addition of SF₆. *Limnology and Oceanography*: 647-656.

- Cook, P., E. Butler, and B. Eyre. 2004. Carbon and nitrogen cycling on intertidal mudflats of a temperate Australian estuary I. Benthic metabolism. *Marine Ecology Progress Series* **280**: 25-38.
- Dauer, D. M., J. A. Ranasinghe, and S. B. Weisberg. 2000. Relationships between benthic community condition, water quality, sediment quality, nutrient loads, and land use patterns in Chesapeake Bay. *Estuaries* **23**: 80-96.
- Degrandpre, M., T. Hammar, S. Smith, and F. Sayles. 1995. In situ measurements of seawater pCO₂. *Limnology and Oceanography* **40**: 969-975.
- Dickson, A. 1981. An exact definition of total alkalinity and a procedure for the estimation of alkalinity and total inorganic carbon from titration data. *Deep Sea Research Part A. Oceanographic Research Papers* **28**: 609-623.
- Dunne, T. 1979. Sediment yield and land use in tropical catchments. *Journal of Hydrology* **42**: 281-300.
- Elsinger, R. J., and W. S. Moore. 1983. Gas exchange in the Pee Dee River based on ²²²Rn evasion. *Geophysical Research Letters* **10**: 443-446.
- Eyre, B. 1998. Transport, retention and transformation of material in Australian estuaries. *Estuaries and Coasts* **21**: 540-551.
- Eyre, B., and A. Ferguson. 2002. Comparison of carbon production and decomposition, benthic nutrient fluxes and denitrification in seagrass, phytoplankton, benthic microalgae-and macroalgae-dominated warm-temperate Australian lagoons. *Marine Ecology Progress Series* **229**: 43-59.

- Faber, P. A., P. L. M. Cook, I. D. Mckelvie, and P. S. Ellis. 2011. Development of a gas diffusion probe for the rapid measurement of pCO₂ in aquatic samples. *Analytica Chimica Acta* **691**: 1-5.
- Feely, R. A., R. Wanninkhof, H. B. Milburn, C. E. Cosca, M. Stapp, and P. P. Murphy. 1998. A new automated underway system for making high precision pCO₂ measurements onboard research ships. *Analytica Chimica Acta* **377**: 185-191.
- Ferguson, A., B. Eyre, and J. Gay. 2003. Organic matter and benthic metabolism in euphotic sediments along shallow sub-tropical estuaries, northern New South Wales, Australia. *Aquatic Microbial Ecology* **33**: 137-154.
- Forja, J. M., T. Ortega, T. A. Delvalls, and A. Gómez-Parra. 2004. Benthic fluxes of inorganic carbon in shallow coastal ecosystems of the Iberian Peninsula. *Marine Chemistry* **85**: 141-156.
- Frankignoulle, M. 1988. Field measurements of air-sea CO₂ exchange. *Limnology and Oceanography* **33**: 313-322.
- Frankignoulle, M. and others 1998. Carbon dioxide emission from European estuaries. *Science* **282**: 434.
- Frankignoulle, M., and A. Borges. 2001. Direct and indirect pCO₂ measurements in a wide range of pCO₂ and salinity values (the Scheldt estuary). *Aquatic Geochemistry* **7**: 267-273.
- Frankignoulle, M., I. Bourge, and R. Wollast. 1996. Atmospheric CO₂ fluxes in a highly polluted estuary (the Scheldt). *Limnology and Oceanography* **41**: 365-369.

- Gattuso, J., M. Frankignoulle, I. Bourge, S. Romaine, and R. Buddemeier. 1998. Effect of calcium carbonate saturation of seawater on coral calcification. *Global and Planetary Change* **18**: 37-46.
- Gazeau, F. and others 2005. Whole-system metabolism and CO₂ fluxes in a Mediterranean Bay dominated by seagrass beds (Palma Bay, NW Mediterranean). *Biogeosciences* **2**: 43-60.
- Gazeau, F., C. Quiblier, J. Jansen, J. Gattuso, J. Middelburg, and C. Heip. 2007. Impact of elevated CO₂ on shellfish calcification. *Geophysical Research Letters* **34**: L07603.
- Goyet, C., D. Walt, and P. Brewer. 1992. Development of a fiber optic sensor for measurement of pCO₂ in sea water: design criteria and sea trials. *Deep Sea Research Part A. Oceanographic Research Papers* **39**: 1015-1026.
- Green, M. A., R. C. Aller, and J. Y. Aller. 1993. Carbonate dissolution and temporal abundances of foraminifera in Long Island Sound sediments. *Limnology and Oceanography*: 331-345.
- Gribsholt, B., and E. Kristensen. 2003. Benthic metabolism and sulfur cycling along an inundation gradient in a tidal *Spartina anglica* salt marsh. *Limnology and Oceanography* **48**: 2151-2162.
- Haese, R. R. 2000. The reactivity of iron, p. 233-261. *Marine geochemistry*. Springer.
- Hammond, D., P. Giordani, W. Berelson, and R. Poletti. 1999. Diagenesis of carbon and nutrients and benthic exchange in sediments of the Northern Adriatic Sea. *Marine Chemistry* **66**: 53-79.

- Hargrave, B., and G. Phillips. 1981. Annual in situ carbon dioxide and oxygen flux across a subtidal marine sediment. *Estuarine, Coastal and Shelf Science* **12**: 725-737.
- Hopkinson, C. 1985. Shallow-water benthic and pelagic metabolism. *Marine Biology* **87**: 19-32.
- Hopkinson, C. S., and J. J. Vallino. 1995. The relationships among man's activities in watersheds and estuaries: a model of runoff effects on patterns of estuarine community metabolism. *Estuaries* **18**: 598-621.
- Howarth, R. W., J. R. Fruci, and D. Sherman. 1991. Inputs of sediment and carbon to an estuarine ecosystem: Influence of land use. *Ecological Applications*: 27-39.
- Hu, X., and W. J. Cai. 2011. An assessment of ocean margin anaerobic processes on oceanic alkalinity budget. *Global Biogeochemical Cycles* **25**: GB3003.
- Jähne, B., G. Heinz, and W. Dietrich. 1987. Measurement of the diffusion coefficients of sparingly soluble gases in water. *Journal of Geophysical Research* **92**: 10767-10710,10776.
- Jickells, T. D., and J. E. Rae. 2005. *Biogeochemistry of intertidal sediments*. Cambridge University Press.
- Koné, Y.-M., and A. Borges. 2008. Dissolved inorganic carbon dynamics in the waters surrounding forested mangroves of the Ca Mau Province (Vietnam). *Estuarine, Coastal and Shelf Science* **77**: 409-421.
- Körtzinger, A. and others 2000. The international at-sea intercomparison of fCO₂ systems during the R/V Meteor Cruise 36/1 in the North Atlantic Ocean. *Marine Chemistry* **72**: 171-192.

- Maher, D., I. Santos, L. Golsby-Smith, J. Gleeson, and B. Eyre. 2013. Groundwater-derived dissolved inorganic and organic carbon exports from a mangrove tidal creek: The missing mangrove carbon sink? *Limnol. Oceanogr* **58**: 475-488.
- Maher, D. T., and B. D. Eyre. 2012. Carbon budgets for three autotrophic Australian estuaries: Implications for global estimates of the coastal air-water CO₂ flux. *Global Biogeochem. Cycles* **26**: GB1032.
- Marino, R., and R. W. Howarth. 1993. Atmospheric oxygen exchange in the Hudson River: Dome measurements and comparison with other natural waters. *Estuaries* **16**: 433-445.
- Martin, J.-M., and M. Meybeck. 1979. Elemental mass-balance of material carried by major world rivers. *Marine Chemistry* **7**: 173-206.
- Matthews, C. J., V. L. St. Louis, and R. H. Hesslein. 2003. Comparison of three techniques used to measure diffusive gas exchange from sheltered aquatic surfaces. *Environmental Science & Technology* **37**: 772-780.
- Middelburg, J. and others 1996. Organic matter mineralization in intertidal sediments along an estuarine gradient. *Marine Ecology Progress Series*. Oldendorf **132**: 157-168.
- Migné, A., D. Davoult, J. J. Bourrand, and G. Boucher. 2005. Benthic primary production, respiration and remineralisation: in situ measurements in the soft-bottom *Abra alba* community of the western English Channel (North Brittany). *Journal of Sea Research* **53**: 223-229.

- Migné, A. and others 2002. A closed-chamber CO₂-flux method for estimating intertidal primary production and respiration under emersed conditions. *Marine Biology* **140**: 865-869.
- Millero, F. 1995. Thermodynamics of the carbon dioxide system in the oceans. *Geochimica et Cosmochimica Acta* **59**: 661-677.
- Millero, F. J., T. B. Graham, F. Huang, H. Bustos-Serrano, and D. Pierrot. 2006. Dissociation constants of carbonic acid in seawater as a function of salinity and temperature. *Marine Chemistry* **100**: 80-94.
- Miyajima, T., Y. Tsuboi, Y. Tanaka, and I. Koike. 2009. Export of inorganic carbon from two Southeast Asian mangrove forests to adjacent estuaries as estimated by the stable isotope composition of dissolved inorganic carbon. *Journal of Geophysical Research* **114**: G01024.
- Neil, D. T., A. R. Orpin, P. V. Ridd, and B. Yu. 2002. Sediment yield and impacts from river catchments to the Great Barrier Reef lagoon: a review. *Marine and Freshwater Research* **53**: 733-752.
- Ortega, T., R. Ponce, J. Forja, and A. Gómez-Parra. 2005. Fluxes of dissolved inorganic carbon in three estuarine systems of the Cantabrian Sea (north of Spain). *Journal of Marine Systems* **53**: 125-142.
- Raymond, P., J. Bauer, and J. Cole. 2000. Atmospheric CO₂ evasion, dissolved inorganic carbon production, and net heterotrophy in the York River estuary. *Limnology and Oceanography* **45**: 1707-1717.
- Raymond, P., N. Caraco, and J. Cole. 1997. Carbon dioxide concentration and atmospheric flux in the Hudson River. *Estuaries and Coasts* **20**: 381-390.

- Raymond, P., and J. Cole. 2001. Gas exchange in rivers and estuaries: Choosing a gas transfer velocity. *Estuaries and Coasts* **24**: 312-317.
- Reeburgh, W. 1983. Rates of biogeochemical processes in anoxic sediments. *Annual Review of Earth and Planetary Sciences* **11**: 269-298.
- Roy, R. and others 1993. The dissociation constants of carbonic acid in seawater at salinities 5 to 45 and temperatures 0 to 45 C. *Marine Chemistry* **44**: 249-267.
- Sabine, C. and others 2004. The oceanic sink for anthropogenic CO₂. *Science* **305**: 367-371.
- Sarmiento, J., and N. Gruber. 2006. *Ocean biogeochemical dynamics*. Princeton University Press.
- Smith, S., and J. Hollibaugh. 1993. Coastal metabolism and the oceanic organic carbon balance. *Reviews of Geophysics* **31**: 75-89.
- Stumm, W., and J. Morgan. 1996. *Aquatic chemistry: chemical equilibria and rates in natural waters*.
- Ternon, J., C. Oudot, A. Dessier, and D. Diverres. 2000. A seasonal tropical sink for atmospheric CO₂ in the Atlantic Ocean: the role of the Amazon River discharge. *Marine Chemistry* **68**: 183-201.
- Therkildsen, M., and B. Lomstein. 1993. Seasonal variation in net benthic C-mineralization in a shallow estuary. *FEMS Microbiology Ecology* **12**: 131-142.
- Thomas, H. and others 2009. Enhanced ocean carbon storage from anaerobic alkalinity generation in coastal sediments. *Biogeosciences* **6**: 267-274.

- Vachon, D., Y. Prairie, and J. Coleb. 2010. The relationship between near-surface turbulence and gas transfer velocity in freshwater systems and its implications for floating chamber measurements of gas exchange. *Limnol. Oceanogr* **55**: 1723-1732.
- Walt, D., and C. Goyet. 1993. Multiple-indicator fiber-optic sensor for high-resolution pCO₂ sea water measurements. *Analytica Chimica Acta* **274**: 47-52.
- Walter, L. M. and others 1993. Dissolution and recrystallization in modern shelf carbonates: evidence from pore water and solid phase chemistry [and discussion]. *Philosophical Transactions of the Royal Society of London. Series A: Physical and Engineering Sciences* **344**: 27-36.
- Walter, L. M., and E. A. Burton. 1990. Dissolution of recent platform carbonate sediments in marine pore fluids. *American Journal of Science* **290**: 601-643.
- Wang, Z., W. Cai, Y. Wang, and B. Upchurch. 2003. A long pathlength liquid-core waveguide sensor for real-time pCO₂ measurements at sea. *Marine Chemistry* **84**: 73-84.
- Wang, Z., Y. Wang, W. Cai, and S. Liu. 2002. A long pathlength spectrophotometric pCO₂ sensor using a gas-permeable liquid-core waveguide. *Talanta* **57**: 69-80.
- Wanninkhof, R. 1992. Relationship between wind speed and gas exchange. *Journal of Geophysical Research* **97**: 7373–7382.
- Wanninkhof, R., and W. R. McGillis. 1999. A cubic relationship between air-sea CO₂ exchange and wind speed. *Geophysical Research Letters* **26**: 1889-1892.

- Wolanski, E., M. Jones, and J. Bunt. 1980. Hydrodynamics of a tidal creek-mangrove swamp system. *Marine and Freshwater Research* **31**: 431-450.
- Zappa, C. and others 2007. Environmental turbulent mixing controls on air-water gas exchange in marine and aquatic systems. *Geophysical Research Letters* **34**: L10601.
- Zappa, C. J., P. A. Raymond, E. A. Terray, and W. R. McGillis. 2003. Variation in surface turbulence and the gas transfer velocity over a tidal cycle in a macro-tidal estuary. *Estuaries* **26**: 1401-1415.
- Zeebe, R., and D. Wolf-Gladrow. 2001. *CO₂ in seawater: equilibrium, kinetics, isotopes*. Elsevier Science.
- Zhai, W., M. Dai, W. Cai, Y. Wang, and Z. Wang. 2005. High partial pressure of CO₂ and its maintaining mechanism in a subtropical estuary: the Pearl River estuary, China. *Marine Chemistry* **93**: 21-32.

2. The role of alkalinity generation in controlling the fluxes of CO₂ during exposure and inundation on tidal flats

P. A. Faber^{1*}, A . J. Kessler¹, J. K. Bull¹, I. D. McKelvie^{2,3}, F. J. R. Meysman⁴, P. L. M. Cook¹

¹ Water Studies Centre, School of Chemistry, Monash University, Victoria 3800, Australia

² School of Chemistry, The University of Melbourne, Victoria 3010, Australia

³ School of Geography, Earth and Environmental Sciences, University of Plymouth, Plymouth PL48AA, England

⁴ Department of Ecosystem Studies, Royal Netherlands Institute for Sea Research (NIOZ), Korringaweg 7, 4401 NT Yerseke, The Netherlands

2.1 Declaration for Thesis Chapter two

Declaration by candidate

In the case of Chapter two, the nature and extent of my contribution to the work was the following:

Nature of contribution	Extent of contribution (%)
Running computer model, some laboratory analysis, data analysis, primary author	75

The following co-authors contributed to the work. If co-authors are students at Monash University, the extent of their contribution in percentage terms must be stated:

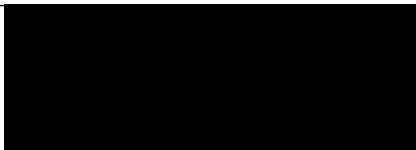
Name	Nature of contribution	Extent of contribution (%) for student co-authors only
Adam Kessler	Assisting in model formulation	5
James Bull	Laboratory analysis of core incubations	
Ian McKelvie	Assistance in laboratory analysis.	
Filip Meysman	Formulation of computer model,	
Perran Cook	Assistance with study design, guidance and manuscript editing, field data collection.	

The undersigned hereby certify that the above declaration correctly reflects the nature and extent of the candidate's and co-authors' contributions to this work*.

Candidate's
Signature

	Date
--	------

Main
Supervisor's
Signature

	Date 18/04/14
---	------------------

2.2 Abstract

Dissolved inorganic carbon (DIC), gaseous CO₂ and alkalinity fluxes from intertidal sediments were investigated during periods of exposure and inundation, using laboratory core incubations, previously published field data and reactive transport model simulations. In the incubations and previous field data, it was found that during periods of alkalinity production, the flux of DIC out of the sediment was greater during inundation than exposure by a factor of up to 1.8. This alkalinity production was attributed to the accumulation of reduced sulfur species within the sediment. This finding was supported by computational simulations which indicated that large amounts of sulfate reduction and reduced sulfur burial (FeS) induce an alkalinity flux from the sediment during high tide conditions. Model simulations also found that the amount of reactive Fe in the sediment was a major driver of net alkalinity production. Our finding that CO₂ fluxes can be significantly lower than total metabolism during exposure has implications for how total metabolism is quantified on tidal flats.

2.3 Introduction

Tidal flats are highly dynamic and biogeochemically active environments, that are characterised by the deposition of allochthonous organic matter as well as high in-situ rates of primary production by microphytobenthos (Joye et al. 2009). The quantification of organic carbon production and mineralisation in these environments is complicated by the fact that tidal flats are periodically inundated. This means that fluxes of inorganic carbon should ideally be measured both during inundation (as dissolved inorganic carbon $\text{DIC} = [\text{CO}_2] + [\text{HCO}_3^-] + [\text{CO}_3^{2-}]$) and exposure (as gaseous CO_2). In practice, the quantification of inorganic carbon fluxes during the inundation of tidal flats is logistically complex because they are covered by a shallow layer of turbid water, and often experience high currents. Moreover, the determination of DIC in aqueous samples is also more time consuming and technically challenging than the analysis of CO_2 in gas samples. Typically, most studies of benthic metabolism on tidal flats only measure gaseous fluxes of CO_2 during exposure (Middelburg et al. 1996; Migné et al. 2005) or DIC flux during inundation (Cai et al. 1999).

Relatively few studies have included direct measurement of inorganic carbon fluxes during both exposure and inundation of tidal flats and these studies show different outcomes. Alongi et al. (1999) found very similar exchange rates during both inundation and exposure. By contrast, Gribsholt and Kristensen (2003) and Cook et al. (2004) found consistently higher rates of inorganic carbon exchange during inundation on un-vegetated tidal flat sediments, where the flux during inundation increased by a factor of ~2. A number of possible explanations exist for these differences. Firstly, solute transport processes are very different between inundation and exposure periods. During inundation, all three forms of the carbonate system (CO_2 , HCO_3^- and CO_3^{2-}) can be transported across the sediment interface, whereas during exposure, only gaseous CO_2 can diffuse into the

atmosphere. Furthermore, bio-irrigation is well known to enhance solute exchange in sediments (Kristensen 1988). This process will cease upon exposure, and would result in a reduction of the CO₂ flux during exposure as compared to the inundated DIC flux. Secondly, alkalinity generation, caused by the burial of reduced metal sulfides and/or calcium carbonate dissolution, is often observed at high rates in shallow waters and intertidal sediments (Ferguson et al. 2003b; Cook et al. 2004; Thomas et al. 2009). Alkalinity cannot escape the sediment during low tide, and so will tend to accumulate near the sediment-water interface. This will lead to a shift towards increased HCO₃⁻ and CO₃²⁻ and decreased CO₂, and hence, a reduced gaseous CO₂ flux during exposure.

However, there are also reasons why the CO₂ flux might be enhanced during exposure. A change in CO₂ transfer during exposure to the atmosphere may occur due to the higher diffusion of CO₂ in the atmosphere (10^{-5} compared to $10^{-9} \text{ m}^2 \text{ s}^{-1}$) and the decreased thickness of the diffusive boundary layer during exposure (Brotas et al. 1990).

To date, none of these factors have been explored, experimentally or theoretically. A basic understanding of the exchange dynamics of inorganic carbon is required for the design of studies aiming to quantify the fluxes of inorganic carbon between tidal flats and the atmosphere and coastal waters. Here, we used data from controlled laboratory experiments, and a numeric diagenetic model to investigate the dynamics of inorganic carbon exchange in the intertidal zone. In particular, we focus on the role of alkalinity generation by anaerobic respiration in the retardation of the CO₂ efflux during exposure relative to DIC export to the water column.

2.4 Materials and methods

2.4.1 Experimental

Muddy sediment (Grain size: 48% 300 μm - 1mm; 8% 200 - 300 μm ; 39% 100 - 200 μm ; 5% 62 - 100 μm and porosity = 0.81 ml water cm^{-3}) was collected from an intertidal flat located in the Yarra Estuary, Australia (37.833° S, 145.0229° E). The sediment was sieved (1 mm mesh) to remove macrofauna and homogenised. The total inorganic carbon content of the sediment was <0.1% w/w. The sediment was then placed in a shallow tray and gently stirred whilst being aerated for 1 day to oxidise reduced solutes before being packed into 8 core liners (7 cm diameter) to a depth of 5 cm. This depth layer was chosen to represent the diagenetically active depth. **Fig. 2.1** represents the experimental setup that was used. The cores had stirrer bars inserted to gently stir the water column. A peristaltic pump system transferred ambient sea water collected from Port Phillip Bay in and out of the cores (Salinity = 35, Temperature = 20°C). The pumping regime followed a regular six hourly cycle of inundation and exposure that mimicked a semi-diurnal tide. The inlet of the tubes in the core was recessed slightly into the sediment surface, so that all the overlying water could be removed, leaving no ponding of water on the surface during exposure. The water was recycled between the cores and a central reservoir, and was unfiltered. The reservoir water was changed periodically so that the TA was maintained between 2.5 and 3 mM. The incubations were conducted in dark. Carbon mineralisation processes in natural systems can be highly dynamic reflecting pulsed inputs of organic matter (OM), for example, deposition of phytodetritus. This pulsed occurrence of carbon mineralisation is highly relevant, driving cycles of solute reduction and oxidation, which in turn drives alkalinity production and consumption. To simulate a pulse of organic matter, half of the cores had 0.38 g baker's yeast added to them after 71 days (+OM treatment), while the remaining cores did not

receive this organic matter input (-OM). During inundation, the flux of DIC was determined by covering the cores with sealed lids and taking 4-5 water samples during sediment inundation. The DIC flux was determined as the slope of DIC concentration versus time multiplied by the water height. The pH was simultaneously measured as the water sample for alkalinity was taken. During exposure, the flux of gaseous CO₂ was measured by sampling the gas headspace of the sealed core. Again, the CO₂ flux was determined as the slope of CO₂ concentration versus time multiplied by the headspace height. CO₂ was sampled using evacuated 3 ml draw blood collection vials (Vacutainers, Becton Dickinson) and analysed using Flow Injection Analysis (Satieperakul et al. 2004). Alkalinity samples were filtered (Bonnet, 0.45 µm polyethersulfone) and preserved with 20 µl HgCl₂ (6% w/v). They were stored in glass vials and refrigerated at 4 °C for less than one week before analysis using a modified Gran titration (Almgren et al. 1983). pH was determined at 20 °C using a pH electrode (Hach PHC301 connected to an HQ40d meter), calibrated with NBS buffers. DIC concentrations in the water column were calculated using alkalinity and pH, with the constants found in Roy et al. (1993). The method for total Fe analysis of the dried sediment was modified from Lord (1982), using a 24 hr citrate/bicarbonate/dithionite extraction for easily extractable Fe, followed by a 24 hr concentrated nitric acid digestion. The extracts were then analysed using atomic absorption spectroscopy (AAS).

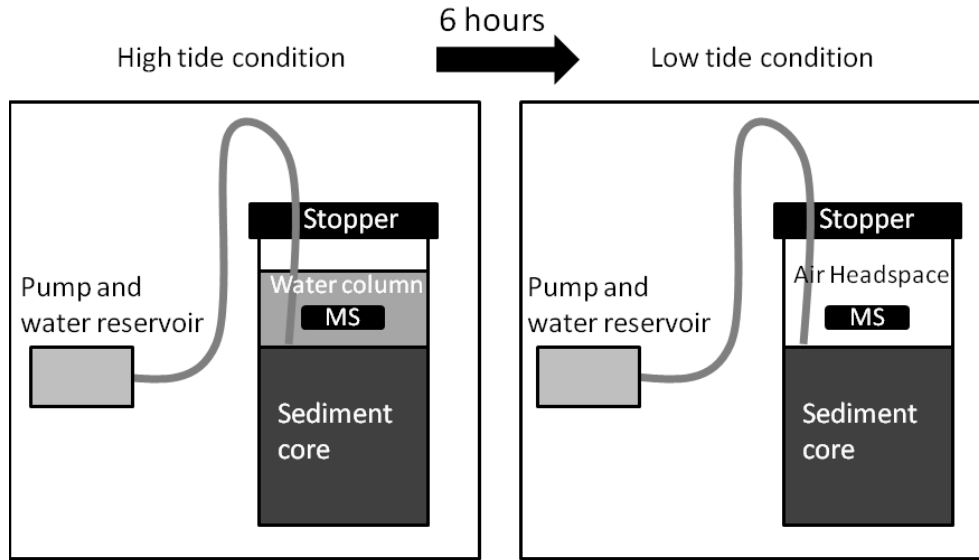


Figure 2.1: Diagram of the experimental setup, showing the conditions of simulated tides. TA and DIC are sampled from the water column during inundation (high tide) and CO₂ is sampled from the headspace during exposure (low tide). MS refers to a magnetic stirrer bar.

2.4.2 Model formulation

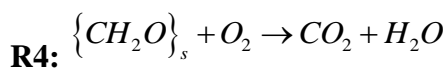
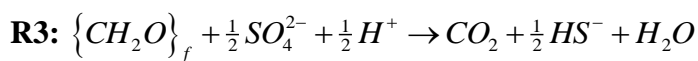
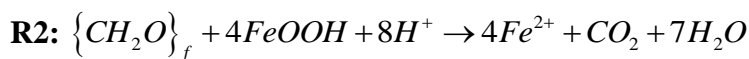
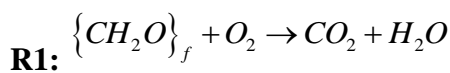
The reactive transport model follows the standard formulation for early diagenetic models of marine sediments (Boudreau 1997; Meysman et al. 2003). The model simulates the depth profiles of solutes and solids, as well as the fluxes across the sediment-water interface, based on the mass balance equations

$$\text{Solute:} \quad \phi \frac{\partial C_i^{PW}}{\partial t} = \frac{\partial}{\partial x} \left[\phi D_i \frac{\partial C_i^{PW}}{\partial x} \right] + \sum_k \nu_{i,k} R_k$$

$$\text{Solids:} \quad (1 - \phi) \frac{\partial C_i^S}{\partial t} = \sum_k \nu_{i,k} R_k$$

where C_i^{PW} and C_i^S are the concentrations of a solute and solid compound respectively. No advective processes are included in the model, as negligible sedimentation occurred during the incubations. The porosity ϕ is assumed constant with depth. For solutes, the only transport process is molecular diffusion. The diffusion coefficient D_i is calculated as a function of temperature and salinity using the R package *marelac* (Soetaert 2010) and subsequently corrected for tortuosity according to the modified Wiessberg relation of Boudreau (1996). The quantities R_k represent the reaction rates, where $\nu_{i,k}$ is the stoichiometric coefficient of the i -th species in the k -th reaction. The reaction set includes three mineralisation pathways (aerobic respiration, dissimilatory iron reduction and sulfate reduction) for two fractions of organic matter (fast and slow decaying), the formation of iron sulfide and pyrite, and the reoxidation of reduced compounds in pore water (ferrous iron, free sulfide) and solid phase (iron sulfides and pyrite). The full set of 13 reactions is given in **Table 2.1**. The rate expressions for these reactions follow the standard kinetic rate laws and are given in **Table 2.2**. For simplicity, we have assumed that processes such as nitrification and denitrification have a negligible effect on alkalinity fluxes in this system.

Table 2.1: Kinetic reactions included in the reaction set



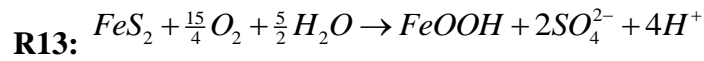
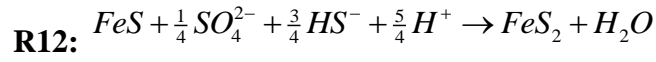
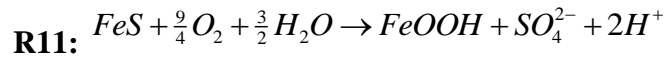
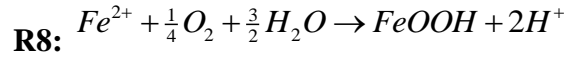
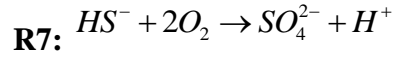
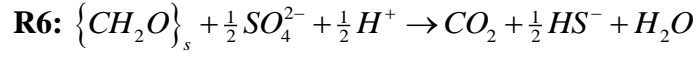
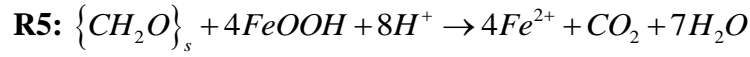


Table 2.2: Kinetic rate expressions for the reactions included in the reaction set

$$R_{\min}^f = (1-\phi)k_{fast} \left[CH_2O_f \right]$$

$$R_{\min}^s = (1-\phi)k_{slow} \left[CH_2O_s \right]$$

$$R_1 = \frac{\left[O_2 \right]}{\left[O_2 \right] + K_{O_2}} R_{\min}^f$$

$$R_2 = \frac{\left[FeOOH \right]}{\left[FeOOH \right] + K_{FeOOH}} \frac{K_{O_2}}{\left[O_2 \right] + K_{O_2}} R_{\min}^f$$

$$R_3 = \frac{[SO_4^{2-}]}{[SO_4^{2-}] + K_{SO_4^{2-}}} \frac{K_{FeOOH}}{[FeOOH] + K_{FeOOH}} \frac{K_{O_2}}{[O_2] + K_{O_2}} R_{\min}^f$$

$$R_4 = \frac{[O_2]}{[O_2] + K_{O_2}} R_{\min}^s$$

$$R_5 = \frac{[FeOOH]}{[FeOOH] + K_{FeOOH}} \frac{K_{O_2}}{[O_2] + K_{O_2}} R_{\min}^s$$

$$R_6 = \frac{[SO_4^{2-}]}{[SO_4^{2-}] + K_{SO_4^{2-}}} \frac{K_{FeOOH}}{[FeOOH] + K_{FeOOH}} \frac{K_{O_2}}{[O_2] + K_{O_2}} R_{\min}^s$$

$$R_7 = \phi k_{H_2S-Ox} [O_2] [HS^-]$$

$$R_8 = \phi k_{Fe-Ox} [Fe^{2+}] [O_2]$$

$$R_9 = (1-\phi) k_{FeOOH-H_2S} [FeOOH] [HS^-]$$

$$R_{10} = \phi k_{FeS.form} [Fe^{2+}] [HS^-]$$

$$R_{11} = (1-\phi) k_{FeS-Ox} [FeS] [O_2]$$

$$R_{12} = (1-\phi) k_{FeS_2.form} [FeS] [HS^-]$$

$$R_{13} = (1-\phi) k_{FeS_2-Ox} [FeS_2] [O_2]$$

2.4.3 pH model

The set of acid-base reactions governing the pH dynamics in the pore water includes the carbonate, borate, sulfide and water equilibria. The impact of dissociation

reactions involving phosphate, ammonium, silicate and dissolved organic compounds was assumed negligible. The associated total alkalinity and total species are hence defined as:

$$A_T = [HCO_3^-] + 2[CO_3^{2-}] + [B(OH)_4^-] + [HS^-] + [OH^-] - [H^+]$$

$$SumCO2 = [CO_2] + [HCO_3^-] + [CO_3^{2-}]$$

$$SumBOH3 = [B(OH)_3] + [B(OH)_4^-]$$

$$SumH2S = [HS^-] + [H_2S]$$

The associated equilibrium constants were calculated as a function of temperature and salinity using AquaEnv, a dedicated R-package for acid-base and CO₂ system calculations (Hofmann et al. 2010). Specifically, for the carbonate equilibria, we used the relationships provided by Millero et al. (2006).

2.4.4 Boundary conditions and initial state

The cyclic process of inundation and exposure was simulated by regular switching between two sets of boundary conditions. Under inundation, the concentration of solutes at the sediment-water interface was fixed to that of the overlying water (which was set at constant pH and solute concentrations), while a fixed flux was imposed for the solids. These fluxes were set to zero for all solid components during the whole simulation period (zero deposition assumed– see above), apart from organic matter, which received a pulse input at 71 days. To model this pulse input, the organic matter was added uniformly to the top 2 mm of the sediment at a total concentration of ~2500 µmol CH₂O g⁻¹ dry sediment and fractionated between the fast-decaying fraction (75%) and the slow-decaying fraction

(25%), a ratio used by Westrich and Berner (1984) (who also included a third, non-reactive fraction in their model.)

Under exposed conditions, only the volatile solutes O₂ and CO₂ have an exchange with the overlying atmosphere, which is modelled using the convective boundary flux $J = k_d (C^{eq} - C)$ with k_d the piston velocity and C^{eq} the gas concentration in equilibrium with the atmosphere. At the lower boundary of the sediment domain a no-flux condition was imposed (fluxes across the bottom boundary are zero) for all compounds over the whole simulation period.

The reduced Fe (FeS and FeS₂) concentration was initially set to 0 and the O₂ concentration in the pore water was set to equilibrium with the atmospheric concentration. A uniform profile of slow-decaying organic matter (~2500 μmol CH₂O g⁻¹ dry sediment), and either 19 or 95 μmol Fe g⁻¹ dry sediment was imposed. These latter values were determined to be the extreme low and high Fe concentrations, as measured by a total Fe extraction at the conclusion of the experiment.

2.4.5 Numerical model solution

A numerical solution procedure was implemented in the open-source programming language R as fully detailed in Soetaert and Meysman (2012). A reactive transport model essentially consists of one partial differential equation (PDE) for each compound. Together with the mass action laws of the acid-base equilibria, these PDEs form a differential-algebraic system, which was solved using an operator splitting approach (Solution method [3b] as explained in Hofmann et al., (2008). Following the method-of-lines, the R-package ReacTran uses a finite difference scheme to expand the spatial derivatives of the PDEs over the sediment grid. This grid was obtained by dividing

the sediment domain (thickness $L = 5$ cm, the approximate depth of the sediment cores in the incubation experiment) into a uniform grid of 100 sediment layers. After finite differencing, the resulting set of ODEs was integrated using the stiff equation solver `vode` from the R-package `deSolve`.

At each time step, the operator splitting approach of the pH model required an additional pH equilibration step. To this end, the numerical integration of the ODE system provided the values of the reaction invariants (TA, SumCO₂, SumH₂S, SumBOH₃) at each future time step. Subsequently, the non-linear system of algebraic acid-base expressions was solved for the unknown proton concentration using the iterative method of Follows et al. (2006). Using this proton concentration (or equally pH value), the full speciation could be calculated of all chemical species involved in the acid-base dissociation reactions. The resulting concentrations of the equilibrium species could then be employed in kinetic rate expressions (specifically, the pore water CO₂ concentration was needed in the rate expression for the air-sea gas transfer of CO₂). Further details on this pH model procedure are given by Hofmann et al., (2008).

2.4.6 Description of model runs

The model was set up to simulate the tidal cycles imposed in the laboratory core incubation experiments, which were exposed and inundated alternately every 6 hours. The model simulations provide flux estimates at each point in time. The fluxes of TA and DIC during inundation and CO₂ fluxes during exposure are reported as the mean over the 6-hour exposure/inundation period. These reported mean values include transient (~30 min) spikes in DIC and TA immediately after inundation. The simulation extended over 120 days (i.e. 240 tidal cycles), with a pulse of organic matter added on day 70,

simulating the addition of the organic matter source in the laboratory experiments. **Table 2.3** lists an overview of parameters values used in model simulations. These were determined from measured properties, literature values or calibrated to the available dataset. All parameter values were kept constant during the whole simulation period (apart from the organic matter input).

Table 2.3: Overview of model parameter values

Constant	Value	Units
Porosity	0.8	-
rho.sed (density of solid sediment)	2.6	g cm ⁻³
Piston velocity	1	cm hr ⁻¹
K.fast (highly labile organic matter)	25	y ⁻¹
K.slow (less labile organic matter)	0.6	y ⁻¹
K_O ₂ (Monod constant for O ₂ consumption)	0.005	μmol cm ⁻³
K_FeOOH (Monod constant for FeOOH reduction)	200*rho.sed	μmol cm ⁻³
K_SO ₄ ²⁻ (Monod constant for SO ₄ ²⁻ reduction)	1.6	μmol cm ⁻³
k_H ₂ S.Ox (Kinetic constant for H ₂ S oxidation)	1.6 x 10 ⁷	μmol ⁻¹ cm ³ y ⁻¹
k_Fe.Ox (Kinetic constant for Fe oxidation)	2.0 x 10 ⁴	μmol ⁻¹ cm ³ y ⁻¹
k_FeS.Ox (Kinetic constant for FeS oxidation)	160	μmol ⁻¹ cm ³ y ⁻¹
k_FeS ₂ .Ox (Kinetic constant for FeS ₂ oxidation)	0	μmol ⁻¹ cm ³ y ⁻¹
k_Fe.H ₂ S (Kinetic constant for FeOOH/H ₂ S redox reaction)	2.57	μmol ⁻¹ cm ³ y ⁻¹
k_FeS.form (Kinetic constant for FeS formation)	1 x 10 ⁸	μmol ⁻¹ cm ³ y ⁻¹
k_FeS ₂ .form (Kinetic constant for FeS ₂ formation)	1	μmol ⁻¹ cm ³ y ⁻¹

2.4.7 Sensitivity model runs

The sensitivity of CO₂ flux to the piston velocity was investigated using simulations, where the piston velocity was varied from 0.05 to 5 cm hr⁻¹. In each simulation, the initial FeOOH concentration was 19 μmol Fe g⁻¹ dry sediment. For each

value of the piston velocity, the average flux of CO₂ during exposure was calculated over the complete simulation period (30 tidal cycles). This procedure was repeated for three different initial values of organic matter concentration (2500, 1000 and 600 $\mu\text{mol C g}^{-1}$ dry sediment for the slow-decaying fraction, and 5, 2.5 and 1.3 $\mu\text{mol C g}^{-1}$ dry sediment for the fast-decaying fraction respectively), to investigate the sensitivity of CO₂ flux to the piston velocity under different amounts of organic matter loading.

The availability of reactive oxidised iron (FeOOH) controls alkalinity production in the sediment, and hence, we performed a second series of simulations to investigate the sensitivity of the model towards the initial sedimentary FeOOH concentration. To determine the effect of FeOOH availability on TA production, simulations were run with a fixed initial concentration of CH₂O ($\sim 2500 \mu\text{mol CH}_2\text{O g}^{-1}$ dry sediment) but with various FeOOH concentrations (7.6, 19 and 95 $\mu\text{mol Fe g}^{-1}$ dry sediment). The values of 19 and 95 $\mu\text{mol Fe g}^{-1}$ dry sediment are the low and high estimates of sediment FeOOH concentrations in the core experiment sediment, respectively. The value of 7.6 $\mu\text{mol Fe g}^{-1}$ dry sediment was chosen as a low value for a comparison with our estimates.

2.5 Results

2.5.1 Experimental

There was little variation in the DIC fluxes over the entire course of the experiment in the –OM treatment with a mean value of $1.3 \text{ mmol m}^{-2} \text{ h}^{-1}$ over the 120 days (**Fig. 2.2**). In the +OM treatment, DIC fluxes were the same as the –OM treatment within experimental uncertainty in the first 70 days of the experiment before the organic matter was added (**Fig. 2.2**). After the organic matter addition, DIC fluxes substantially increased to a maximum of $\sim 5.0 \text{ mmol m}^{-2} \text{ h}^{-1}$, and then decreased again to $\sim 2.0 \text{ mmol m}^{-2} \text{ h}^{-1}$.

$^2 \text{ h}^{-1}$ over a time period of 40 days after organic matter addition. Alkalinity fluxes were initially high in both -OM and +OM treatments, steadily decreasing from $>1.4 \text{ mmol m}^{-2} \text{ h}^{-1}$ at the start of the experiment to attain a negligible alkalinity flux after 60 days. The most likely explanation for this observation is that there was build-up of iron sulfides, whose rate of formation slowed over time. We hypothesize that initially, a large pool of Fe(III) was formed during sediment pre-treatment, which was subsequently gradually turned into metal sulfides. Dissimilatory iron reduction produces alkalinity (TA:DIC = 8, see R9 in **Table 2.2**), but as the pool of Fe(III) is depleted, alkalinity production will decrease over time. After the pulsed addition of organic matter, alkalinity fluxes increased rapidly to a maximum of $3.0 \text{ mmol m}^{-2} \text{ h}^{-1}$ before decreasing again rapidly. The CO_2 fluxes during exposure were initially very low in both treatments ($\sim 0.10 \text{ mmol m}^{-2} \text{ h}^{-1}$). In the -OM treatment, the CO_2 flux increased after 60 d, coinciding with the decrease and cessation of alkalinity fluxes (fluxes not significantly different from zero, shown by the error bars). In the +OM treatment, there was an increase in CO_2 fluxes after the addition of organic matter, reaching a maximum of $\sim 2.5 \text{ mmol m}^{-2} \text{ h}^{-1}$. The CO_2 fluxes decreased again to $\sim 0.60 \text{ mmol m}^{-2} \text{ h}^{-1}$ at the conclusion of the experiment.

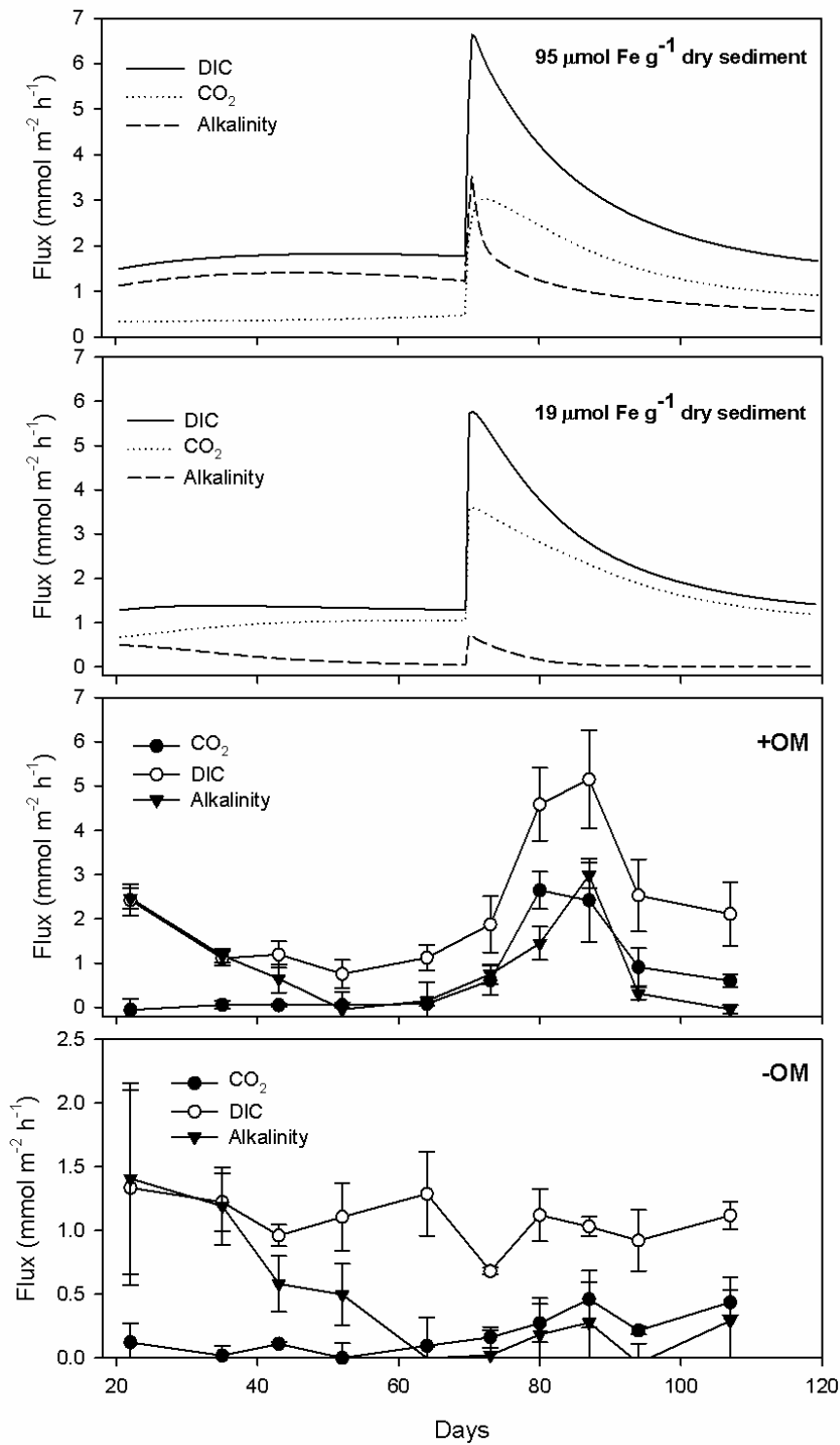


Figure 2.2: Simulated mean fluxes of CO₂ during exposure (CO₂), dissolved inorganic carbon (DIC) and alkalinity during inundation in the computer simulation with 95 and 19 μmol Fe/g sediment (d/w) and laboratory core incubation fluxes with (+OM) and without (-OM) added organic matter. Error bars are standard deviations across 10 replicates.

2.5.2 Model simulations

To match with the laboratory experiments, the data from the model were truncated before 20 days (**Fig. 2.2**). From day 20 to 70, the simulation yielded inundated DIC fluxes between ~ 1.2 and $\sim 1.4 \text{ mmol m}^{-2} \text{ h}^{-1}$. Immediately after the OM addition at day 70, the DIC flux increased to a maximum of $\sim 5.7 \text{ mmol m}^{-2} \text{ h}^{-1}$. The TA flux decreased from ~ 0.48 to $\sim 0.040 \text{ mmol m}^{-2} \text{ h}^{-1}$ before the OM addition, then increased to a maximum of $\sim 0.74 \text{ mmol m}^{-2} \text{ h}^{-1}$ after the addition. The CO_2 flux during exposure was between ~ 0.66 and $\sim 1.0 \text{ mmol m}^{-2} \text{ h}^{-1}$ before the OM addition, and rose to a maximum of $\sim 3.6 \text{ mmol m}^{-2} \text{ h}^{-1}$ after the addition of the OM, then decreasing again to $\sim 1.2 \text{ mmol m}^{-2} \text{ h}^{-1}$ by the end of the simulation. The peak flux during the simulation is shifted forward in time relative to the core incubations indicating a delayed response of organic matter mineralisation under experimental conditions. This is expected, as the bacterial community first needs to grow to consume the bioavailable organic matter. In the computer simulation, no lag phase occurs, as the model formulation does not include population growth, and thus assumes an instantaneous response of microbial metabolism.

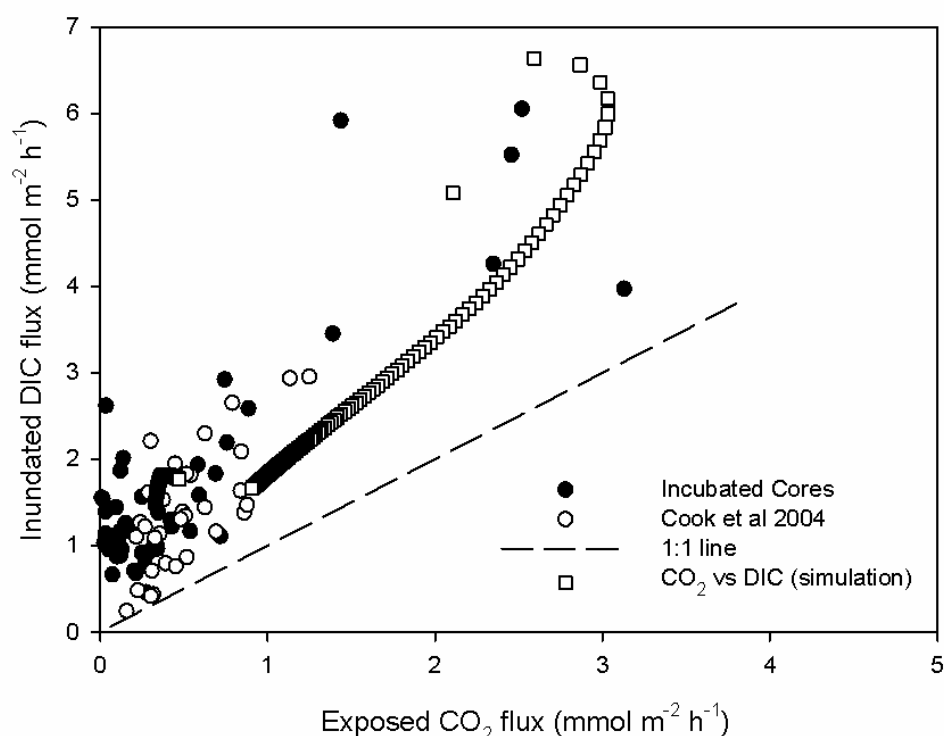


Figure 2.3: Fluxes of dissolved inorganic carbon (DIC) versus exposed CO₂ fluxes for two experimental data sets, and a model simulation. Incubated core experiments represent both the + and – OM treatments.

In the model simulations, DIC fluxes were consistently higher during inundation than CO₂ fluxes during the corresponding exposure periods (**Fig. 2.3**). The discrepancy between DIC and gaseous CO₂ fluxes appears to increase with increasing respiration, shown by the divergence of the simulation data from the 1:1 line as DIC flux increases. This pattern was very similar to that previously observed for intact sediments collected from tidal flats (Cook et al. 2004) (**Fig. 2.3**).

The fluxes of gaseous CO₂ during exposure and the fluxes of DIC and TA during exposure were highly sensitive to initial Fe concentrations in the sediment. This can be evaluated by calculating the mean fluxes over the period before the organic matter pulse (**Fig. 2.4**). The high Fe concentration resulted in a lower CO₂ flux during exposure (~0.65

vs $\sim 0.35 \text{ mmol m}^{-2} \text{ h}^{-1}$ for the 19 and $95 \text{ } \mu\text{mol Fe g}^{-1}$ dry sediment). There was also a large discrepancy between alkalinity fluxes, where the high Fe concentration resulted in a higher TA flux ($0.80 \text{ mmol m}^{-2} \text{ h}^{-1}$ versus $1.4 \text{ mmol m}^{-2} \text{ h}^{-1}$ for the 19 and $95 \text{ } \mu\text{mol Fe g}^{-1}$ dry sediment simulations). The difference between DIC fluxes were smaller, with a flux of $\sim 1.8 \text{ mmol m}^{-2} \text{ h}^{-1}$ for the simulation with $95 \text{ } \mu\text{mol Fe g}^{-1}$ dry sediment, and $\sim 1.6 \text{ mmol m}^{-2} \text{ h}^{-1}$ for the simulation with $19 \text{ } \mu\text{mol Fe g}^{-1}$ dry sediment.

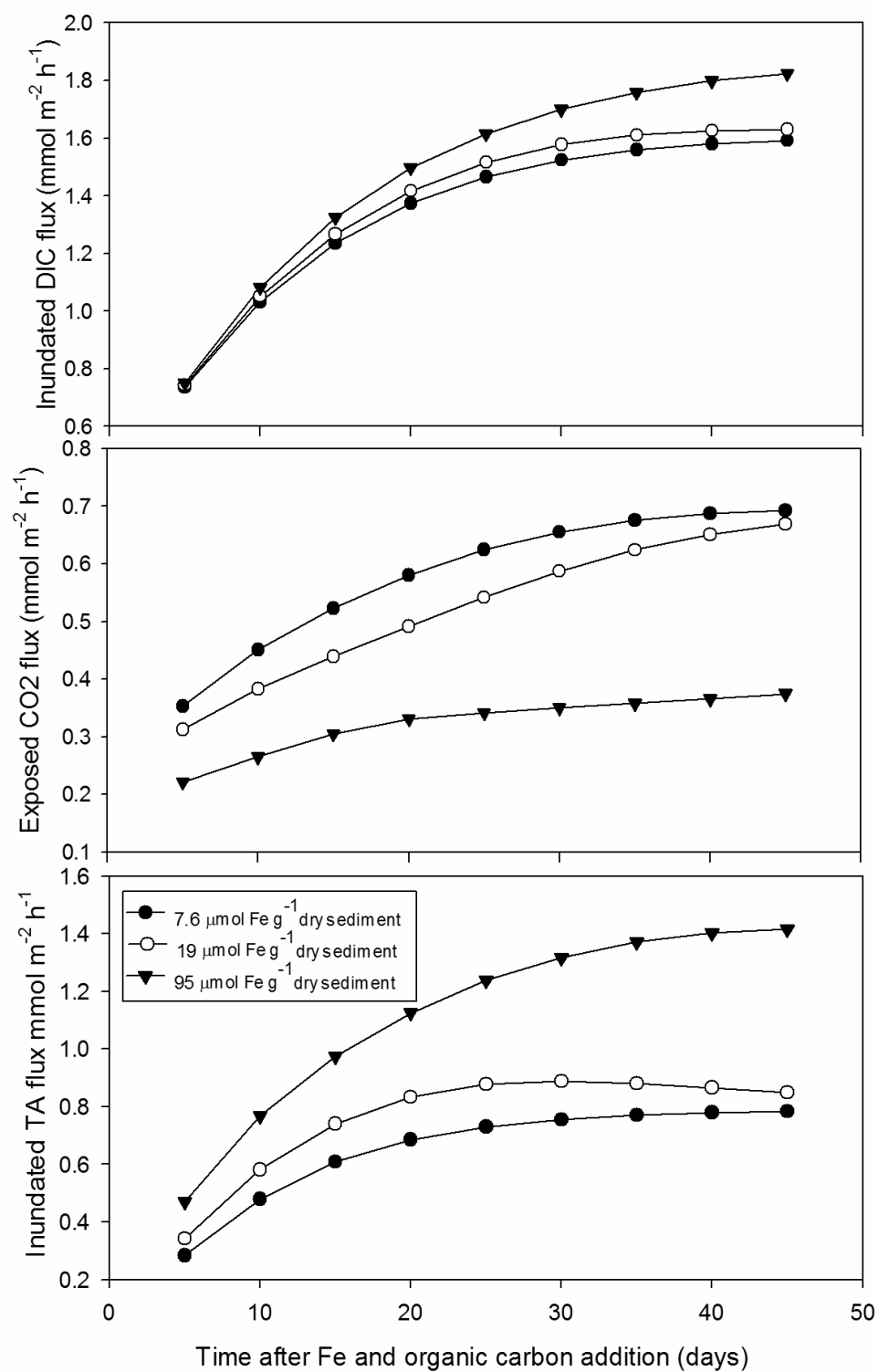


Figure 2.4: Fluxes of dissolved inorganic carbon (DIC), exposed CO_2 and alkalinity fluxes for a simulation of a 50 day period with an imposed profile of 7.6, 19 and 95 $\mu\text{mol g}^{-1}$ sediment (d/w) FeOOH .

2.5.3 Simulation profiles

The profile of FeOOH in the top 0.5 cm of sediment changed dramatically upon the addition of the organic matter pulse to the top 0.2 cm (**Fig. 2.5**). The profile taken two tidal cycles before the pulse shows the FeOOH reaching $\sim 15 \mu\text{mol Fe g}^{-1}$ dry sediment in the surface layer, and decreasing with increasing depth. One tidal cycle after the addition of organic matter, FeOOH has begun to oxidise, with the concentration in the top 0.2 cm falling to a maximum of $2 \mu\text{mol Fe g}^{-1}$ dry sediment in the surface layer. Below 0.2 cm, the FeOOH profile is similar between the two times, as the organic matter concentration has not changed in this domain.

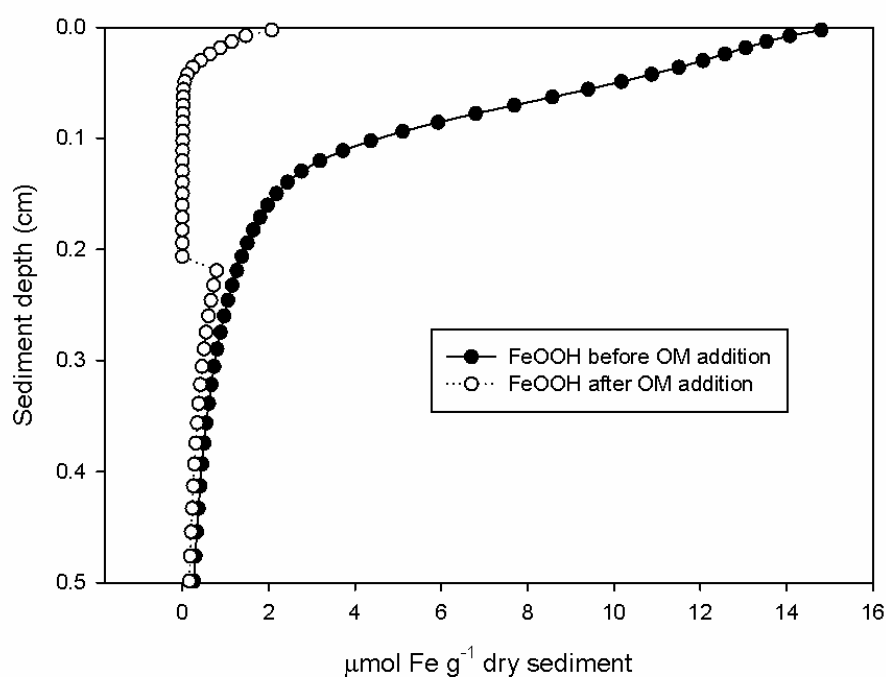
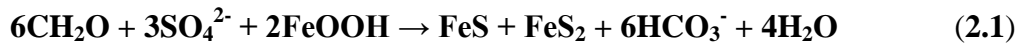


Figure 2.5: A simulation showing the FeOOH concentration before and after an organic matter pulse with initial FeOOH concentration of $19 \mu\text{mol g}^{-1}$ sediment (d/w). Note: The step around 0.2 cm is due to the pulse of organic matter added to only the top 0.2 cm.

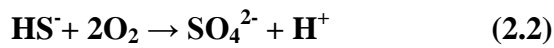
2.6 Discussion

2.6.1 Alkalinity producing reactions

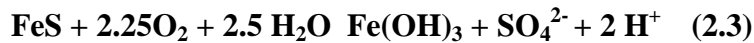
The production of alkalinity can be attributed to several key processes; ammonia release, net denitrification, net sulfate reduction and to a lesser extent, dissolved organic carbon release (Hammond et al. 1999). Berner et al. (1970) proposed the idea of sulfate reduction as an alkalinity producing process. It was noted that sulfate reduction coupled with the precipitation of the stable iron sulfides FeS and FeS₂ produces one mole of alkalinity per mole of carbon mineralised (Berner et al. 1970) (**Eq. 2.1**):



In this representation of sulfate reduction, the supply of Fe (III) to the sediment enables the burial of reduced sulfur compounds as iron sulfides (FeS) or pyrite (FeS₂). This burial of reduced sulfur prevents sulfide oxidation and hence it prevents the alkalinity generated by sulfate reduction being consumed again (**Eq. 2.2**).



Upon exposure to oxygen, iron sulfides can also oxidise, leading to alkalinity consumption (and hence no net alkalinity generation by sulfate reduction) (**Eq. 2.3**)



However, the rate of this reaction is typically lower than that of free sulfide oxidation (see **Table 2.3**). More importantly, one requires a suitable transport process, that either moves the reduced sulfur compounds upwards to the oxic zone (like bioturbation), or oppositely, transfers oxygen down into anoxic layers (like bio-irrigation). In the experimental setup here, such transport processes are not present.

Hu and Cai (2011a) reviewed the factors controlling alkalinity generation in ocean margins in sediment and concluded that the burial of pyrite and the denitrification of NO_3^- derived from the continents were the only net sources of alkalinity in ocean margin sediments. As the cycling of sulfur is closely linked with that of iron, we included both sulfur and iron geochemistry in the diagenetic model. In our experiments, denitrification was unlikely to be a significant source of alkalinity generation because of the lack of NO_3^- in the overlying water of our incubations. Coupled nitrification denitrification will not result in significant net alkalinity generation (Hu and Cai 2011a). Consequently, we did not model the effect of denitrification on alkalinity in this model. Dissolved organic matter and HPO_4^{2-} have been shown to contribute to alkalinity fluxes (Cai et al. 2010), but reactions involving sulfur (and its interactions with iron) are the major processes controlling the alkalinity balance within the sediment, and hence only these processes are considered. We are confident that the model used here represents the critical anaerobic alkalinity-generating processes that are important in our experimental set up.

2.6.2 Model sensitivity towards piston velocity

At piston velocities $>1 \text{ cm hr}^{-1}$ the CO_2 efflux reached a stable value, and this asymptotic CO_2 efflux increased proportionally with initial organic matter content (or total mineralisation) (**Fig. 2.6**). Decreasing the piston velocity below 0.5 cm hr^{-1} reduced CO_2 fluxes during sediment exposure. This can be attributed to the slower efflux of CO_2 for a given CO_2 concentration gradient (transport control), and a slower flux of O_2 into the sediment resulting in less aerobic respiration. Indeed, we found the rate of aerobic respiration to decrease with decreasing piston velocity (data not shown). Initially we thought that the alkalinity flux would remain constant upon changing piston velocity. It

was noted, however, that there was an increase in alkalinity production by 7% as the piston velocity was decreased from 5 to 0.05 (data not shown) indicating that anaerobic respiration accounted for a greater proportion of the total respiration. Higher respiration rates were more sensitive to decreasing piston velocities. We concluded that when the piston velocity is greater than 1 cm hr^{-1} , exchange will be limited by production of CO_2 (reaction control), rather than transport across the air-water interface (**Fig 2.6**). For the remainder of the simulations, the piston velocity was fixed at 1 cm hr^{-1} , the lowest of values found by various researchers across the water-air interface in estuarine and riverine systems, as summarised by Raymond et al. (2000).

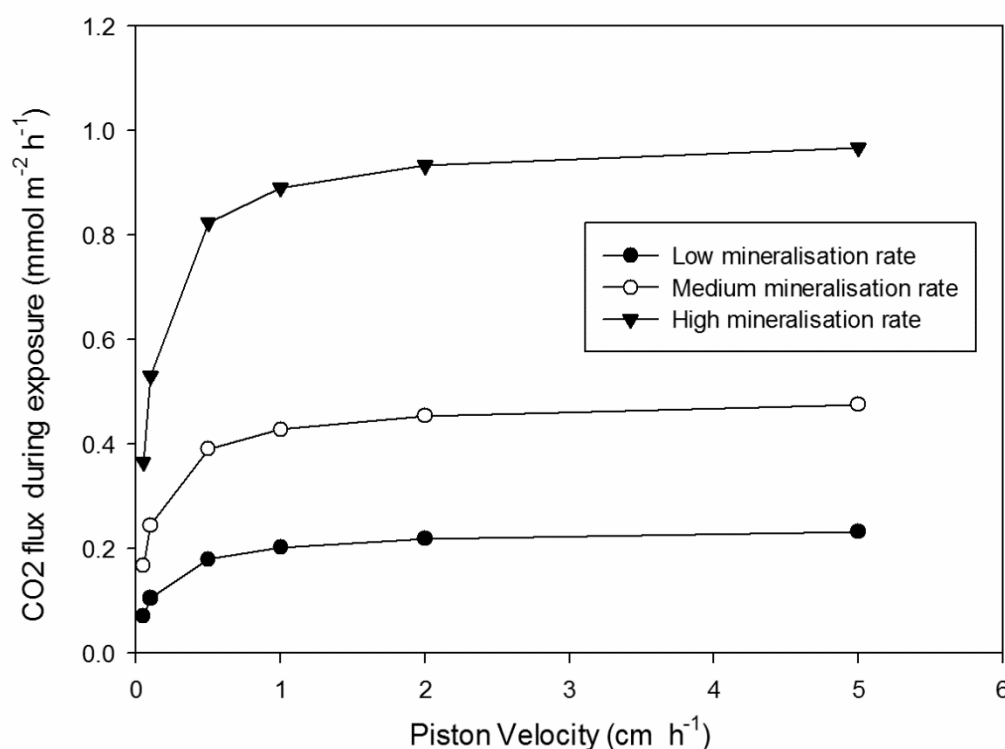


Figure 2.6: Exposed flux of CO_2 with varying piston velocity and respiration rate. Low, medium and high mineralisation rates refer to peak DIC productions of approx. 600, 1300 and $2600 \mu\text{mol m}^{-2} \text{h}^{-1}$ respectively

2.6.3 Agreement of simulations with experimental data

There was a general agreement between experimental flux data and the model simulations. Both model and experimental data showed that DIC fluxes from the sediment during tidal inundation are higher than CO₂ fluxes during exposure. This difference was most pronounced at the start of the experiment and after the addition of organic matter. At the start of the experiments there was a rapid alkalinity generation which can be explained by the formation of FeS as the Fe(III) initially present within the surface sediment was reduced. After the pulse of organic matter, the oxygen penetration in the sediment is reduced, and a higher rate of anaerobic carbon mineralisation takes place. This leads then to increased rates of reduced sulfur production, FeS burial and net alkalinity production. The reduction of Fe in the surface of the sediment leads to a transient alkalinity flux and associated increase in the discrepancy between gaseous CO₂ flux and DIC flux (**Fig. 2.5**). This observation is seen in both the model and the laboratory incubations, although there is a slight offset due to the fact that there is a delay in the maximum respiration rate in the laboratory incubations compared to the model.

In our simulations, reduced sulfur production continues after FeOOH is exhausted, but it is reoxidised as free sulfide diffuses upwards into the oxygenated surface layers of sediment. Nonetheless, a relatively small alkalinity flux still leaves the sediment, as there is some build up of H₂S in the sediment pore waters (The diffusion of sulfide into the oxic layer, and its subsequent oxidation is slower than its production within the deeper layers of the sediment).

The dynamics of this simulation/experiment have strong environmental relevance being representative of a resuspension event or the deposition of fresh sediment from the catchment and the deposition of organic matter. This highlights the importance of environmental dynamics in controlling the relative loss of CO₂ and DIC from intertidal

sediment. Indeed, in coastal sediments, periodically high fluxes of alkalinity are observed following periods of high organic matter input (Ferguson et al. 2003a). Hargrave and Phillips (1981) describe the significance of short term organic matter deposition, with high supply rates, relative to mineralisation rates, causing a burial of organic matter in deeper, anoxic layers of the sediment.

2.6.4 Model sensitivity towards sedimentary iron

The sensitivity of the model (**Fig. 2.7**) to solid-phase iron (Fe) suggests that the delivery of fresh (oxidised) Fe controls how much mineralised carbon is exported to the atmosphere (as CO₂) versus the ocean (as alkalinity). In the simulation, a large input of Fe leads to a higher rate of alkalinity production through FeS₂ burial (FeOOH consumption), and a corresponding lower CO₂ efflux during exposure (**Fig. 2.4**). The sensitivity of the model to Fe agrees with the literature (Berner et al. 1970; Hu and Cai 2011a), which suggests that FeS₂ burial is the most important process controlling alkalinity production. The present work shows that in high carbon systems such as intertidal sediments, Fe will be the limiting species in pyrite burial, despite the role of carbon as the mediating species in pyrite burial globally (Hu and Cai 2011a).

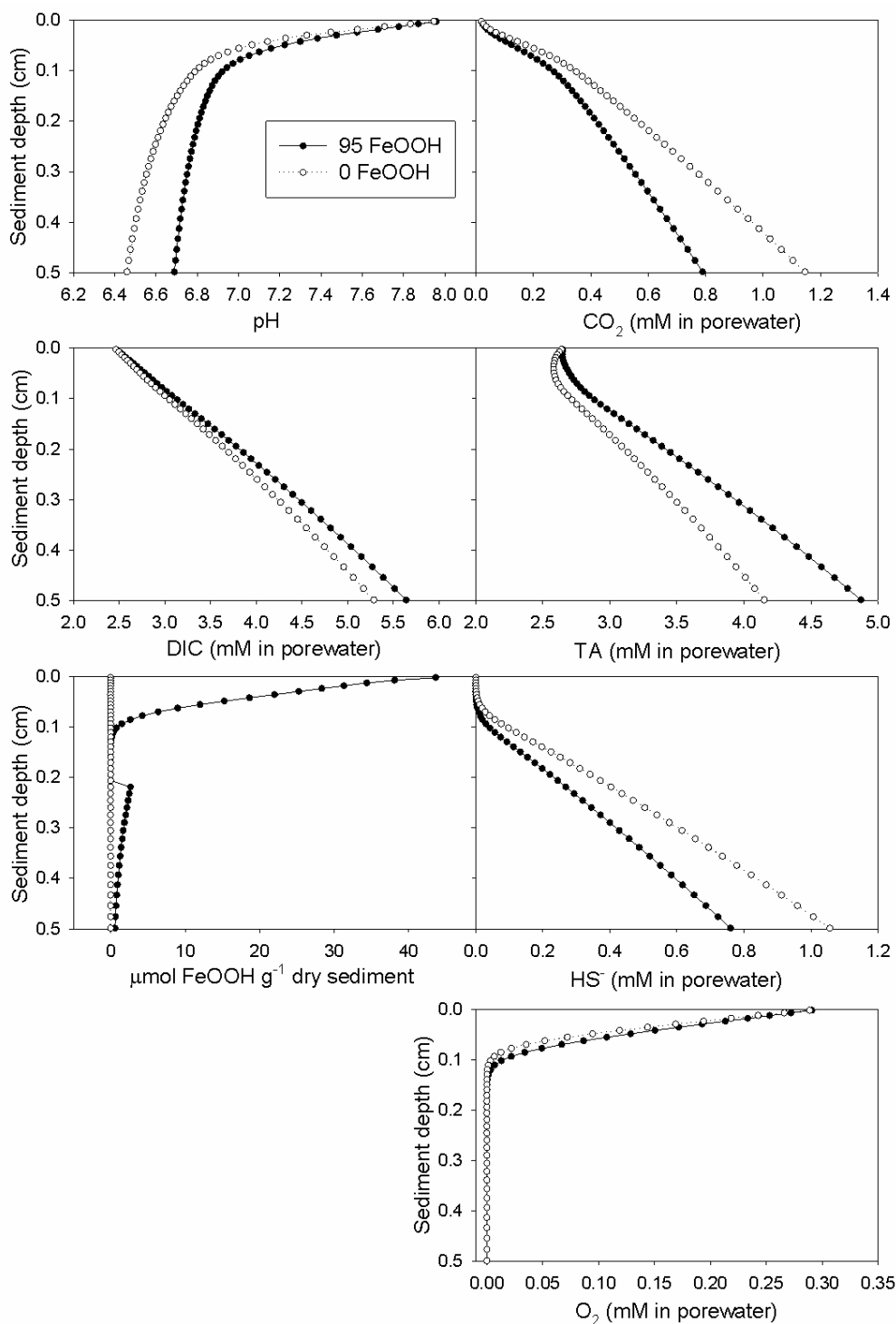


Figure 2.7: Profiles of pH, CO₂, DIC, TA, FeOOH and HS⁻ and O₂ from two simulations.

Empty circles represent a simulation with no FeOOH, whereas filled circles represent 95 $\mu\text{mol g}^{-1}$ sediment (d/w) FeOOH.

The temporal change of TA fluxes also differs considerably. TA flux stabilises after 30 days in the simulations with the lower Fe concentrations, whereas at higher Fe concentrations, TA flux continues to increase. This is due to the reduction of all the oxidised Fe, creating a higher net production of alkalinity. For simulations with little or no Fe, there is a higher temporary sink of HS^- in the sediment pore waters during intense alkalinity production (**Fig. 2.7**) as insoluble iron sulfides cannot form. Subsequent alkalinity consumption occurs as the HS^- is re-oxidised. The effect of the reoxidation of reduced sulfur can be seen in **Figure 2.7**, which shows the simulation with no FeOOH having lower pH, and thus higher CO_2 concentration, than the simulation with $95 \mu\text{mol Fe g}^{-1}$ dry sediment. The alkalinity concentration (as indicated by HCO_3^- and CO_3^{2-}) throughout the FeOOH containing profile is also considerably higher. During periods where respiration is extremely high, HS^- has the potential to by-pass the small oxic zone in the sediment, and so the HS^- can reach the water column before it is re-oxidised. In this situation, the numeric simulation will show a net alkalinity flux from the sediment. In reality, immediate re-oxidation of HS^- in the overlying water column will directly consume this alkalinity.

With regard to carbon budgets, the effect of anaerobic carbon metabolism is important as higher alkalinity export to the ocean creates a higher CO_2 buffering capacity for the uptake of atmospheric CO_2 . The effect of anaerobic alkalinity production on atmospheric carbon uptake in coastal seas has been estimated at up to 60% of the total uptake (Thomas et al. 2009). This is an upper estimate, as it neglects alkalinity consumed during nitrification (Hu and Cai 2011a). In regions with high anthropogenic disturbance, large amounts of terrestrial carbon is exported towards coastal oceans (Frankignoulle et al. 1996; Frankignoulle et al. 1998; Abril et al. 2002). Increased organic carbon loading in estuaries due to anthropogenic land use represents an anthropogenic carbon source to the

atmosphere upon its breakdown. More anthropogenically disturbed catchments will also export more sediment and hence more Fe(III) (Walling 1999; Asselman et al. 2003) to estuaries, which may partially offset larger CO₂ emissions from increased labile organic carbon export to estuaries. The significance of this offset remains to be investigated.

2.7 Conclusions

The laboratory data and field data (Cook et al. 2004) and computer simulations clearly show that gaseous CO₂ fluxes during exposure on tidal flats are likely to underestimate total carbon mineralisation. This finding has clear implications for research in this field, given that total inorganic carbon fluxes for intertidal sediments have generally been estimated using only gaseous CO₂ fluxes on the exposed sediments (Middelburg et al. 1996; Migné et al. 2005). The results of this study demonstrate the importance of considering both exposed and inundated fluxes in studies of intertidal metabolism, which may be quite different, depending on the extent to which there is a net accumulation of reduced solutes.

2.8 Acknowledgements

P. Faber acknowledges the assistance of an Australian Postgraduate Association scholarship. This work was supported by a Monash University faculty of science early career researcher grant, as well as Monash researcher accelerator grant to PC. We thank Hans Røy for stimulating discussions on this work.

2.9 References

- Abril, G., Nogueira, M., Etcheber, H., Cabecadas, G., Lemaire, E., and Brogueira, M.: Behaviour of organic carbon in nine contrasting european estuaries, *Estuarine, Coastal and Shelf Science*, 54, 241-262, 2002.
- Almgren, T., Dyrssen, D., and Fonselius, S.: Determination of alkalinity and total carbonate., in: *Methods of seawater analysis*, edited by: Grasshoff, K., Ehrhardt, M., and Kremling, K., Springer-Verlag, Chemie, Weinheim, 99-123, 1983.
- Alongi, D., Tirendi, F., Dixon, P., Trott, L., and Brunskill, G.: Mineralization of organic matter in intertidal sediments of a tropical semi-enclosed delta, *Estuarine, Coastal and Shelf Science*, 48, 451-467, 1999.
- Asselman, N. E. M., Middelkoop, H., and Van Dijk, P. M.: The impact of changes in climate and land use on soil erosion, transport and deposition of suspended sediment in the river rhine, *Hydrological Processes*, 17, 3225-3244, 2003.
- Berner, R. A., Scott, M. R., and Thomlinson, C.: Carbonate alkalinity in the pore waters of anoxic marine sediments, *Limnology and Oceanography*, 544-549, 1970.
- Boudreau, B. P.: The diffusive tortuosity of fine-grained unlithified sediments, *Geochimica et Cosmochimica Acta*, 60, 3139-3142, 1996.
- Boudreau, B. P.: *Diagenetic models and their implementation: Modelling transport and reactions in aquatic sediments*, Springer, Berlin and New York, 1997.
- Brotas, V., Amorim-Ferreira, A., Vale, C., and Catarino, F.: Oxygen profiles in intertidal sediments of ria formosa (s. Portugal), *Hydrobiologia*, 207, 123-130, 1990.

- Cai, W., Pomeroy, L., Moran, M., and Wang, Y.: Oxygen and carbon dioxide mass balance for the estuarine-intertidal marsh complex of five rivers in the southeastern us, *Limnology and Oceanography*, 44, 639-649, 1999.
- Cai, W. J., Luther, G. W., Cornwell, J. C., and Giblin, A. E.: Carbon cycling and the coupling between proton and electron transfer reactions in aquatic sediments in lake champlain, *Aquatic Geochemistry*, 16, 421-446, 2010.
- Cook, P., Butler, E., and Eyre, B.: Carbon and nitrogen cycling on intertidal mudflats of a temperate australian estuary i. Benthic metabolism, *Marine Ecology Progress Series*, 280, 25-38, 2004.
- Ferguson, A., Eyre, B., and Gay, J.: Organic matter and benthic metabolism in euphotic sediments along shallow sub-tropical estuaries, northern new south wales, australia, *Aquatic Microbial Ecology*, 33, 137-154, 2003a.
- Ferguson, A. J. P., Eyre, B. D., and Gay, J. M.: Organic matter and benthic metabolism in euphotic sediments along shallow sub-tropical estuaries, northern new south wales, australia, *Aquat. Microb. Ecol.*, 33, 137-154, 2003b.
- Follows, M. J., Ito, T., and Dutkiewicz, S.: On the solution of the carbonate chemistry system in ocean biogeochemistry models, *Ocean Modelling*, 12, 290-301, 2006.
- Frankignoulle, M., Bourge, I., and Wollast, R.: Atmospheric co₂ fluxes in a highly polluted estuary (the scheldt), *Limnology and Oceanography*, 41, 365-369, 1996.
- Frankignoulle, M., Abril, G., Borges, A., Bourge, I., Canon, C., Delille, B., Libert, E., and Théate, J.: Carbon dioxide emission from european estuaries, *Science*, 282, 434, 1998.

- Gribsholt, B., and Kristensen, E.: Benthic metabolism and sulfur cycling along an inundation gradient in a tidal *spartina anglica* salt marsh, *Limnology and Oceanography*, 48, 2151-2162, 2003.
- Hammond, D., Giordani, P., Berelson, W., and Poletti, R.: Diagenesis of carbon and nutrients and benthic exchange in sediments of the northern adriatic sea, *Marine Chemistry*, 66, 53-79, 1999.
- Hargrave, B., and Phillips, G.: Annual in situ carbon dioxide and oxygen flux across a subtidal marine sediment, *Estuarine, Coastal and Shelf Science*, 12, 725-737, 1981.
- Hofmann, A., Meysman, F., Soetaert, K., and Middelburg, J.: A step-by-step procedure for ph model construction in aquatic systems, *Biogeosciences*, 5, 227-251, 2008.
- Hofmann, A. F., Soetaert, K., Middelburg, J. J., and Meysman, F. J. R.: Aquaenv: An aquatic acid–base modelling environment in r, *Aquatic Geochemistry*, 16, 507-546, 2010.
- Hu, X., and Cai, W. J.: An assessment of ocean margin anaerobic processes on oceanic alkalinity budget, *Global Biogeochemical Cycles*, 25, 1-11, 2011.
- Joye, S. B., de Beer, D., Cook, P. L. M., and Perillo, G.: Biogeochemical dynamics of coastal tidal flats, *Coastal wetlands: an integrated ecosystem approach*, 345, 2009.
- Kristensen, E.: Benthic fauna and biogeochemical processes in marine sediments: Microbial activities and fluxes, in: *Nitrogen cycling in coastal marine environments*, edited by: Blackburn, T. H., and Sorensen, J., John Wiley and Sons, Chichester, 275-299, 1988.

- Lord, C. J.: A selective and precise method for pyrite determination in sedimentary materials, *Journal of Sedimentary Research*, 52, 664, 1982.
- Meysman, F. J. R., Middelburg, J. J., Herman, P. M. J., and Heip, C. H. R.: Reactive transport in surface sediments. II. Media: An object-oriented problem-solving environment for early diagenesis, *Computers & geosciences*, 29, 301-318, 2003.
- Middelburg, J., Klaver, G., Nieuwenhuize, J., Wielemaker, A., De Haas, W., Vlug, T., and Van der Nat, J.: Organic matter mineralization in intertidal sediments along an estuarine gradient, *Marine Ecology Progress Series*. Oldendorf, 132, 157-168, 1996.
- Migné, A., Davoult, D., Bourrand, J. J., and Boucher, G.: Benthic primary production, respiration and remineralisation: In situ measurements in the soft-bottom abra alba community of the western english channel (north brittany), *Journal of Sea Research*, 53, 223-229, 2005.
- Raymond, P., Bauer, J., and Cole, J.: Atmospheric CO₂ evasion, dissolved inorganic carbon production, and net heterotrophy in the York river estuary, *Limnology and Oceanography*, 45, 1707-1717, 2000.
- Roy, R., Roy, L., Vogel, K., Porter-Moore, C., Pearson, T., Good, C., Millero, F., and Campbell, D.: The dissociation constants of carbonic acid in seawater at salinities 5 to 45 and temperatures 0 to 45 °C, *Marine Chemistry*, 44, 249-267, 1993.
- Satienperakul, S., Cardwell, T. J., Cattrall, R. W., McKelvie, I. D., Taylor, D. M., and Kolev, S. D.: Determination of carbon dioxide in gaseous samples by gas diffusion-flow injection, *Talanta*, 62, 631-636, 2004.

- Soetaert, K., and Meysman, F.: Reactive transport in aquatic ecosystems: Rapid model prototyping in the open source software r, *Environ. Model. Softw.*, 32, 49-60, 2012.
- Soetaert, K., Petzoldt, T., Meysman, F.J.R.: Marelac: Tools for aquatic sciences. R package version 2.1.1., 2010.
- Thomas, H., Schiettecatte, L., Suykens, K., Koné, Y., Shadwick, E., Prowe, F., Bozec, Y., de Baar, H. J. W., and Borges, A.: Enhanced ocean carbon storage from anaerobic alkalinity generation in coastal sediments, *Biogeosciences*, 6, 267-274, 2009.
- Walling, D.: Linking land use, erosion and sediment yields in river basins, *Hydrobiologia*, 410, 223-240, 1999.
- Westrich, J. T., and Berner, R. A.: The role of sedimentary organic matter in bacterial sulfate reduction: The g model tested, *Limnology and Oceanography*, 29, 236-249, 1984.

3. Porewater exchange driven by tidal pumping causes alkalinity export in two intertidal inlets

Authors: Peter A. Faber¹, Victor Evrard¹, Ryan J. Woodland¹, Ian C. Cartwright², Perran L.M. Cook¹

¹ Water Studies Centre, School of Chemistry, Monash University, Victoria 3800, Australia

² School of Geosciences, Monash University, Victoria 3800, Australia

3.1 Declaration for Thesis Chapter Three

Declaration by candidate

In the case of Chapter [insert chapter number], the nature and extent of my contribution to the work was the following:

Nature of contribution	Extent of contribution (%)
Field work, laboratory analysis, data analysis and primary author	82.5

The following co-authors contributed to the work. If co-authors are students at Monash University, the extent of their contribution in percentage terms must be stated:

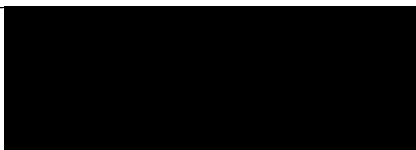
Name	Nature of contribution	Extent of contribution (%) for student co-authors only
Perran Cook	Field work, assistance with study design, guidance and manuscript editing.	10
Ryan Woodland	Field work and manuscript editing.	2.5
Victor Evrard	Field work and manuscript editing.	2.5
Ian Cartwright	Assistance with ^{222}Rn analysis and manuscript editing.	2.5

The undersigned hereby certify that the above declaration correctly reflects the nature and extent of the candidate's and co-authors' contributions to this work*.

Candidate's
Signature

	Date
--	------

Main
Supervisor's
Signature

	Date 18/04/14
---	------------------

We acknowledge Vera Eate, Keralee Browne, Michael Bourke and Todd Scicluna for their assistance in the field and laboratory and Matt Edmunds at Australian Marine Ecology for skippering the R/V *Orca II*. This work was supported by Melbourne Water and the Australian Research Council (DP1096457).

3.2 Abstract

Carbon and alkalinity export from two adjacent intertidal inlets with different terrestrial inputs were investigated. One inlet receives a small creek from an agriculturally dominated catchment, leading to the input of terrestrially sourced material; whereas, the other is relatively isolated from terrestrial inputs. Using time series measurements, we calculated the total advective exchange of dissolved organic carbon (DOC) ($0\text{--}25\text{ mmol m}^{-2}\text{ d}^{-1}$), dissolved inorganic carbon (DIC) ($130\text{--}450\text{ mmol m}^{-2}\text{ d}^{-1}$), total alkalinity (TA) ($46\text{--}310\text{ mmol m}^{-2}\text{ d}^{-1}$) and the nutrients nitrate ($1.0\text{--}1.1\text{ mmol m}^{-2}\text{ d}^{-1}$), ammonia ($0.0043\text{--}0.10\text{ mmol m}^{-2}\text{ d}^{-1}$), and phosphorus ($0.016\text{--}0.25\text{ mmol m}^{-2}\text{ d}^{-1}$). ^{222}Rn data indicated that porewater exchange played an important part in controlling carbon export from the sediment as an advective flux. The residence time of porewater within both inlets was $\sim 6.6\text{--}7.4\text{ h}$, indicating that porewater exchange is driven by tidal pumping. The inlet with the greater amount of terrestrial inputs exported much more TA (310 vs. $46\text{ mmol m}^{-2}\text{ d}^{-1}$), suggesting that the extent of land-to-sea connectivity influences how carbon is exported. We hypothesize this is due to the increased input of iron from terrestrial sources, which fosters net TA production through the burial of reduced sulfur species as iron sulfides. However, a simple mass balance showed the TA fluxes observed over 24 h were higher than could be sustained continuously with iron input from the catchment ($0.49\text{ mmol Fe m}^{-2}\text{ d}^{-1}$), meaning that the observed TA fluxes could not be sustained on long times scales. It is most likely that there are periods of net sulfur reduction and net oxidation in response to wave action and calm conditions, highlighting the importance of long term monitoring over different seasons and weather patterns to obtain representative budgets.

3.3 Introduction

The export of inorganic carbon from coastal ocean and estuarine systems attracts considerable interest as these systems have been recognised as significant components of the global carbon cycle and important areas of organic matter mineralisation (Smith and Hollibaugh 1993). Coastal mudflats are typically highly reactive, being areas of allochthonous organic matter deposition as well as having high in-situ rates of primary production by mangroves, microphytobenthos and seagrass (Joye et al. 2009). Following mineralisation of organic material, dissolved inorganic carbon (DIC) can be exported as either CO_2 , or carbonate alkalinity (A_c ; $A_c = [\text{HCO}_3^-] + 2[\text{CO}_3^{2-}]$). These two products have different fates as CO_2 is able to evade into the atmosphere, whereas A_c remains dissolved and is exported to the ocean. When A_c is produced it acts as a buffer allowing the uptake of more CO_2 from the atmosphere or from other respiration processes. The export of total alkalinity (TA), of which A_c is the major component, has been shown to dominate carbon export in coastal mudflat systems (Thomas et al. 2009) and the fate of mineralised organic carbon is therefore relevant to global carbon budgets. The production of A_c may be closely linked to the burial of reduced sulfur (S) species because sulfate can act as an electron acceptor in the absence of oxygen. Burial of reduced S as iron sulfides such as iron monosulfide (FeS) and pyrite (FeS_2) prevents its reoxidation and allows a net production of A_c . As a consequence, the availability of iron (Fe) acts as a driver of A_c export (Faber et al. 2012). Typically, the supply of fresh Fe is derived from terrestrial sources and is transported as suspended particles in rivers and streams. Because of this, the strength of the link between land and coastal marine systems is expected to influence the extent of alkalinity export from near-shore coastal waters to the ocean.

Another source of exported A_c and DIC is carbonate dissolution in the sediment porewater (Berelson et al. 1998; Brasse et al. 1999), which may occur as a result of acid

production from sulfide reoxidation or aerobic respiration (Walter and Burton 1990; Walter et al. 1993). In sediments with low Fe content such as those with low amounts of terrestrial inputs, hydrogen sulfide (H_2S) oxidation within the sediment may be a major source of acid, which contributes to carbonate dissolution (Aller 1982; Walter and Burton 1990; Walter et al. 1993). The potential influence of Fe inputs on carbonate dissolution suggest that this should be considered when comparing sediments with and without terrestrial inputs.

Metabolism has been extensively measured on tidal flats (e.g. Migné et al. 2002; Cook et al. 2004; Spilmont et al. 2006), mainly through the use of in situ benthic chambers. Although these techniques are useful in determining diffusive fluxes of solutes and gases from cohesive sediments, they neglect the effect of processes such as porewater exchange and do not account for whole system fluxes driven by advective flow. Several recent studies (e.g. Bouillon et al. 2007; Koné and Borges 2008; Miyajima et al. 2009) have considered porewater exchange in their studies of mangrove systems and found that this is a significant driver of dissolved organic carbon (DOC) and DIC export. Bouillon et al. (2008a) suggest that DIC export from mangrove systems may be much more important than previously understood. Maher et al. (2013) also found this to be the case, with DIC export from a mangrove tidal creek being an order of magnitude greater than DOC export.

For measuring the extent of porewater exchange, ^{222}Rn can be used as a conservative tracer because it is chemically unreactive (noble gas) and is produced in easily measurable amounts within sediments as part of the ^{238}U to ^{206}Pb decay chain. The high concentration of the parent isotope ^{226}Ra in minerals means that porewater ^{222}Rn activities can be much higher than in surface water. This provides a way to differentiate surface water from porewater even if they have similar concentrations of other substances. For instance, the contribution of porewater to the draining water of an intertidal inlet can

be estimated using channel ^{222}Rn measurements by comparing them with a measurement of a porewater ^{222}Rn endmember (Burnett and Dulaiova 2003). Because ^{222}Rn has a known half-life (3.8 d) and it reaches secular equilibrium with ^{226}Ra contained in minerals within sediments, emanation experiments allow the porewater endmember to be easily constrained. The residence time of porewater can also be estimated (Hoehn and Von Gunten 1989) and can allow determination of the mechanism of porewater exchange, which in intertidal zones is expected to be linked to the tidal cycle. This information may help to provide an understanding into the dynamics of organic and inorganic carbon in intertidal mudflats.

In addition, depending on their CO_2 fixation mechanism during photosynthesis, primary producers differ in their carbon isotope (i.e., $\delta^{13}\text{C}$) composition (O'leary 1981). Sources of organic carbon in these systems may include autochthonous organic matter such as seagrass, mangrove detritus and benthic microalgae, as well as terrestrially-sourced allochthonous material. It is expected that the $\delta^{13}\text{C}$ of exported DIC will differ depending on the local sources of organic matter being degraded. Values of $\delta^{13}\text{C}$ have been successfully used to determine the sources of DIC exported to the sea in mangrove dominated systems (Bouillon et al. 2008b; Miyajima et al. 2009; Maher et al. 2013). Carbonate dissolution will also influence the $\delta^{13}\text{C}$ of DIC as carbonates have relatively high $\delta^{13}\text{C}$ values, which aids in determining the relative importance of this process in driving alkalinity export.

In this study, we undertook a carbon budget to assess and compare the export of DIC, TA and CO_2 into the coastal ocean and atmosphere at two different sites with contrasting terrestrial influences and determined the drivers behind alkalinity export. This study is relevant to our understanding of cohesive sediment habitats, particularly regarding the likely changes in the delivery of nutrients that will occur as riverine inputs

change with increasing anthropogenic demand and altered precipitation regimes. This work also has relevance to studies of mangrove systems, of which few include consider advective DIC fluxes in their budgets (Maher et al. 2013).

3.4 Methods

3.4.1 Field sites

The two field sites are in the northern part of Western Port (WP), a large macrotidal embayment in southeast Australia (**Figure 3.1**). The area contains extensive seagrass (primarily *Zostera muelleri*) beds and intertidal mudflats fringed by mangrove forest (primarily *Avicennia marina*), as well as deeper subtidal channels. The major difference between these two sites is that Watson Inlet (WI: -38.2361°, 145.2610°) receives freshwater input (~3100 ML yr⁻¹) from Watson Creek (WC) . The course of WC is through a region of intensive agriculture and therefore delivers significant amounts of anthropogenic nutrients to WI. During the summer sampling period which this study focuses on, there were no freshwater inputs from WC due to low rainfall. In contrast, Chinaman Inlet (CI: -38.241197, 145.316677) does not receive any freshwater inputs and influences from terrestrial catchments on this site are negligible. Estimates of the areas of each inlet and the different habitats are presented in **Table 1**. Both sites had similar coverage of seagrass (26% and 23% for WI and CI, respectively), mangrove (43% and 53% for WI and CI, respectively) and bare sediment (24% and 21% for WI and CI, respectively). These two sites were chosen to provide a comparison between the carbon dynamics of geographically similar coastal regions.

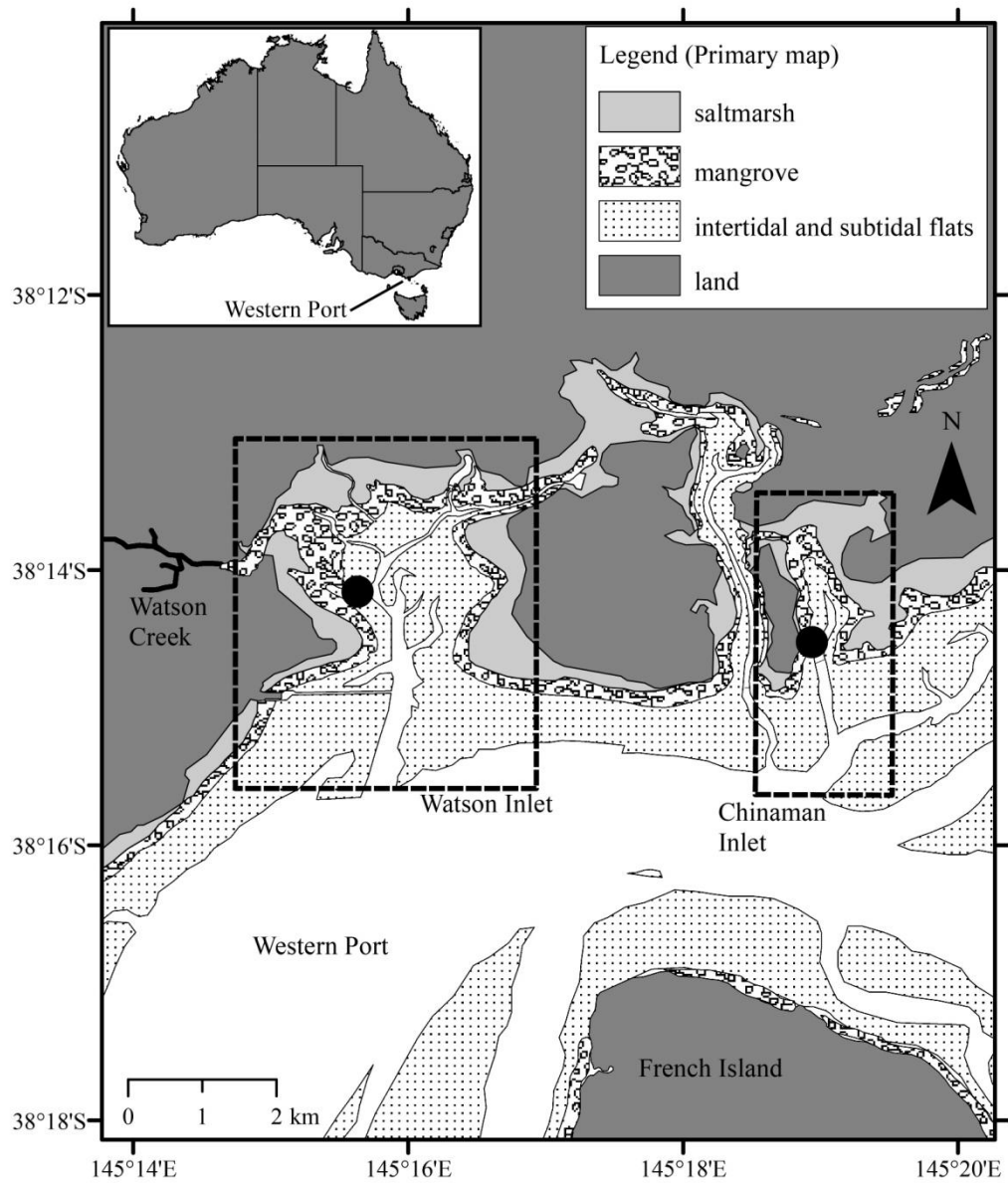


Figure 3.1: (A) Map of Australia, adapted from (Evrard et al. 2013) with approximate location of Western Port. (B) Map of Watson Inlet (WI), Watson Creek (WC), and Chinaman Inlet (CI) in the north-eastern corner of Western Port (WP). The dots represent approximate locations for the time series sampling.

Table 3.1: Coverage of different habitat at Watson Inlet (WI) and Chinaman Inlet (CI) as areas and percentage of total areas.

Habitat	WI area (m ²)	WI (% of total)	CI area (m ²)	CI (% of total)
Seagrass	1.07 x10 ⁶	26.4	2.60 x10 ⁵	23.2
Mangrove	1.77 x10 ⁶	43.4	5.89 x10 ⁵	52.6
Bare	9.84 x10 ⁵	24.1	2.39 x10 ⁵	21.4
Channel	2.50 x10 ⁵	6.1	3.13 x10 ⁴	2.8
Total	4.08 x10 ⁶	100	1.12 x10 ⁶	100

3.4.2 In situ monitoring of water parameters and sampling

Both sites were sampled during 24 hour time-series in spring (22-24 November 2011) and summer (21-23 February 2012). This sampling regime allowed us to observe a range of conditions elicited by tidal and diurnal effects. For the purpose of this study, we focused on the summer sampling period and used the spring period as a temporal comparison for TA fluxes.

Sampling at each site was performed on-board the R/V *Orca II*, anchored mid-channel close to the inlet entrance. At each site, an acoustic Doppler current profiler (ADCP; Argonaut-XR, Sontek Yellow Springs Instruments) was deployed at the bottom of the tidal channel and recorded water current velocities and water height at 1 Hz. A bathymetry survey of the cross section of the channel where the ADCP was deployed was conducted to calculate the volume of water exchange between the inlets and the bay. Observations from the ADCP were averaged hourly to match the frequency of the other time series data that were collected. A Hydrolab® sonde DS5X multiprobe was used to log temperature, dissolved oxygen (DO), pH, turbidity, salinity and chlorophyll-a in the surface water hourly during the monitoring periods. These hourly measurements

corresponded with sampling times for TA, $\delta^{13}\text{C}_{\text{DIC}}$, nutrients and calculated flow and tide height data. Hourly samples of ambient water were also taken for total nitrogen (TN) and total phosphorus (TP) and stored in a cooler on ice until return to the laboratory where they were stored at 4°C before analysis. Samples for nitrogen oxides (NO_x), ammonium (NH_4^+), total dissolved nitrogen (TDN), total dissolved phosphorus (TDP) and filterable reactive phosphorus (FRP) were collected by filtering water through a 0.45 μm Bonnet® filter and storing the filtrate in a cooler as above, and frozen upon return to the laboratory. Samples for TA were similarly filtered and refrigerated in a cooler but were not allowed to freeze before analysis. For dissolved organic carbon (DOC) samples, 100 mL of water was filtered through precombusted Whatman GF/F filters into precombusted brown-glass vials and preserved with 2 drops of concentrated HCl. Particulate organic carbon (POC) was sampled by passing water through precombusted Whatman GF/F filters and storing the filter along with retained material at $\sim -20^\circ\text{C}$ in aluminum foil until analysis. Water samples for $\delta^{13}\text{C}_{\text{DIC}}$ analysis were collected in 12 mL Exetainer vials (Labco®) and preserved with 20 μL of 6% w:w HgCl_2 solution. Care was taken to limit atmospheric exchange of CO_2 during sampling by using a ~ 10 cm piece of tubing attached to a syringe to overfill the vial and avoid the formation of bubbles.

3.4.3 Nutrient Analysis

Nutrient samples (NO_x , NO_2^- , NH_4^+ , TN, TP, and FRP) were analysed via flow injection analysis (FIA) (Lachat Quick-Chem 8500 Flow Injection Analyser, with a spectrophotometric detector). DOC and POC were analysed using a total organic carbon (TOC) analyser (Shimadzu TOC-VSCH). Standards, spikes and reference materials were within acceptable limits and analysed following the procedures in Standard Methods for Water and Wastewater (2005).

3.4.4 Estimation of carbonate dissolution

Samples of draining porewater and channel water were collected for the analysis of Ca^{2+} and Na^{+} and refrigerated until analysis. These were analysed by ion chromatography using a Dionex 2100 equipped with a cation exchange column (CS12A), and the $\text{Ca}^{2+}:\text{Na}^{+}$ ratio was determined with high precision (relative standard deviation (RSD) = 0.2%). The $\text{Ca}^{2+}:\text{Na}^{+}$ in porewater was compared to the background ratio in WP and the contribution of carbonate dissolution to both TA and DIC was calculated based on the fact that for 1 mol of CaCO_3 dissolved, 2 mol of alkalinity and 1 mol of DIC are produced.

3.4.5 TA measurement and calculation of DIC and Pco_2

TA was measured using a modified Gran titration (Almgren et al. 1983) and a NBS buffer calibrated pH electrode attached to a portable Hach® HQ40d meter. The RSD was <1%. TA and pH were used to calculate Pco_2 and DIC (Zeebe and Wolf-Gladrow 2001; Borges et al. 2004a). Frankignoulle and Borges (2001) found that this method of calculating Pco_2 is suitable for estuarine waters and gave accurate results relative to direct measurements. The concentrations of DIC and Pco_2 were calculated using the R-package Aquaenv (Hofmann et al. 2010). Aquaenv accounts for the effects of salinity and temperature on the equilibrium constants (K_1 , K_2) and Henry's constant (K_H), using the relationships of Millero (1995). We accounted for evaporation in our flux calculations by adjusting TA and DIC to the minimum salinity measured during the time series at each site, which was assumed to be the background concentration in WP. This allowed us to determine fluxes for whole system exports of TA and DIC without incurring significant errors associated with evaporation.

3.4.6 $\delta^{13}\text{C}$ of dissolved inorganic carbon

A 4 mL He headspace was placed in the preserved 12 mL water samples to which a 0.1 mL of H_3PO_4 (1 mol L^{-1}) was added to liberate DIC as CO_2 . Before analysis, vials were shaken vigorously for ~5 min and allowed to stand for several hours to ensure equilibrium of CO_2 with the headspace. DIC present in the headspace was analysed on an ANCA GSL2 elemental analyser interfaced to a Hydra 20-22 continuous-flow isotope ratio mass-spectrometer (Sercon). Analytical precision was $\pm 0.1\text{‰}$ for ^{13}C and stable isotope data are expressed in the delta notation ($\delta^{13}\text{C}$) relative to the stable isotopic ratio of the Vienna Pee Dee Belemnite standard ($R_{\text{VPDB}} = 0.0111797$).

3.4.7 CO_2 flux calculations

CO_2 flux from both systems was estimated using P_{CO_2} , wind speed, and current (Borges et al. 2004a). Wind speed data was acquired from the Australian Government Bureau of Meteorology and was measured at Her Majesty's Australian Ship Cerberus weather station (-38.3670° , 145.1870°), approximately 20 km southwest of the sampling sites. Current and depth data was obtained using the ADCP. CO_2 flux (F) was calculated using **Eq. 3.1**.

$$F = k([\text{CO}_2]_{\text{water}} - [\text{CO}_2]_{\text{air}}) \quad (3.1)$$

where k is the gas transfer velocity, $[\text{CO}_2]_{\text{water}}$ is the concentration of measured CO_2 in water and $[\text{CO}_2]_{\text{air}}$ is the concentration of CO_2 in water at equilibrium with the atmosphere. These terms are calculated using **Eq. 3.2**.

$$[\text{CO}_2] = K_{\text{H}} \times P_{\text{CO}_2} \quad (3.2)$$

where K_{H} is the Henry's constant for the in situ temperature and salinity of the sample.

We used the 2012 international average of $394 \mu\text{atm}$ for the partial pressure of CO_2 in air (www.co2now.org).

To calculate k from wind speed, current and depth, we used **Eq. 3.3**. (Borges et al. 2004a; Borges et al. 2004b):

$$k=1+1.719w^{0.5}h^{-0.5}+2.58u \quad (3.3)$$

where w is current in cm s^{-1} , h is depth in m and u is wind speed in m s^{-1} . We assumed in our calculation of k that wind attenuation from vegetation was negligible because the inlets are quite wide and the prevailing wind during the sampling period was onshore (southwest to southwesterly).

The k value was normalised to a Schmidt number of 660 (Sc_{CO_2} ; the Schmidt number of CO_2 at 20°C in seawater (Wanninkhof 1992)). As the Schmidt number is highly sensitive to temperature, we corrected k for temperature by calculating the Schmidt number using the equations in Wanninkhof (1992). The adjusted k (k_{CO_2}) was calculated using **Eq. 3.4**.

$$\frac{k_{660}}{k_{CO_2}} = \left(\frac{660}{Sc_{CO_2}} \right)^n \quad (3.4)$$

The value of n depends on the process that dominates diffusion. A value of -0.5 was chosen based on an estimate of best fit (Jähne et al. 1987) that has been used for similar analyses (Wanninkhof 1992; Raymond et al. 2000).

3.4.8 Seagrass export measurements

The tidal exchange of unattached seagrass wrack was monitored with a 1 x 0.5 m fixed-frame net (1 cm stretch mesh) attached to the bow of the research vessel at water level. The net was monitored continuously throughout the 23 h sampling cycle and the collected wrack was emptied when the net filled or showed evidence of an upstream pressure front, and prior to each transition between phases of the tidal cycle (e.g., rising to slack). The wrack samples were bagged separately and stored at -20°C . In the laboratory,

wrack samples were cleaned of small fish and invertebrates, dried to constant weight at 60°C, and then weighed to the nearest mg. Subsamples of seagrass wrack were analysed for % C content ($= 32.9 \pm 3.8$ standard deviation (SD) %) to allow conversion of bulk dry weight to seagrass carbon (SGC).

The relationship between SGC and current velocity was modeled using least-squares regression to fit a 2-parameter quadratic model. Mean current velocity was estimated as the average in-channel current velocity observed with the ADCP during each collection interval. These models were then used to calculate the directional flux of SGC for a 1 m x 0.5 m cell over the full 23 h sampling period at 1 min intervals. By assuming that the positively buoyant seagrass wrack was primarily limited to the upper 0.5 m of the water column and homogenously distributed within that zone, we were able to scale our estimates to total net SGC flux for each inlet by multiplying the flux values by the cross-sectional width of each channel (WI = 78.1 m; CI = 39 m).

3.4.9 Porewater input and residence time

Measurements of ^{222}Rn were made continuously during the time series using a RAD-7 radon-in-air monitor (DurrIDGE). Water from ~ 20 cm under the surface was continuously pumped from the channel via an on-board pump and allowed to equilibrate with air in an air-water gas exchanger (Burnett et al. 2001; Burnett and Dulaiova 2003).

Porewater and sediment sampling was conducted on 18–19 March 2013 for WI and CI, respectively, with sampling taking place during low tide. Draining porewater was collected from small channels on the mudflats of each inlet by excavating a ~20 cm hole in the sediment, into which a 200 mL glass bottle was placed so that it would collect the draining porewater (porewater draining across the surface only was collected). The bottle was capped with a glass stopper and transported to the lab to determine the ^{222}Rn activity

(A_t). Care was taken to avoid additional exposure to the atmosphere, which would cause loss of ^{222}Rn and an underestimation of residence time. To determine the ^{222}Rn activity for porewater at steady state (A_e), we collected sediment samples and kept them in 1 L Schott bottles with ~100 mL of seawater for ~3 wk. After this period, steady state is assumed, as well as equilibrium between the ^{222}Rn in the water column and the sediment. The water column was removed, and measured for ^{222}Rn . Activities of ^{222}Rn were determined using a portable radon-in-air monitor (RAD-7, DurrIDGE Company Incorporated) following methods described by Burnett and Dulaiova (2006) and are expressed in Bq m^{-3} . Measurement times were 2 h and relative precision is <10%. Calculation of ^{222}Rn activities were corrected for salinity and temperature as described by Schubert et al. (2012) because they affect the partitioning of the gas between dissolved and gaseous phases.

In order to estimate fluxes of porewater from the inlet, measurements during the time series were used in a simple ^{222}Rn mass balance, which was used to calculate total porewater export using porewater ^{222}Rn activities according to the mass balance **Eq. 3.5**.

$$F_{pw} = F_{ts}(\text{Rn}_{ts} + \text{Rn}_F) / \text{Rn}_{pw} \quad (3.5)$$

where F_{pw} and F_{ts} are the fluxes of porewater and water during the time series, respectively, in $\text{m}^3 \text{d}^{-1}$, Rn_{pw} and Rn_{ts} are activities of ^{222}Rn in the porewater and channel during the time series, respectively, and Rn_F is the loss in ^{222}Rn activity due to evasion to the atmosphere in the period between porewater drainage and sampling during the time series. The hourly F_{pw} values were integrated to obtain daily exports. We assumed that the radioactive decay of ^{222}Rn was negligible due to the short time (relative to its half-life, 3.8 d) between porewater drainage and its measurement. We calculated the flux of ^{222}Rn to the atmosphere by using ^{222}Rn measurements and k values in a way analogous to our CO_2 flux calculations. To estimate Rn_F we multiplied this calculated flux with the time

between porewater drainage and sampling, which was estimated using current in m s^{-1} obtained from the ADCP measurements, and the estimated average distance between drainage sites and the sampling location. This distance was estimated as half the length of the channel within each inlet, relative to the sampling site. This estimate assumes that porewater discharge is spatially uniform along the extent of the channel. We used porewater units of cm d^{-1} ($\text{cm}^3 \text{ cm}^{-2} \text{ d}^{-1}$) which was calculated using the whole areas of each of the inlets.

We estimated residence time of porewater with a ^{222}Rn dating method outlined by Hoehn and Von Gunten (1989), and Lamontagne and Cook (2007). The relationship between ^{222}Rn ingrowth and residence time is given by **Eq. 3.6**.

$$A_t = A_e (1 - e^{-\lambda t}) \quad (3.6)$$

where A_t is the activity of ^{222}Rn in the porewater, A_e is the activity of ^{222}Rn in water at equilibrium with its parent nuclide within the sediment, λ is the radioactive decay constant of ^{222}Rn (0.18 d^{-1}), and t is the residence time in days.

3.4.10 Core extractions and incubation

At both sites, triplicate intact sediment cores from mangrove, seagrass, bare sediment and channel habitats were taken during the February 2012 sampling campaign. Three replicate 20–25 cm sediment cores with 10–15 cm overlying water were taken using 30 cm x 6.6 cm inner diameter transparent polycarbonate core liners. The cores were then sealed using rubber stoppers and transported at a constant temperature back to the laboratory. The sealed cores were incubated at in situ temperature in either light or darkness and stirred continuously with a magnetic stirrer. The lights used were 25 x 50 W halogen down lights, at a height of ~50 cm, with a light intensity of ~400 $\mu\text{mol photons m}^{-2} \text{ s}^{-1}$ at the sediment surface. Samples for TA were taken from the cores every two hours

and pH was measured simultaneously to obtain a four point time series. Sampled water was replaced from a reservoir of water that was collected at the field site. The TA and the pH in the reservoir were also measured at each time point to allow corrections for changes in TA and DIC due to dilution of the core water column. The fluxes of TA and DIC were calculated for each core using least-squares linear regressions of the four time series points. The average flux of triplicate cores was taken for each condition and site. Measurements of pH were taken using a calibrated portable Hach® HQ40d meter.

3.5 Results

3.5.1 Time series

Results from hourly monitoring of mean flow, tide height, salinity, pH, DO, P_{CO_2} , TA, DIC $\delta^{13}C$, ^{222}Rn , and nutrients (**Fig. 3.2**) show that many of the measurements appeared to follow a tidal influence with higher values of salinity, pH, P_{CO_2} , DIC, TA, and ^{222}Rn during the outgoing tide. The ranges of TA, DIC, and P_{CO_2} measurements throughout the time series were greater at WI. Evaporation was significant at both sites with salinity maxima of 37.2 at WI and 36.2 at CI occurring during low tide (panel C, D). Background salinity for each site was assumed to be the lowest measured value, which occurred during high tide and was 35.9 and 35.6 for WI and CI, respectively. We assumed that during high tide the measured value of each parameter represented background WP values, as the incoming water in the channel was from WP and had not yet been in contact with the intertidal flats. At this time, salinity was at a minimum due to the small effect of evaporation in WP relative to the intertidal areas of the inlets.

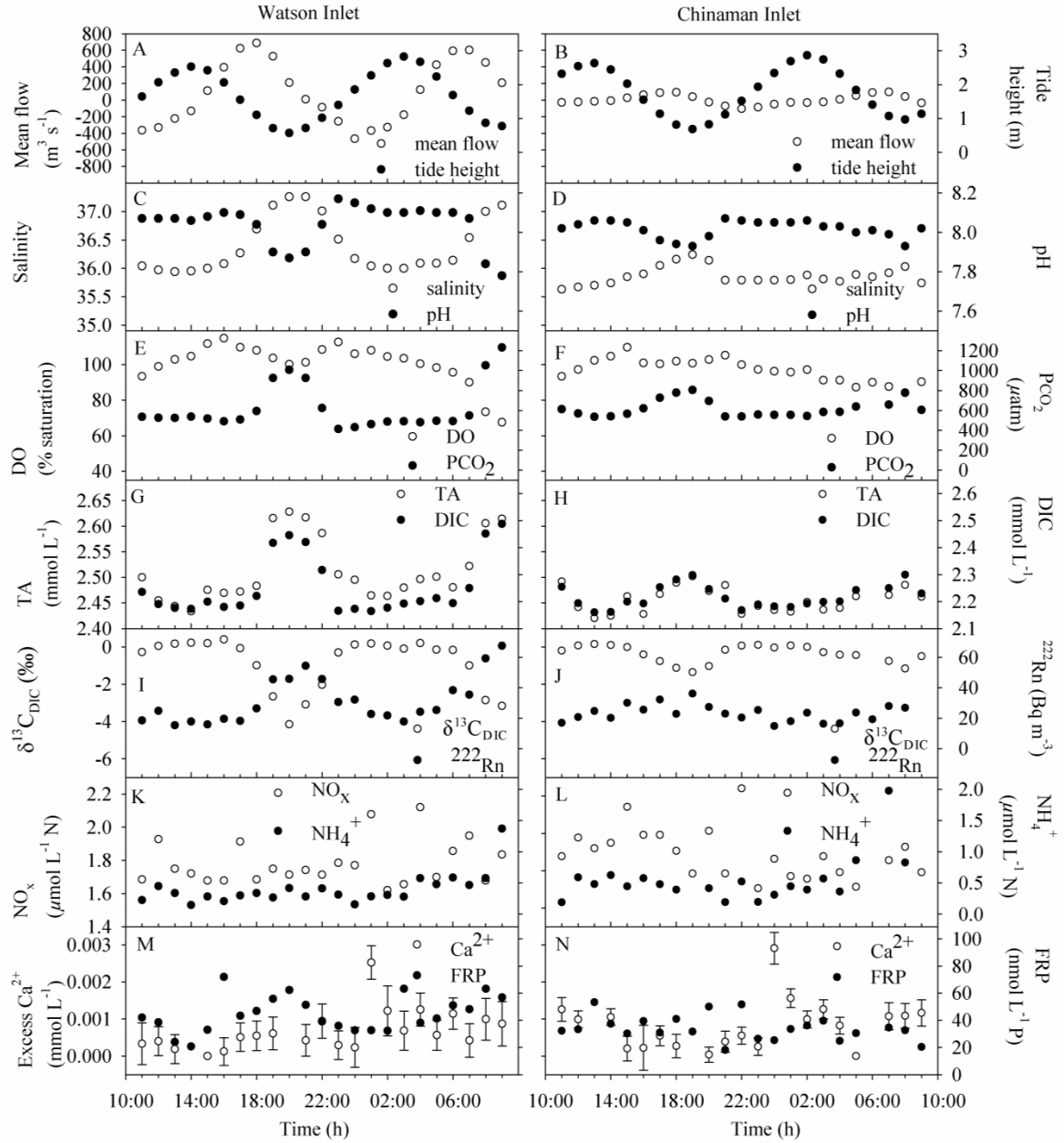


Figure 3.2: Time series measurements of mean flow, tide height, salinity, pH, DO, Pco₂, TA, DIC, Excess Ca²⁺, δ¹³C, ²²²Rn, NH₄⁺, NO_x and FRP for Watson Inlet (left column) and Chinaman Inlet (right column). The error bars on Ca²⁺ represent ± one standard deviation.

There was little change in Pco₂ and pH between day and night, but tidal effects on these parameters were obvious. At WI, DO ranged between 68% and 115% saturation,

and between 84% and 110% at CI (panel E, F). Percentages of DO appear to be influenced by both tide, and photosynthesis during daylight hours.

The concentrations of TA and DIC in the inlets were higher during outgoing tides, when porewater was draining from the tidal flats (panel G, H). The concentration of TA changed by 8%, increasing $\sim 0.2 \text{ mmol L}^{-1}$ above the measured background concentration at WI, compared to 3% and $\sim 0.1 \text{ mmol L}^{-1}$ in CI. The higher concentration of TA and DIC at WI corresponded with higher ^{222}Rn measurements (panel I, J), indicating that the increased TA and DIC concentrations were related to higher proportions of porewater. Measurements of $\delta^{13}\text{C}_{\text{DIC}}$ (panel I, J) followed distinct tidal trends at both WI and CI, with minima occurring during low tide.

The measured concentrations of NO_x , NH_4^+ (panel K, L) and FRP (panels M, N) during the time series also varied with the tidal cycle. The measured concentration of NO_x was $1.6\text{--}2.1 \text{ } \mu\text{mol L}^{-1}$ in WI and $1.7\text{--}2.2 \text{ } \mu\text{mol L}^{-1}$ in CI. The measured concentration of NH_4^+ was $0.15\text{--}1.4 \text{ } \mu\text{mol L}^{-1}$ in WI and $0.19\text{--}2.0 \text{ } \mu\text{mol L}^{-1}$ in CI. The concentration of FRP followed a more consistent tidal pattern in WI and was $21\text{--}72 \text{ nmol L}^{-1}$ in WI and $18\text{--}52 \text{ nmol L}^{-1}$ in CI. The total amounts of exported NO_x , NH_4^+ and FRP were calculated to be 1.0 , 0.10 and $0.25 \text{ mmol m}^{-2} \text{ d}^{-1}$, respectively, for WI and 1.1 , 0.0043 and $0.016 \text{ mmol m}^{-2} \text{ d}^{-1}$, respectively, for CI. These export values are calculated using the total inlet area (intertidal + subtidal areas) at each site.

3.5.2 Porewater

The concentrations of TA and DIC were similar in the draining porewater from both sites and Pco_2 varied considerably in both sites, from subsaturated to supersaturated, relative to the atmosphere ($240\text{--}870 \text{ } \mu\text{atm}$ at WI and $310\text{--}1160 \text{ } \mu\text{atm}$ at CI). The concentrations of NH_4^+ , TDN, TN, FRP, TDP, and TP were all higher in the porewater

samples than the background in both sites (**Table 3.2**); whereas, NO_x was lower in the porewater samples. The measured concentration of DOC was the same as the background at CI (0.20 mmol L^{-1}), but higher than the background at WI (0.25 mmol L^{-1}).

The porosity of sediment differed slightly between the sites, and was 0.54 and 0.49 for WI and CI, respectively. At WI, porewater had a mean ^{222}Rn concentration of 240 Bq m^{-3} (**Table 3.2**) and channel water during the time series ranged between 15 and 68 Bq m^{-3} (**Fig. 3.2**, panel I, J). Porewater at CI had a similar mean ^{222}Rn concentration of 252 Bq m^{-3} ; however, the fluctuation in ^{222}Rn concentration measured during the time series in the inlet channel was lower and ranged between 15 and 36 Bq m^{-3} . The net porewater exports, which have the units cm d^{-1} (or $\text{cm}^3 \text{ cm}^{-2} \text{ d}^{-1}$) are calculated for the entire inlet area (**Table 3.2**). The porewater export at WI was calculated to be 27 ± 2.6 (SD) cm d^{-1} which was ~5 times greater than at CI ($6.7 \pm 1.2 \text{ cm d}^{-1}$) (**Table 3.2**). The residence times were calculated (**Eq. 3.6**) using the activity of ^{222}Rn at equilibrium with its parent nuclide within the sediment (A_e) which was 4593 and 4305 Bq m^{-3} at WI and CI, respectively, and the mean measured activity of ^{222}Rn in the sampled porewater (A_i) (**Table 3.2**). The residence times of porewater within the sediment were 6.6 and 7.4 h for WI and CI, respectively, indicating that porewater exchange was controlled by the tidal cycle, which led to the observed tidal patterns in many of the measured parameters during the time series (**Fig. 3.2**). $\text{Ca}^{2+}:\text{Na}^+$ ratios were slightly elevated in the porewater with means of 2.1226×10^{-2} (range = 2.1164×10^{-2} – 2.1278×10^{-2}) and 2.1173×10^{-2} (range = 2.1138×10^{-2} – 2.1211×10^{-2}) for WI and CI, respectively, compared to background WP ratios of 2.1066×10^{-2} and 2.1003×10^{-2} for WI and CI, respectively.

Table 3.2: Porewater analysis of carbon species and nutrients, including relevant ^{222}Rn measurements and the total volume of exported porewater for Watson Inlet (WI), Chinaman Inlet (CI), and Western Port (WP). *RSD for measurement method.

Porewater measurements	WI porewater	RSD (%)	CI porewater	RSD (%)	WP (background)
Pco_2 (μatm)	240–870		310–1160		540
DIC (mmol L^{-1})	2.6	9.32	2.66	7.48	2.17
TA (mmol L^{-1})	3.22	5.24	3.18	2.82	2.43
$\delta^{13}\text{C}$ (‰)	-2.8–0.5		-1.5–0.8		0.19
Salinity	38.9	0.8	38.4	0.5	35.8
pH	8.0–8.4		7.8–8.3		8.1
NH_3 (mmol L^{-1})	1.4×10^{-3}	39	4.0×10^{-3}	35	3.1×10^{-4}
FRP (mmol L^{-1})	9.7×10^{-5}	41	1.5×10^{-4}	23	3.7×10^{-5}
NO_x (mmol L^{-1})	2.5×10^{-4}	37	7.0×10^{-4}	81	1.8×10^{-3}
TDP (mmol L^{-1})	3.9×10^{-4}	37	3.2×10^{-4}	0	1.7×10^{-4}
TDN (mmol L^{-1})	2.1×10^{-2}	12	2.4×10^{-2}	4.3	2.7×10^{-2}
TP (mmol L^{-1})	3.2×10^{-3}	42	5.4×10^{-3}	68	2.6×10^{-4}
TN (mmol L^{-1})	4.7×10^{-2}	28	6.9×10^{-2}	56	2.7×10^{-2}
DOC (mmol L^{-1})	0.25	9.1	0.2	9.8	0.2
$A_t^{222}\text{Rn}$ (Bq m^{-3})	240	10	252	18	21.2
Residence time* (h)	6.6	11	7.4	20	
Exported pore water** (cm d^{-1})	27 ± 2.6	-	6.7 ± 1.2	-	
Sediment measurements	WI		CI		
$A_e^{222}\text{Rn}$ (Bq m^{-3})	4593	-	4305	-	
$\delta^{13}\text{C}$ (‰)	-18.6	0.2‰*	-18	0.2‰*	
Organic carbon content (%)	0.6		0.6		

* Residence time was calculated using equation 3.6.** Exported pore water was

calculated using the mass balance equation 3.5

3.5.3 Advective carbon fluxes

Instantaneous advective fluxes of DIC, TA, and CO₂ from each estuary showed a net export of these species (**Fig. 3.3**). The instantaneous advective flux of each carbon species was taken as the excess (= measured value – background value), which flowed in and out, through the entrance of the inlets. This accounted for amounts of these species which re-entered the inlet after transition to flood tide, allowing the net export to be determined. At WI, maximum instantaneous advective exports were $4.8 \times 10^5 \text{ mol h}^{-1}$, $3.5 \times 10^5 \text{ mol h}^{-1}$, and $3.0 \times 10^4 \text{ mol h}^{-1}$ for DIC, TA, and CO₂, respectively. At CI, maximum exports were lower, with values of $4.1 \times 10^4 \text{ mol h}^{-1}$, $2.3 \times 10^4 \text{ mol h}^{-1}$, and $2.5 \times 10^3 \text{ mol h}^{-1}$, for DIC, TA, and CO₂, respectively. The instantaneous fluxes were integrated to calculate daily advective exports of CO₂, DIC, and TA (**Table 3.3**) for the total inlet areas. Also included in this table is the estimated atmospheric CO₂ flux and estimated fluxes from SGC, POC, and DOC. At WI, daily exports were calculated to be $460 \text{ mmol m}^{-2} \text{ d}^{-1}$, $310 \text{ mmol m}^{-2} \text{ d}^{-1}$ and $46 \text{ mmol m}^{-2} \text{ d}^{-1}$ for DIC, TA, and CO₂, respectively, whereas CI exports were $140 \text{ mmol m}^{-2} \text{ d}^{-1}$, $46 \text{ mmol m}^{-2} \text{ d}^{-1}$, and $27 \text{ mmol m}^{-2} \text{ d}^{-1}$, respectively (CO₂ emitted to the atmosphere is included in these daily export values). The advective TA flux was also calculated for the time series conducted during spring and it was found that these fluxes were $110 \text{ mmol m}^{-2} \text{ d}^{-1}$ and $130 \text{ mmol m}^{-2} \text{ d}^{-1}$ for WI and CI, respectively.

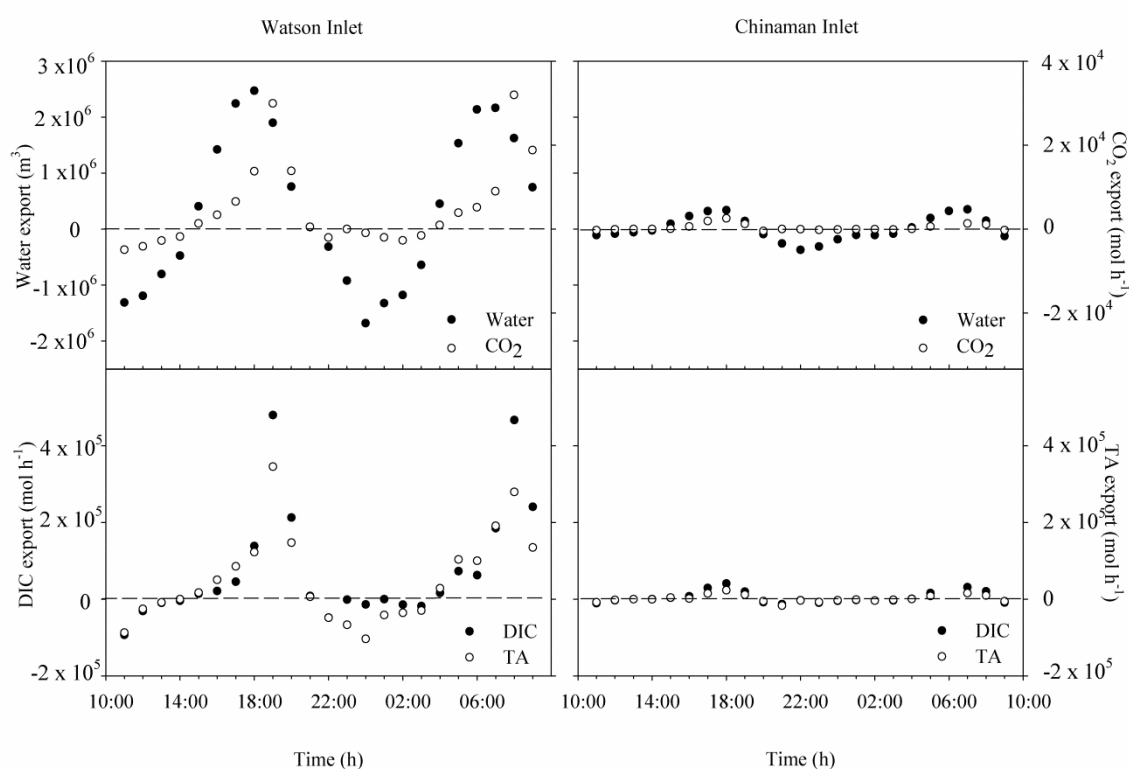


Figure 3.3: Export of water, CO₂, DIC, and TA from the inlets to WP during the time series campaigns for Watson Inlet (left) and Chinaman Inlet (right). Positive values represent export out of the inlets. The dotted line represents zero export.

Table 3.3: Carbon budget of Watson Inlet and Chinaman Inlet as a total export, an area integrated flux and as a percentage of total C export.

Component of C budget	Watson Inlet		Chinaman Inlet	
	Carbon export (mmol m ⁻² day)	% of total C export	Carbon export (mmol m ⁻² day)	% of total C export
Atmospheric CO ₂ flux	17	3	19	11
Advective CO ₂ flux	30	6	8	5
Total CO ₂ flux	46	9	27	17
Advective DIC flux	440	90	120	76
Total inorganic carbon flux	460	93	140	87

Total TA export	310		46	
SGC	19	4	-18	-11
POC	5	1	2	1
DOC	25	5	0	0
Net C export	490	-	130	-
TA from cores	-26	-	20	-
TA during spring	110	-	130	-

Flux of SGC ranged from 0.12–3.8 mol h⁻¹ at WI and 0.020–0.67 mol h⁻¹ at CI over the tidal cycle. Peak SGC flux rates were observed during rising and falling tide stages at both sites with mean flux = 0.76±1.1 (SD) g h⁻¹ in current velocities > 0.02 m s⁻¹; flux rates declined to 0.071±0.065 mol h⁻¹ when current velocities fell below 0.02 m s⁻¹. There was a significant curvilinear relationship between SGC flux and mean current velocity ($n = 14$; adj- $R^2 = 0.44$; $p = 0.02$). Scaled flux rates over the full sampling period yielded daily SGC flux estimates of ~19 mmol m⁻² d⁻¹ for WI and ~-18 mmol m⁻² d⁻¹ for CI. The positive flux rate at the WI site indicates a net export of SGC; whereas, the negative flux at CI indicates a net import of SGC.

3.5.4 Carbon isotope signatures

Keeling plots (**Fig. 3.4**) were produced to determine the $\delta^{13}\text{C}$ end-member of the DIC source (Keeling 1958; Karlsson et al. 2007), with the y-intercept of the $\delta^{13}\text{C}_{\text{DIC}}$ vs. 1/DIC plot representing the isotope ratio of the DIC source. During the time series, $\delta^{13}\text{C}$ concentrations changed typically with the tide with the lowest $\delta^{13}\text{C}_{\text{DIC}}$ occurring at low tide. This ranged from -4.2‰ to 0.4‰ in WI and -1.4‰ to 0.2‰ in CI (**Fig. 3.2**, panel I, J). Keeling plots made using the time series data had y-intercepts of -24.6‰ and -20.4‰ for WI and CI, respectively (**Table 3.4**). Plots made using five replicate porewater samples showed a more positive $\delta^{13}\text{C}_{\text{DIC}}$ value of -15.4‰ and -13.3‰ for WI and CI, respectively. The sediment $\delta^{13}\text{C}$ on bare and seagrass-vegetated mudflats was -19.5‰ for

WI and -18‰ for CI. Mean seagrass $\delta^{13}\text{C}$ was $-13.7 \pm 1\text{‰}$ and $-12.7 \pm 1\text{‰}$ for WI and CI, respectively, and mangrove leaf $\delta^{13}\text{C}$ was found to be -25.5‰ .

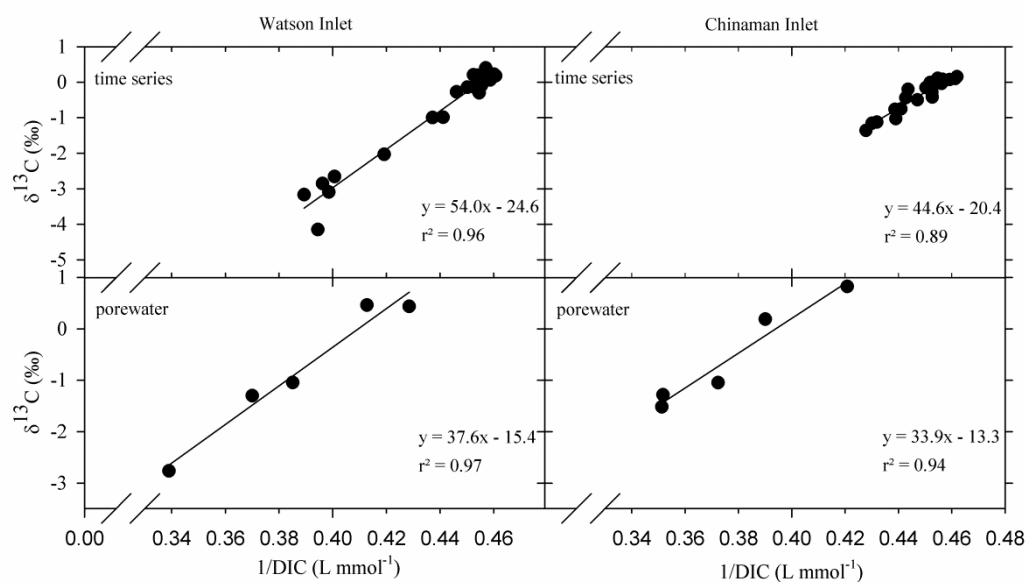


Figure 3.4: Keeling plots of time series measurements (top) and porewater samples (bottom) for Watson Inlet (WI) and Chinaman Inlet (CI). The linear regression equations displayed show the y-intercept which represent the $\delta^{13}\text{C}$ end-member. Note: the x-axes are truncated.

Table 3.4: Keeling plot y-intercepts for the time series and porewater samples at Watson Inlet (WI) and Chinaman Inlet (CI).

	Time series y-intercept	Porewater y-intercept
WI	-24.6	-15.4
CI	-20.4	-13.3

3.6 Discussion

To summarise the key findings of this study, we present a conceptual diagram (Fig. 3.5), which illustrates the dominance of TA export and other key processes. These include (1) sedimentation and fresh Fe input, (2) sulfate reduction, (3) FeS and FeS₂ burial, (4) TA export through porewater drainage, (5) DOC and POC export, (6) SGC export, and (7) TA from carbonate dissolution within the sediment and subsequent export through porewater drainage.

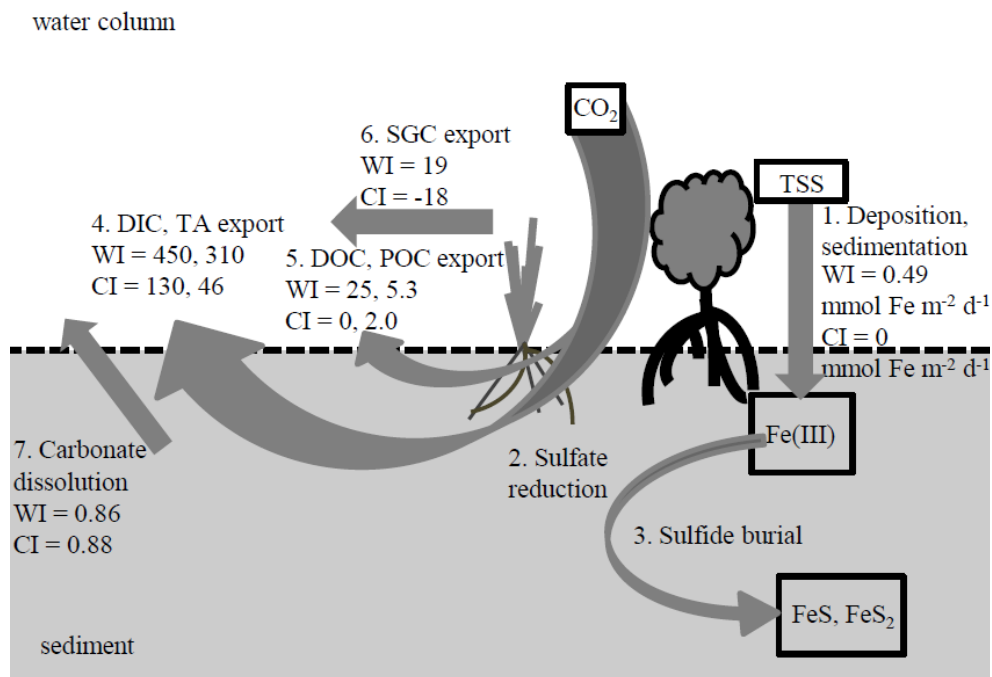
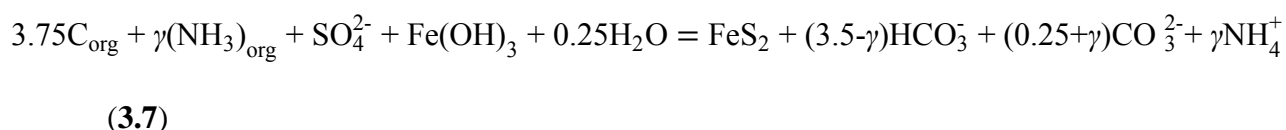


Figure 3.5: Conceptual diagram of the components of carbon export from the intertidal zones of the inlets. The dashed line represents the sediment water interface. Processes 1-3 represent inputs of Fe, sulfate reduction, and FeS and FeS₂ burial. The large arrow represents the carbon pump, taking in CO₂ from the atmosphere and releasing it as 4. DIC, 5. DOC and POC and 6. SGC. Also included is carbonate dissolution (7). Units are $\text{mmol C m}^{-2} \text{ d}^{-1}$ for carbon, $\text{mmol TA m}^{-2} \text{ d}^{-1}$ for TA and $\text{mmol Fe m}^{-2} \text{ d}^{-1}$ for Fe.

3.6.1 Alkalinity export

The major processes driving alkalinity production have been shown to include net denitrification, ammonia release, carbonate dissolution and sulfate reduction (Hammond et al. 1999). In a recent review, Hu and Cai (2011a) concluded that denitrification of external sources of nitrate and sulfate reduction followed by FeS₂ burial produce alkalinity relevant to ocean budgets on a global scale. In WI and CI, denitrification rates were extremely low ($< 10 \mu\text{mol m}^{-2} \text{h}^{-1}$, (Evrard et al. 2013)) and so alkalinity production due to denitrification was assumed to be negligible compared to alkalinity produced by sulfate reduction and carbonate dissolution. Berner et al. (1970) showed that sulfate reduction followed by FeS and FeS₂ burial (**Fig. 3.5**, processes 2 and 3) allowed 1 mole of alkalinity to be produced for every mole of organic matter broken down. Although several examples of different stoichiometry for the production of alkalinity during FeS₂ formation exist (Hammond et al. 1999), the **Eq. 3.7** is often used to describe respiration of organic matter with an oxidation state of zero and yields ~0.81 mole of alkalinity for every mole of organic matter broken down through sulfate reduction:



where γ is 3.75 divided by the C:N ratio, which we assumed to be 5 (Hammond et al. 1999). This reaction assumes the formation of FeS₂, which is more resistant to oxidation and is formed on much longer time scales than FeS. The burial of FeS and FeS₂ is important in producing net alkalinity because sulfide reoxidation is prevented, which would consume any alkalinity produced. Although internal cycling of Fe would cause instantaneous alkalinity fluxes during net FeS formation, no net alkalinity would be produced over the longer term due to periodic reoxidation of stored sulfides (Faber et al.

2012). For this reason, fresh Fe derived from allochthonous sources would need to be supplied for a net alkalinity export via sulfate reduction to occur (**Fig. 3.5**, process 1).

We estimated the total amount of Fe added to WI from WC using total suspended solids (TSS) values and daily flow data for the two years preceding the 2012 sampling period. TSS was estimated from logged turbidity measurements using a linear relationship between the two, which was calculated from a separate data set for WC. For Fe:TSS we used a ratio of 0.05, which is a high estimate based on typical Fe concentrations found in riverine TSS (Martin and Meybeck 1979). At WI, the estimated amount of Fe added from WC was $\sim 0.49 \text{ mmol Fe m}^{-2} \text{ d}^{-1}$, a value much lower than which would account for the observed alkalinity exports. According to **Eq. 3.7**, this quantity of Fe would cause a net alkalinity export of $2.3 \text{ mmol m}^{-2} \text{ d}^{-1}$, which is far less than the observed value of $310 \text{ mmol m}^{-2} \text{ d}^{-1}$. Three possible explanations for this large discrepancy exist: 1) alkalinity production from carbonate dissolution, 2) temporal variability in net sulfate reduction including periods of net reduction and re-oxidation which are not captured by our sampling strategy, and 3) temporal variability in the factor(s) driving alkalinity export such as porewater exchange.

Carbonate dissolution (**Fig. 3.5**, process 7.) has long been recognised as an alkalinity producing reaction (Berner et al. 1970; Walter and Burton 1990) and has been shown to be associated with sulfide oxidation and aerobic respiration, which enable carbonate dissolution by producing acid in the sediment porewater. Carbonate dissolution within sediments would elevate both alkalinity and DIC exports. Here we can gain insight into the extent of carbonate dissolution by looking at the export of Ca^{2+} compared to a conservative ion such as Na^+ . The $\text{Ca}^{2+}:\text{Na}^+$ was elevated in the porewater samples at 0.02123 and 0.02117 for WI and CI, respectively, compared to the background ratio of 0.02107 and 0.02100, respectively. The slightly elevated $\text{Ca}^{2+}:\text{Na}^+$ indicates that

carbonate dissolution was occurring within the porewater. Based on the excess ratio of 0.00016 and 0.00017 for WI and CI, the amount of excess Ca^{2+} can be estimated and was found to be 0.86 and 0.88 $\mu\text{mol Ca}^{2+} \text{ L}^{-1}$ which represents ~0.2% of the total TA and DIC in the porewater exported at both sites. These values may be associated with some error as the presence of carbonate bearing sediments may have been heterogeneous within the intertidal zones of the inlets and our sampling regime may not have captured samples with a greater extent of carbonate dissolution. Trends in $\text{Ca}^{2+}:\text{Na}^{+}$ in the time series measurements were not apparent, and the contribution of carbonate dissolution to alkalinity in the channel was determined to be a maximum of ~3 $\mu\text{mol L}^{-1}$, which was calculated from excess Ca^{2+} concentrations observed during the time series (**Fig. 3.2**). Considering the excess alkalinity is as high as 200 $\mu\text{mol L}^{-1}$, this contribution is negligible.

The balance between net sulfate reduction and oxidation is known to be highly temporally variable (for a review, see Burdige 2011). During periods of high wind and turbulence, sediment may be resuspended leading to the reoxidation of FeS and FeS_2 causing an alkalinity consumption (via the production of acid). Moreover, Ferguson et al. (2003a) showed that anaerobic mineralisation increased during periods of high organic matter supply, followed by aerobic mineralisation and the reoxidation of reduced S species when the organic matter supply reduced. It is therefore most likely that there is a net consumption of alkalinity in winter when storms are more frequent and organic matter supplies lower, and a net production in the warmer, calmer periods. We also anecdotally observed considerable changes in seagrass density at the same site on an interannual basis. It is well known that the presence of seagrass roots have a considerable influence on sulfate reduction, and this may be through both the direct effect of DOC exudation (Isaksen and Finster 1996) or particle trapping (Evrard et al. 2005). The loss and

accumulation of seagrass on longer time scales is therefore also likely to affect alkalinity fluxes.

Tide height was observed to have a marked influence on the amount of TA and DIC export at both sites. The export of TA from CI during the spring sampling was seen to be ~3 times higher than during summer, which corresponded with a ~10 cm higher high tide. Due to the extensive mudflats and mangroves at the upper reaches of the intertidal zone, a 10 cm increase in water height corresponded to a relatively large increase in inundated then drained sediment during the tidal cycle, and an accompanying increase in porewater exchange. Based on ADCP measurements during the time series, this small increase in tide height caused ~3 times the volume of water to be exchanged in CI. This tide difference also resulted in large differences in the quantity of porewater exported with 2.8 times more porewater draining from sediments during spring (6.7 ± 1.2 vs. 18.9 ± 3.4 cm d⁻¹). This was also the case in WI, where a TA export ~3 times higher during summer (**Table 3.3**) is associated with a ~10 cm higher high tide and ~1.6 times more porewater export (27 ± 2.6 vs. 16.8 ± 1.6 cm d⁻¹). The importance of tide height in causing alkalinity export appears to be greater than the seasonal differences between the summer and spring sampling periods, although this is uncertain given the limited data sets.

3.6.2 Porewater exchange

During summer, WI (negligible creek flow) and CI showed characteristics of ‘inverse estuaries’, where salinity changes are due to evaporation from the intertidal areas rather than freshwater input, with salinity values being a mirror image of tide height (Wolanski and Ridd 1986; Bouillon et al. 2007). This is typical of mangrove creeks without a freshwater input and with high evaporation rates.

Bouillon et al. (2007) used DO, salinity and DOC as tracers to estimate the porewater contribution to a mangrove creek during low tide and found that exchange of porewater is an important driver of high concentrations of P_{CO_2} , DIC and TA. In terms of biogeochemical processes, intertidal zones function very efficiently relative to shelf sediments as they are under the influence of tidal pumping and are exposed to large amounts of terrestrially derived organic carbon and Fe. Sulfate reduction in the intertidal zones of estuaries and their adjacent marshes may be the source of a significant proportion of alkalinity observed in estuarine waters (Cai and Wang 1998; Wang and Cai 2004). Compared to WI, the generally lower ^{222}Rn concentrations during the CI time series suggests that porewater contributes a lower proportion of water within the inlet during low tide, resulting in a lower net export of porewater. The porewater export estimates of $27 \pm 2.6 \text{ cm d}^{-1}$ from WI and $6.7 \pm 1.2 \text{ cm d}^{-1}$ from CI (**Table 3.2**) are associated with sources of uncertainty such as the variability in porewater ^{222}Rn , which has been observed to be highly temporally variable (Atkins et al. 2013). The ^{222}Rn activities of the porewater endmember samples had relatively little variability (220-277 and 205-302 $Bq \text{ m}^{-3}$ for WI and CI, respectively), which may be reflective of the fact that we collected draining porewater which, to some extent, may have accounted for the heterogeneity of ^{222}Rn activities within the sediment because the water would have drained from a large area of intertidal sediment. Nonetheless, due to practical constraints, we were unable to take samples of draining porewater from within the upper reaches of the inlets or during the whole outgoing tide and this is recognized as a source of uncertainty in our estimates.

To give confidence to our estimates of porewater input, we used another mass balance approach using TA as a tracer. If we assume all the excess alkalinity measured

during the time series is derived from advective porewater exchange and that TA acts conservatively during export, then we can estimate porewater export using **Eq 3.8**.

$$PW = \frac{TA_{TE} \cdot A}{(TA_{PW} - TA_{WP})} \cdot 100 \quad (3.8)$$

Where PW is the exported porewater in cm d^{-1} , TA_{TE} is the total export of TA from the inlet in mol d^{-1} , TA_{PW} is concentration of TA in the porewater in mmol L^{-1} , TA_{WP} is the TA concentration measured in WP, and A is the area of the inlet in m^2 .

We obtained values of $48.9 \pm 11 \text{ cm d}^{-1}$ and $7.6 \pm 1.2 \text{ cm d}^{-1}$ for WI and CI, respectively, which is in close agreement with the estimates from the ^{222}Rn mass balance. It is likely that the difference between these estimates is due to heterogeneity of both ^{222}Rn activity and TA production within the sediment. The similarity of the porewater export estimates and the estimates obtained using the TA tracer, as well as the similarity between the calculated residence time of draining porewater (6.6-7.4) and a tidal cycle (~6 h), gives us confidence in the porewater export estimates. For comparison, recent work in an Australian tidal creek showed average porewater exports of $56.7 \pm 14.2 \text{ cm d}^{-1}$ (Atkins et al. 2013).

The reasons for the generally higher porewater export in WI may include differences in geomorphology between the sites, porosity, or faunal burrow density, all of which can influence porewater exchange. In a parallel study at the same sites, Evrard et al. (2013) found that although the abundance of macrofauna were similar at both sites, densities of the crab *Halicarcinus ovatus* were significantly higher at WI. Water exchange during tidal cycles is known to be significantly greater in areas replete with macropores or burrows created by intertidal species of crabs or other macrofauna (Ridd 1996; Xin et al. 2009). Concomitant with passive porewater draining through macrofauna burrows, bioirrigation will also significantly affect the microbial composition and subsequently the biogeochemistry of marine sediments (Kristensen and Kostka 2005). Seasonal changes in

burrow density or bioirrigation may have an influence on biogeochemical processes, for instance sulfate reduction or sulfide reoxidation, although any seasonal changes of these factors have yet to be investigated. Recent research observed crab burrows being a major influence on porewater exchange and also suggested that newly formed crab burrows exposed old sediments to porewater exchange and played a role in controlling nutrient fluxes (Gleeson et al. 2013).

The porewater concentrations of most N and P species were higher than background concentrations in WP, indicating that porewater exchange is a source of these species. The concentration of NO_x was found to be lower in the sediment porewater, possibly due to denitrification or uptake by seagrass, which was abundant on the intertidal zone where the porewater was sampled, or microphytobenthos. To determine whether the inlets were a significant source of nutrients to WP, the instantaneous fluxes and total exports were calculated and were found to be negligible relative to background WP concentrations (data quoted in results text) due to the efficient internal cycling of N and P and rapid uptake of nutrients by seagrass and possibly microphytobenthos.

3.6.3 Carbon budget

This study highlights the importance of porewater exchange in driving alkalinity exports, extending the work of Maher et al. (2013). Previous studies have made use of cores to estimate benthic metabolism and carbon fluxes from intertidal sediments (Cook et al. 2004), but these are subject to errors caused by the heterogeneity of complex systems and they ignore fluxes driven by porewater exchange by accounting only for diffusive fluxes. The alkalinity fluxes observed in the sediment core incubations were very different from the advective fluxes calculated (**Table 3.3**), and it is assumed that this was due to factors associated with core sampling or incubations rather than due to in situ

biogeochemical processes. For instance, the cores were not subject to tidal flooding and ebbing, which will change biogeochemical factors associated with TA and DIC fluxes by stopping advective fluxes through the porewater. The consumption of alkalinity in WI may be due to the effects of fauna trapped inside the core, causing disturbance, or disturbance around the edges of the core during sampling. WI has a larger amount of Fe inputs so is expected to have larger amounts of FeS which can be oxidised. Total CO₂ fluxes represented 9% and 17% of total carbon flux for WI and CI, respectively). This occurred as both an atmospheric flux contributing 3% and 11% of total carbon flux for WI and CI, respectively, and as an advective flux to WP, representing 6% and 5% of total carbon flux for WI and CI, respectively. After advective export of CO₂, it is expected that it will either escape to the atmosphere or take part in other processes such as photosynthesis. Advective fluxes of both CO₂ and DIC were ~5 times higher at WI, whereas TA flux in WI is close to an order of magnitude higher. The production of alkalinity is significant to global carbon budgets due to a two-fold effect on atmospheric carbon dioxide: firstly, carbon is retained as alkalinity rather than being lost to the atmosphere as CO₂, and is exported to the ocean; secondly, alkalinity acts as buffer, facilitating the uptake of extra CO₂. Thomas et al. (2009) estimated that anaerobic organic matter degradation (sulfate reduction and denitrification) in coastal sediments produced alkalinity on a scale that was relevant to global carbon budgets, causing as much as 60% of the total CO₂ uptake by shelf and marginal seas. At both WI and CI, DIC export was considerably higher than TA export. This discrepancy cannot be accounted for by the supersaturation of CO₂ in the advected water alone, as this only contributed ~6% and ~5% of DIC in WI and CI, respectively. The dominance of DIC export relative to CO₂ fluxes to the atmosphere may be due to CO₂ being uptaken by alkalinity rich porewater which buffers its uptake. This is suggested by the measurements of P_{CO2} from the porewater

samples, some of which exhibit P_{CO_2} values which are subsaturated ($240 \mu\text{atm}$) with regard to atmospheric P_{CO_2} . Similarly, supersaturated ($1160 \mu\text{atm}$) pCO_2 in porewater samples indicate that aerobic processes are important in DIC production and probably control a large proportion of DIC export. Thomas et al. (2009) describe a seasonal uptake of atmospheric and respired CO_2 because in the sites of anaerobic alkalinity generation, aerobic respiration was limited. In our study, it appears that uptake of CO_2 occurs instantaneously as a result of simultaneous aerobic processes in oxic zones of the sediment, which provides enough CO_2 to quickly cause supersaturation in draining porewater.

The estimated export of DOC from CI was essentially nil, whereas WI exported a small quantity of DOC compared to DIC export, representing ~5% of total carbon export. The calculated export of seagrass (**Fig. 3.5**, process 6) was included in the carbon budget and was 19 and -18 mmol SGC d^{-1} in WI and CI, respectively (**Table 3.3**). At WI, the net export of seagrass accounted for ~4% of total carbon export. Conversely, the net import of seagrass at CI accounted for ~11% of total DIC export. The large seagrass import rates in CI suggests that mineralisation of organic matter in the imported seagrass may be a significant source of DIC production. These estimates of SGC flux are probably representative of local seagrass wrack dynamics under typical conditions at this time of year; however, our estimates do not take into account the modulating role of recurrent events such as the spring-neap tidal cycle, nor pulsed events such as those associated with storms. These events can exert a strong influence on wrack deposition and advection, particularly in enclosed coastal areas (Mateo et al. 2006). The POC fraction of the carbon budget (**Table 3.3**) accounted for ~1% of total carbon export in both sites.

Our data indicates that DIC export dominates carbon export from this system, and given that these systems contain extensive areas of mangrove forest, may provide

valuable information pertaining to the uncertainties in carbon export from mangrove systems (Bouillon et al. 2008a). The production of large amounts of alkalinity in WI indicates that fluxes of DIC and subsequent export to WP are probably higher than CO₂ lost to the atmosphere from the water or exposed sediments as observed in previous work (Faber et al. 2012).

3.6.4 DIC sources

Mangroves have been shown to contribute large amounts of organic matter as DOC (Dittmar et al. 2006) and detritus (Jennerjahn and Ittekkot 2002) to adjacent coastal systems and have been shown to act as effective CO₂ pumps to the coastal ocean by taking carbon from the atmosphere and releasing it into coastal waters as DIC and DOC (Miyajima et al. 2009; Maher et al. 2013). The systems we studied contain various sources of organic carbon, owing to the fact that WI and CI are systems with extensive bare and seagrass-vegetated mudflats and fringed by mangrove forest. WI in particular, drains numerous mangrove creeks. Mangrove leaf $\delta^{13}\text{C}$ was found to be -25.5‰ and seagrass was -13.7 – -12.7‰, with microphytobenthos having a $\delta^{13}\text{C}$ of around -18‰. For ease of elucidating the sources of DIC in these systems, we assumed two main contributors: 1. mangrove, which may include DIC produced from small amounts of terrestrial organic matter and DIC inputs to WI from WC, and 2. benthic, which includes DIC inputs from seagrass and microphytobenthos. The $\delta^{13}\text{C}_{\text{DIC}}$ end-member value for the time series, of -24.6 and -20.4 for WI and CI, respectively, (**Table 3.4**) suggests that the DIC produced was from a combination of mangrove and benthic sources. The calculated contribution of DIC from mangrove sources was 88-93% in WI and 32-59% in CI, with the remainder coming from benthic sources.

Differences between the $\delta^{13}\text{C}_{\text{DIC}}$ end-members of the time series (channel) and the porewater (**Fig. 3.4, Table 3.4**) were -15.4 and -13.3 for WI and CI, respectively, and were most likely a result of spatial variation in the source of mineralised organic matter in the inlets. The $\delta^{13}\text{C}_{\text{DIC}}$ end-member of the sediment porewater was similar to the $\delta^{13}\text{C}$ of seagrass, indicating that on the mudflats where porewater samples were taken, mineralised seagrass organic matter was the dominant source of DIC.

The difference in the sources of DIC between sites can be explained by the presence of more extensive mangrove creeks in WI (which are major sites of porewater drainage), and the observation of a large import of seagrass at CI which would contribute a large amount of seagrass organic matter to the system. The contribution of carbonate dissolution to carbonate export was too small to affect $\delta^{13}\text{C}_{\text{DIC}}$.

In summary, we found the tidal flats to be active carbon pumps which transform organic matter into alkalinity. The driving mechanism for this is the breakdown of mangrove and terrestrially derived organic matter as well as benthic vegetation. Because much of the carbon exported in these systems is from mangroves, this finding is relevant to recent discussion regarding the extent of carbon mineralisation and subsequent export in mangroves (Bouillon et al. 2008a). In agreement with Maher et al. (2013), our data suggests that export of carbon as DIC may be the major component of the previously unaccounted for fraction of carbon exported by mangroves and that this occurs through porewater exchange which is probably facilitated by macrofaunal burrows. We have identified that this DIC export is mostly alkalinity and is $140 - 460 \text{ mmol m}^{-2} \text{ d}^{-1}$. We make the note however that modes of inorganic carbon export (DIC vs. loss to the atmosphere as CO_2) may change depending upon the availability of oxidised Fe. The driver of alkalinity production was most likely the burial of reduced sulfides: however, fresh Fe inputs were not high enough to account for the observed alkalinity export,

indicating recycling of Fe. As such, there is considerable uncertainty in the temporal variability in alkalinity export in coastal zones highlighting the need to monitor alkalinity fluxes over a range of weather patterns and seasons. Although the alkalinity exported from intertidal zones may not facilitate a net uptake of atmospheric CO₂ as observed by Thomas et al. (2009), these systems can act as an effective carbon pump, with mangroves, seagrass and microphytobenthos taking in atmospheric carbon and ultimately exporting it as mostly alkalinity through porewater exchange.

3.7 References

- Aller, R. C. 1982. Carbonate dissolution in nearshore terrigenous muds: The role of physical and biological reworking. *The Journal of Geology* **90**: 79-95,
- Almgren, T., D. Dyrssen, and S. Fonselius. 1983. Determination of alkalinity and total carbonate., p. 99-123. *In* K. Grasshoff, M. Ehrhardt and K. Kremling [eds.], *Methods of seawater analysis*. Springer-Verlag.
- Apha-Awwa-Wef. 2005. Standard methods for the examination of water and wastewater, the 21st. edition. American Public Health Association,
- Atkins, M. L., I. R. Santos, S. Ruiz-Halpern, and D. T. Maher. 2013. Carbon dioxide dynamics driven by groundwater discharge in a coastal floodplain creek. *Journal of Hydrology* **493**: 30-42,
- Berelson, W., D. Heggie, A. Longmore, T. Kilgore, G. Nicholson, and G. Skyring. 1998. Benthic nutrient recycling in Port Phillip Bay, Australia. *Estuarine, Coastal and Shelf Science* **46**: 917-934,
- Berner, R. A., M. R. Scott, and C. Thomlinson. 1970. Carbonate alkalinity in the pore waters of anoxic marine sediments. *Limnology and Oceanography*: 544-549,
- Borges, A., B. Delille, L. Schiettecatte, F. Gazeau, G. Abril, and M. Frankignoulle. 2004a. Gas transfer velocities of CO₂ in three European estuaries (Randers Fjord, Scheldt, and Thames). *Limnology and Oceanography*: 1630-1641,
- Borges, A. V., J.-P. Vanderborght, L.-S. Schiettecatte, F. Gazeau, S. Ferrón-Smith, B. Delille, and M. Frankignoulle. 2004b. Variability of the gas transfer velocity of CO₂ in a macrotidal estuary (the Scheldt). *Estuaries* **27**: 593-603,
- Bouillon, S., A. V. Borges, E. Castañeda-Moya, K. Diele, T. Dittmar, N. C. Duke, E. Kristensen, S. Y. Lee, C. Marchand, and J. J. Middelburg. 2008a. Mangrove

- production and carbon sinks: a revision of global budget estimates. *Global Biogeochemical Cycles* **22**: GB2013, doi:10.1029/2007GB003052
- Bouillon, S., R. Connolly, and S. Lee. 2008b. Organic matter exchange and cycling in mangrove ecosystems: recent insights from stable isotope studies. *Journal of Sea Research* **59**: 44-58,
- Bouillon, S., J. Middelburg, F. Dehairs, A. Borges, G. Abril, M. Flindt, S. Ulomi, and E. Kristensen. 2007. Importance of intertidal sediment processes and porewater exchange on the water column biogeochemistry in a pristine mangrove creek (Ras Dege, Tanzania). *Biogeosciences Discussions* **4**: 317-348,
- Brasse, S., A. Reimer, R. Seifert, and W. Michaelis. 1999. The influence of intertidal mudflats on the dissolved inorganic carbon and total alkalinity distribution in the German Bight, southeastern North Sea. *Journal of Sea Research* **42**: 93-103,
- Burdige, D. J. 2011. Estuarine and Coastal Sediments – Coupled Biogeochemical Cycling, p. 279-316. *In* E. Wolanski and D. McLusky [eds.], *Treatise on Estuarine and Coastal Science*. Academic Press.
- Burnett, W., G. Kim, and D. Lane-Smith. 2001. A continuous monitor for assessment of ²²²Rn in the coastal ocean. *Journal of Radioanalytical and Nuclear Chemistry* **249**: 167-172,
- Burnett, W. C., and H. Dulaiova. 2003. Estimating the dynamics of groundwater input into the coastal zone via continuous radon-222 measurements. *Journal of environmental radioactivity* **69**: 21-35,
- Cai, W., and Y. Wang. 1998. The chemistry, fluxes, and sources of carbon dioxide in the estuarine waters of the Satilla and Altamaha Rivers, Georgia. *Limnology and Oceanography* **43**: 657-668,

- Cook, P., E. Butler, and B. Eyre. 2004. Carbon and nitrogen cycling on intertidal mudflats of a temperate Australian estuary I. Benthic metabolism. *Marine Ecology Progress Series* **280**: 25-38,
- Dittmar, T., N. Hertkorn, G. Kattner, and R. J. Lara. 2006. Mangroves, a major source of dissolved organic carbon to the oceans. *Global Biogeochemical Cycles* **20**: GB1012, doi:10.1029/2005GB002570
- Evrard, V., V. Eate, R. Woodland, J. Ross, A. O'brien, M. Keough, A. Longmore, R. Wilson, and P. Cook. 2013. Nutrient processing on tidal flats in Western Port: Interactions with ecology and implications for bay-wide nutrient budgets. Melbourne Water, Melbourne.
- Evrard, V., W. Kiswa, T. J. Bouma, and J. J. Middelburg. 2005. Nutrient dynamics of seagrass ecosystems: ^{15}N evidence for the importance of particulate organic matter and root systems. *Marine ecology. Progress series* **295**: 49-55,
- Faber, P., A. Kessler, J. Bull, I. McKelvie, F. Meysman, and P. Cook. 2012. The role of alkalinity generation in controlling the fluxes of CO_2 during exposure and inundation on tidal flats. *Biogeosciences* **9**: 4087-4097,
- Ferguson, A., B. Eyre, and J. Gay. 2003. Organic matter and benthic metabolism in euphotic sediments along shallow sub-tropical estuaries, northern New South Wales, Australia. *Aquatic Microbial Ecology* **33**: 137-154,
- Frankignoulle, M., and A. Borges. 2001. Direct and indirect pCO_2 measurements in a wide range of pCO_2 and salinity values (the Scheldt estuary). *Aquatic Geochemistry* **7**: 267-273,
- Gleeson, J., I. R. Santos, D. T. Maher, and L. Golsby-Smith. 2013. Groundwater-surface water exchange in a mangrove tidal creek: Evidence from natural geochemical tracers and implications for nutrient budgets. *Marine Chemistry*,

- Hammond, D., P. Giordani, W. Berelson, and R. Poletti. 1999. Diagenesis of carbon and nutrients and benthic exchange in sediments of the Northern Adriatic Sea. *Marine Chemistry* **66**: 53-79,
- Hoehn, E., and H. Von Gunten. 1989. Radon in groundwater: A tool to assess infiltration from surface waters to aquifers. *Water Resources Research* **25**: 1795-1803,
- Hofmann, A. F., K. Soetaert, J. J. Middelburg, and F. J. R. Meysman. 2010. AquaEnv: An aquatic acid–base modelling environment in R. *Aquatic Geochemistry* **16**: 507-546,
- Hu, X., and W. J. Cai. 2011. An assessment of ocean margin anaerobic processes on oceanic alkalinity budget. *Global Biogeochemical Cycles* **25**: 1-11,
- Isaksen, M., and K. Finster. 1996. Sulphate reduction in the root zone of the seagrass *Zostera noltii* on the intertidal flats of a coastal lagoon (Arcachon, France). *Marine Ecology Progress Series* **137**: 187-194,
- Jähne, B., G. Heinz, and W. Dietrich. 1987. Measurement of the diffusion coefficients of sparingly soluble gases in water. *Journal of Geophysical Research* **92**: 10767-10710,10776,
- Jennerjahn, T. C., and V. Ittekkot. 2002. Relevance of mangroves for the production and deposition of organic matter along tropical continental margins. *Naturwissenschaften* **89**: 23-30,
- Joye, S. B., D. De Beer, P. L. M. Cook, and G. Perillo. 2009. Biogeochemical dynamics of coastal tidal flats, Chapter. Elsevier Science.
- Karlsson, J., M. Jansson, and A. Jonsson. 2007. Respiration of allochthonous organic carbon in unproductive forest lakes determined by the Keeling plot method. *Limnology and Oceanography* **52**: 603-608,

- Keeling, C. 1958. The concentration and isotopic abundances of atmospheric carbon dioxide in rural areas. *Geochimica et Cosmochimica Acta* **13**: 322-334,
- Koné, Y.-M., and A. Borges. 2008. Dissolved inorganic carbon dynamics in the waters surrounding forested mangroves of the Ca Mau Province (Vietnam). *Estuarine, Coastal and Shelf Science* **77**: 409-421,
- Kristensen, E., and J. Kostka. 2005. Macrofaunal burrows and irrigation in marine sediment: microbiological and biogeochemical interactions, p. 125-157. *In* E. Kristensen, J. Kostka and R. Haese [eds.], *Interactions between macro- and microorganisms in marine sediments*. Coastal and Estuarine Studies. American Geophysical Union.
- Lamontagne, S., and P. G. Cook. 2007. Estimation of hyporheic water residence time in situ using ^{222}Rn disequilibrium. *Limnol. Oceanogr.: Methods* **5**: 407-416,
- Maher, D., I. Santos, L. Golsby-Smith, J. Gleeson, and B. Eyre. 2013. Groundwater-derived dissolved inorganic and organic carbon exports from a mangrove tidal creek: The missing mangrove carbon sink? *Limnol. Oceanogr.* **58**: 475-488,
- Martin, J.-M., and M. Meybeck. 1979. Elemental mass-balance of material carried by major world rivers. *Marine Chemistry* **7**: 173-206,
- Mateo, M. A., J. Cebrián, K. Dunton, and T. Mutchler. 2006. Carbon flux in seagrass ecosystems, p. 159-192. *In* A. W. D. Larkum, R. J. Orth and C. M. Duarte [eds.], *Seagrasses: Biology, ecology and conservation*. Springer.
- Migné, A., D. Davoult, N. Spilmont, D. Menu, G. Boucher, J. P. Gattuso, and H. Rybarczyk. 2002. A closed-chamber CO_2 -flux method for estimating intertidal primary production and respiration under emersed conditions. *Marine Biology* **140**: 865-869,

- Millero, F. 1995. Thermodynamics of the carbon dioxide system in the oceans. *Geochimica et Cosmochimica Acta* **59**: 661-677,
- Miyajima, T., Y. Tsuboi, Y. Tanaka, and I. Koike. 2009. Export of inorganic carbon from two Southeast Asian mangrove forests to adjacent estuaries as estimated by the stable isotope composition of dissolved inorganic carbon. *Journal of Geophysical Research* **114**: G01024, doi:10.1029/2008JG000861
- O'leary, M. 1981. Carbon isotope fractionation in plants. *Phytochemistry* **20**: 553-567,
- Raymond, P., J. Bauer, and J. Cole. 2000. Atmospheric CO₂ evasion, dissolved inorganic carbon production, and net heterotrophy in the York River estuary. *Limnology and Oceanography* **45**: 1707-1717,
- Ridd, P. V. 1996. Flow through animal burrows in mangrove creeks. *Estuarine, Coastal and Shelf Science* **43**: 617-625,
- Schubert, M., A. Paschke, E. Lieberman, and W. C. Burnett. 2012. Air–water partitioning of ²²²Rn and its dependence on water temperature and salinity. *Environmental Science & Technology* **46**: 3905-3911,
- Smith, S., and J. Hollibaugh. 1993. Coastal metabolism and the oceanic organic carbon balance. *Reviews of Geophysics* **31**: 75-89,
- Spilmont, N., D. Davoult, and A. Migné. 2006. Benthic primary production during emersion: in situ measurements and potential primary production in the Seine Estuary (English Channel, France). *Marine Pollution Bulletin* **53**: 49-55,
- Thomas, H., L. Schiettecatte, K. Suykens, Y. Koné, E. Shadwick, F. Prowe, Y. Bozec, H. J. W. De Baar, and A. Borges. 2009. Enhanced ocean carbon storage from anaerobic alkalinity generation in coastal sediments. *Biogeosciences* **6**: 267-274,
- Walter, L. M., S. A. Bischof, W. P. Patterson, T. W. Lyons, R. O'nions, M. Gruszczynski, B. Sellwood, and M. Coleman. 1993. Dissolution and recrystallization in modern

- shelf carbonates: Evidence from pore water and solid phase chemistry [and discussion]. *Philosophical Transactions of the Royal Society of London. Series A: Physical and Engineering Sciences* **344**: 27-36,
- Walter, L. M., and E. A. Burton. 1990. Dissolution of recent platform carbonate sediments in marine pore fluids. *American Journal of Science* **290**: 601-643,
- Wang, Z., and W. Cai. 2004. Carbon dioxide degassing and inorganic carbon export from a marsh-dominated estuary (the Duplin River): A marsh CO₂ pump. *Limnology and Oceanography* **49**: 341-354,
- Wanninkhof, R. 1992. Relationship between wind speed and gas exchange. *Journal of Geophysical Research* **97**: 7373–7382,
- Wolanski, E., and P. Ridd. 1986. Tidal mixing and trapping in mangrove swamps. *Estuarine, Coastal and Shelf Science* **23**: 759-771,
- Xin, P., G. Jin, L. Li, and D. A. Barry. 2009. Effects of crab burrows on pore water flows in salt marshes. *Advances in water resources* **32**: 439-449,
- Zeebe, R., and D. Wolf-Gladrow. 2001. CO₂ in seawater: Equilibrium, kinetics, isotopes, Chapter. Elsevier Science.

4. Trends in alkalinity and inorganic carbon fluxes from estuaries across a land use gradient in South Eastern Australia

Peter A Faber¹, Ryan Woodland¹, Victor Evrard¹, Perran L M Cook¹

¹ Water Studies Centre, School of Chemistry, Monash University, Victoria 3800, Australia

4.1 Declaration for Thesis Chapter Four

Declaration by candidate

In the case of Chapter Four the nature and extent of my contribution to the work was the following:

Nature of contribution	Extent of contribution (%)
The majority of field work, laboratory analysis, data analysis and primary author	82.5

The following co-authors contributed to the work. If co-authors are students at Monash University, the extent of their contribution in percentage terms must be stated:


Name	Nature of contribution	Extent of contribution (%) for student co-authors only
Perran Cook	Assistance with study design, guidance and manuscript editing.	
Ryan Woodland	Assistance with field work, defining catchment impact and providing Appendix A	
Victor Evrard	Assistance with field work	

The undersigned hereby certify that the above declaration correctly reflects the nature and extent of the candidate's and co-authors' contributions to this work*.

Candidate's
Signature

	Date
--	------

Main
Supervisor's
Signature

	Date 18/04/14
---	------------------

4.2 Abstract

We used measurements of $\delta^{13}\text{C}_{\text{DIC}}$, Dissolved inorganic carbon (DIC), total alkalinity (TA) and calculated partial pressure of carbon dioxide (pCO_2) to determine the dominant modes of carbon transformation (photosynthesis, aerobic respiration, alkalinity generation, conservative) in eight Southern Australian temperate estuaries. By comparing estuaries with varying catchment land uses, we were able to calculate budgets and determine the differences in carbon dynamics under different degrees of land use impact. Most of the estuaries showed clear non-conservative mixing behaviour of DIC, TA and $\delta^{13}\text{C}_{\text{DIC}}$. The estuaries ranged between large sources and sinks of atmospheric CO_2 , with fluxes from $-17 - 502 \text{ mmol m}^{-2} \text{ d}^{-1}$. Differences in fluxes varied considerably between sampling periods highlighting the dynamic nature of carbon fluxes in estuaries. It was found that in highly impacted estuaries, there were often high rates of DIC production within the estuary (up to $510 \text{ mmol m}^{-2} \text{ d}^{-1}$) and this was often accompanied by high production of total alkalinity (up to $273 \text{ mmol m}^{-2} \text{ d}^{-1}$) indicating intense anaerobic respiration. Some estuaries exported large amounts of DIC (often as CO_2 efflux across the air-water interface) and exported little or no alkalinity indicating that their dominant mode of carbon transformation was aerobic respiration. The high rates of alkalinity production in systems dominated by anaerobic carbon transformation can be linked to increased Fe inputs from the catchment, which allows net alkalinity production via the burial of reduced sulfur following sulfate reduction. More impacted estuaries had higher rates of alkalinity production in general, but the relationship is complex in that the balance between iron sulfide burial and its reoxidation is a major factor influencing alkalinity fluxes, and the controllers on this balance are not well understood in estuaries.

4.3 Introduction

Estuaries have long been recognised as important links between terrestrial and coastal ecosystems, acting as transporters of terrestrially sourced materials to the coastal ocean (Martens and Goldhaber 1978). They are spatially and temporally diverse (Middelburg et al. 1996) and subject to tidal and seasonal variability and changes along the estuarine gradient. Due to typically high deposition rates of terrestrial and marine particulate matter in the lower estuary, these regions are hot spots for intense biological activity. Because estuaries act as an interface between the land and coastal ocean, the effects of anthropogenic land use on estuarine processes are likely to be pronounced (Smith and Hollibaugh 1993) and biogeochemical pathways may be noticeably altered (Rabouille et al. 2001). In recent times, anthropogenic influences on estuaries have attracted considerable interest due to environmental and economic concerns regarding phenomena such as algal blooms, eutrophication and fish deaths, which can negatively impact important industries such as fisheries and tourism. On a global scale, anthropogenic influences on biogeochemical pathways may be relevant to global carbon budgets, especially in the face of increased world population and associated increases in agriculture and urbanisation. Likewise, changes in climate such as precipitation regimes can considerably change inputs of carbon into rivers (Bauer et al. 2013).

4.3.1 Anaerobic alkalinity production

Alkalinity export from coastal regions can occur as a result of several processes, such as net denitrification, ammonia release, carbonate dissolution and sulfate reduction (Hammond et al. 1999). Among these, net denitrification and sulfate reduction have been shown to significantly contribute to the global fluxes of alkalinity from coastal marine

systems (Chen 2002; Thomas et al. 2009; Hu and Cai 2011a). Alkalinity budgets are also important when considering ocean carbon budgets, for instance, Thomas et al. (2009) showed that anaerobic alkalinity production in mudflats of the North Sea could facilitate up to 20-25% of the total uptake of atmospheric CO₂ in the area. Anaerobic alkalinity production accompanies organic carbon metabolism in the absence of oxygen. Within anoxic zones of sediments, organic carbon mineralisation relies on electron acceptors other than oxygen (Reeburgh 1983), including nitrate (NO₃⁻) and sulfate (SO₄²⁻) resulting in the processes of denitrification and sulfate reduction respectively (Berner et al. 1970; Canfield et al. 1993). The supply of Fe plays an important role in sulfate reduction, by forming FeS/FeS₂ which prevents reoxidation of the sulfide formed by sulfate reduction, allowing net alkalinity fluxes to occur. Anaerobic alkalinity production is important in coastal areas with significant inputs of oxidised Fe and NO₃⁻, and has been shown to be relevant globally to oceanic alkalinity fluxes (Chen 2002; Hu and Cai 2011a). Within intertidal areas, the importance of Fe to the carbon budget has been noted in our previous work (Faber et al. 2012), (Faber et al. submitted, Chapter 3) as it can control the fate of mineralised carbon by allowing net alkalinity fluxes.

With regard to the actual extent of alkalinity flux from coastal oceans, there is some uncertainty, with global estimates being highly variable. Hu and Cai (2011a) recently estimated an alkalinity flux of 4-5 Tmol yr⁻¹, produced by anaerobic processes in oceanic margins. This estimate is better constrained than previous estimates of 16- 31 Tmol yr⁻¹ (Chen 2002; Thomas et al. 2009) and is much lower. Nonetheless, this estimate still contains uncertainty, especially with regard to the contribution of sulfate reduction coupled with FeS/FeS₂ burial.

4.3.2 Fe input to estuaries

Fe is transported from catchments to coastal oceans in rivers, mostly as Fe-organic matter colloids (Boyle et al. 1977; Martin and Meybeck 1979; Haese 2000). The particulate nature of Fe entering estuaries leads to highly non-conservative mixing behaviour whereby ~90% of the Fe from the river water settles before entering the ocean (Boyle et al. 1977). For this reason, estuaries are particularly rich in Fe and are particularly influenced by changes in catchments, which control Fe supply to rivers. Increasing sediment supply to estuaries due to increases in anthropogenic land uses in river catchments has been well documented in the literature (Dunne 1979; Howarth et al. 1991; Hopkinson and Vallino 1995; Allan et al. 1997; Dauer et al. 2000; Neil et al. 2002). For instance, estimates of a fourfold increase in sediment delivery to the Great Barrier Reef lagoon of Australia since European settlement indicate that the main driver of increased sedimentation load is the increase in urbanisation and agriculture in river catchments (Alongi and Mckinnon 2005).

4.3.3 Determination of how catchment land use affects inorganic carbon and alkalinity export

Anthropogenic influences in catchments can significantly change carbon dynamics in estuaries. For instance, agriculture within catchments, which increases loadings of inorganic nutrients and organic carbon to rivers can cause more intense photosynthesis or respiration than would otherwise occur. This can have a direct effect on inorganic carbon cycling and whether an estuarine system acts as a sink or source of carbon to the atmosphere or ocean. In order to produce more constrained carbon budgets, consideration of anaerobic alkalinity production is vital. In previous work, we simulated

the effect of increasing Fe concentrations in intertidal sediments and determined that a large alkalinity flux resulted due to the enhanced storage of reduced sulfur (as FeS/FeS₂) in the sediment (Faber et al. 2012).

Changes in Fe loadings in an estuarine system may be one mechanism through which land use can affect alkalinity export. Widespread data on Fe loading to estuaries are generally not available, however total phosphorus has been extensively monitored in the state of Victoria. Given that there is a close positive correlation between TP and amorphous Fe (Ekholm et al. 2000; Jordan et al. 2008), we used long term TP as a proxy for Fe supply into estuaries in the present study.

Studying estuaries with different catchment land uses provides an opportunity to determine the variability of carbon dynamics in SE Australian estuarine systems as well as determining potential anthropogenic impacts on DIC and alkalinity production. In this paper, we make use of longitudinal and time series sampling campaigns to investigate carbon dynamics in eight contrasting SE Australian estuaries. Measurements of TA, DIC and $\delta^{13}\text{C}_{\text{DIC}}$ allow determination of the processes which are influencing the carbon cycle within the mixing zone of the estuary, and a basic approach to quantifying catchment impact (low, moderate or high) is used to make inferences about how catchment land use affects DIC and alkalinity export from estuaries.

4.4 Methods

4.4.1 Sites

Eight estuaries across Victoria, SE Australia were selected (**Fig. 4.1**) based on availability of data and covering a range of catchment land uses. Three general catchment land uses were recognised; forested, agricultural and urbanised, and a level of relative impact (low,

moderate and high) based on proportions of different types of catchment land use and effective total phosphorous (TP) loading data from 1990-2013, was applied to each site (**Table 4.1**) (See **Appendix 4A** at the end of this chapter for details). Historical effective TP loadings were considered in our measure of land use impact, as highly impacted catchments tend to export higher amounts of eroded material, which includes TP (Ekholm et al. 2000). The eight sites varied considerably in their surface area (**Table 4.1**) and geomorphology. Estuary surface areas were estimated from aerial images and included the extent of the estuary covered during a longitudinal sampling survey, which included both freshwater and saltwater endmembers.

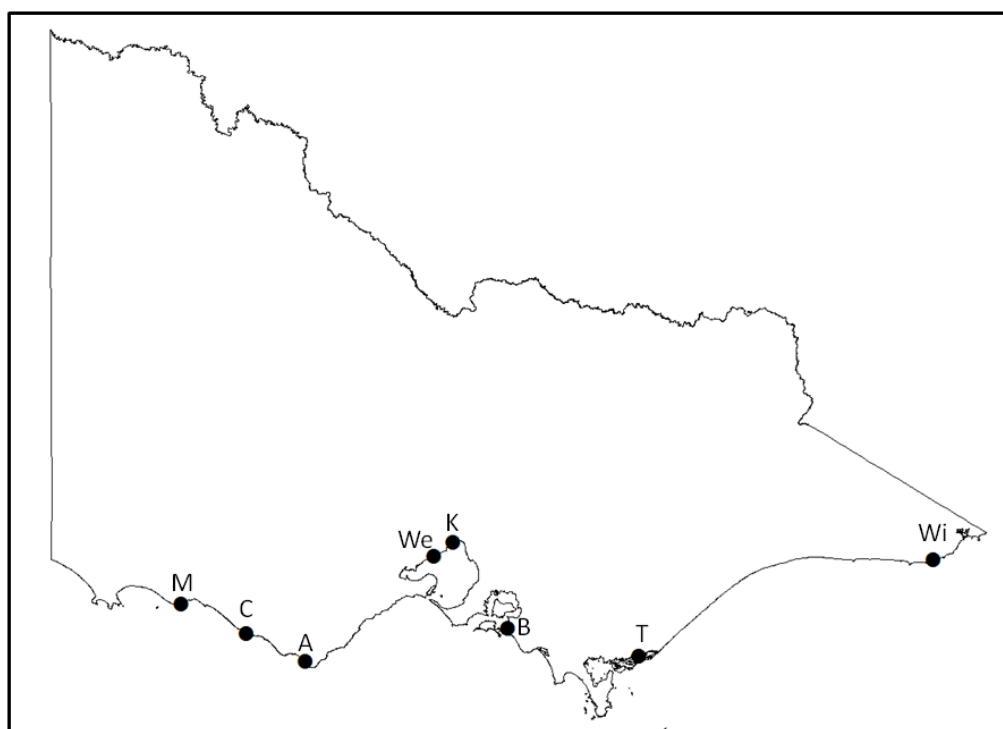


Figure 4.1: Estuary field sites in Victoria, SE Australia. From left to right; Moyne (M), Curdies (C), Aire (A), Werribee (We), Kororoit (K), Bass (B), Tarra (T) and Wingan (Wi).

The Aire (A), Curdies (C), Moyne (M) and Wingan (Wi) are wave dominated estuaries (According to National Land and Water Resources Audit: [URL: www.ozcoasts.gov.au/search_data/glossary_nlwra.jsp](http://www.ozcoasts.gov.au/search_data/glossary_nlwra.jsp)) . The Aire (A), Curdies (C) and Wingan (Wi) contained central basins and the Aire and Curdies were either closed or nearly closed during the sampling periods. The tidal influences on closed estuaries were negligible. The Aire and the Moyne (M) contained large saline lakes upstream of the main sampling areas. The Werribee (We) is a river dominated estuary whereas the Bass (B), Tarra (T) and Kororoit (K) are tide dominated estuaries and typically more narrow and consisted of a channel with a large intertidal zone of mangroves. The Kororoit estuary was partially isolated from Port Philip, a shallow bay, by a large and shallow sandbar which appeared to limit water exchange.

Table 4.1: Site abbreviation, total estuary surface area, effective total phosphorous (TP) loading from 1990-2013, catchment impact and primary catchment land use. Note effective TP loading is normalized to the surface area of the estuary.

Site	Site abbreviation	Total area (m ²)	Effective TP loading (g m ⁻² yr ⁻¹)	Relative impact	Dominant catchment land use
Aire	A	861000	0.15	Low	Forested
Bass	B	187000	2.2	High	Agriculture
Curdies	C	3380000	2.4	High	Agriculture
Kororoit	K	165000	2.7	High	Agriculture/urbanised
Moyne	M	1340000	0.51	Moderate	Agriculture
Tarra	T	357000	0.99	Moderate	Agriculture
Werribee	We	681000	1.6	High	Agriculture/urbanised
Wingan	Wi	1300000	0.16	Low	Forested

4.4.2 Sampling

Two sampling strategies were used; a longitudinal survey which included six sites covering the navigable extent of each estuary, and a time series which included both phases of tidal and diel cycle. For the longitudinal survey, the first and last sites were ocean and riverine (freshwater) end members respectively. The six sites were chosen to include a range of salinity values, but this was not always possible, as it depended on river flow and site accessibility. The longitudinal survey was conducted on board a small boat and samples for surface water were collected. If the water column at a site was stratified (determined from salinity profiles), bottom water was sampled using a Niskin bottle. At each site, samples were taken for total alkalinity (TA), dissolved inorganic carbon (DIC), partial pressure of CO₂ (pCO₂), $\delta^{13}\text{C}$, nitrate/nitrite (NO_x), ammonium (NH₄⁺), filterable reactive phosphorous (FRP), total phosphorous (TP) and total nitrogen (TN). Accompanying these samples, a Hydrolab DS5X multiprobe was used to measure temperature, salinity, pH, turbidity, chlorophyll-a, depth and dissolved oxygen (DO). The time, date and position coordinates were noted for each site. The time series sampling was conducted at a location close to the estuary mouth, within the main channel of the estuary. During the time series sampling, surface water was taken from the channel and sampled for TA, DIC, pCO₂ and $\delta^{13}\text{C}$ and multiprobe measurements, as above. For each time series survey, samples were taken over a 24 hr period of time, including samples after sunset and before sunrise to ensure a wide range of diel and tidal effects were sampled.

Samples of NO_x, NH₄⁺ and FRP were prepared by filtering water with a 0.45 μm Bonnet® filter and storing the filtrate in a cooler and frozen upon return to the laboratory. Total nitrogen (TN), total phosphorous (TP) were sampled by collecting unfiltered water and storing as above. Samples for TA were filtered a 0.45 μm Bonnet® and refrigerated in a cooler but were not allowed to freeze before analysis. For $\delta^{13}\text{C}_{\text{DIC}}$, DIC and pCO₂,

samples were taken using 12 ml Exetainer vials (Labco®, UK) and preserved with 20 µL of 6% w/w HgCl₂ solution. Atmospheric exchange of CO₂ was limited during sampling by having a ~10 cm piece of tubing attached to a syringe which was used to fill the vial, avoiding the formation of bubbles.

4.4.3 $\delta^{13}\text{C}$ of dissolved inorganic carbon

A 4 mL He headspace was placed in the preserved 12 mL water samples to which a 0.1 mL of H₃PO₄ (1 M) was added to liberate DIC as CO₂. Before analysis, vials were shaken vigorously for ~5 min to ensure equilibrium of CO₂ with the headspace. DIC present in the headspace was analysed on an ANCA GSL2 elemental analyser interfaced to a Hydra 20-22 continuous-flow isotope ratio mass-spectrometer (Sercon Ltd., UK). Analytical precision was $\pm 0.1\text{‰}$ for ^{13}C and stable isotope data are expressed in the delta notation ($\delta^{13}\text{C}$) relative to the stable isotopic ratio of the Vienna Pee Dee Belemnite standard ($R_{\text{VPDB}} = 0.0111797$).

4.4.4 Determination of DIC, pCO₂ and TA

Although DIC can be calculated from TA and pH (Zeebe and Wolf-Gladrow 2001), measurement of DIC using flow injection analysis (FIA) is fast, simple and effective, and is not subject to errors associated with in situ pH measurements which may occur due to the changing ionic strength in estuarine waters. DIC was measured using a FIA system with a gas diffusion membrane and acidic carrier stream. CO₂ liberated from the acidified sample diffuses across the membrane into a buffered acceptor stream, decreasing the pH of the solution. Bromothymol blue was used as an indicator in the acceptor stream, and its colour change due to pH change was detected photometrically.

Measurements were performed with a precision (RSD) of ~2%. Quantification of TA was using a modified Gran titration (Almgren et al. 1983) and a NBS buffer calibrated pH electrode attached to a portable Hach® HQ40d meter. The pCO₂ was calculated using TA and pH measurements (Zeebe and Wolf-Gladrow 2001) and our calculations included corrections of the equilibrium and Henry's constants for salinity and temperature.

4.4.5 CO₂ flux calculations

Fluxes of CO₂ across the water-air interface were estimated using pCO₂ measurements and wind speed obtained from the Bureau of Meteorology (Wanninkhof 1992; Raymond and Cole 2001). For each site, the closest weather station (generally within 10 km) was used to provide wind speed data. To estimate the overall CO₂ flux from each estuary, pCO₂ values from the time series were used and the CO₂ flux was calculated hourly and averaged. Our flux estimates do not account for the effect flow may have on the gas transfer coefficient due to lack of data. It is expected however that in some estuaries, flow may considerably increase CO₂ fluxes, therefore our estimates are probably lower than actual values. At the sites that lacked time series data, CO₂ flux estimates were calculated by averaging fluxes of CO₂ at each longitudinal sampling site, except the most upstream, which was excluded as it was representative of river water. In the flux calculation, the average wind speed over the sampling period was used to calculate the gas transfer coefficient. This method makes the assumption that pCO₂ change over the diurnal cycle is negligible.

4.4.6 Dissolved inorganic carbon and alkalinity budgets

At steady state, total fluxes of inorganic carbon to the ocean can be estimated as the sum of fluvial inputs into the estuary and the inputs or removal fluxes within the estuary (Kaul and Froelich 1984). The components of our inorganic carbon budget are shown as a schematic diagram (**Fig. 4.2**), which includes fluvial input of DIC (FI_{DIC}), total export of DIC to the ocean (TE_{DIC}), DIC flux within the estuary (EF_{DIC}) and the atmospheric flux of CO_2 (F_{CO_2}).

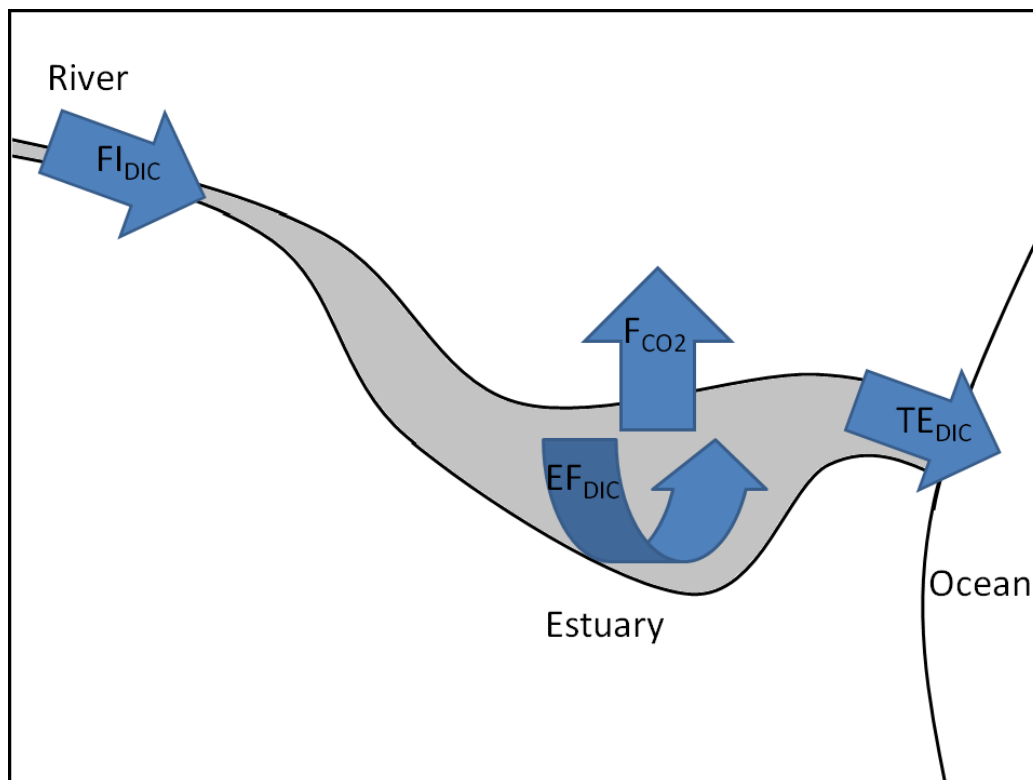


Figure 4.2: Diagram indicating fluxes within an open-mouth estuary, including fluvial input of DIC (FI_{DIC}), estuarine flux of DIC (EF_{DIC}), CO_2 flux across the water-atmosphere interface (F_{CO_2}) and total export of DIC (TE_{DIC}).

Mass balances for DIC were constructed using fluvial inputs of DIC, atmospheric CO_2 fluxes and DIC exports to the ocean (see: (Gazeau et al. 2005a)). For several of the

estuaries, export to the ocean was assumed to be negligible due to the estuary mouth being closed. In these systems, fluvial inputs and CO₂ fluxes to the atmosphere were still considered, though it was noted that during the sampling time, DIC export to the ocean was probably not an important process.

Fluvial input of DIC (FI_{DIC}) in mmol m⁻² d⁻¹ was estimated using **Eq. 4.1**

$$FI_{DIC} = (\rho DIC_0 Q)/S \quad (4.1)$$

Where DIC₀ is the DIC measured in the freshwater endmember in mmol kg⁻¹, ρ is the density of the water in kg m⁻³ at this site, Q is the average riverine flow during the sampling period in m³ d⁻¹ and S is the surface area of the estuary in m² (as measured from the estuary mouth to the upstream site.)

The total export of DIC to the ocean (TE_{DIC}) in mmol m⁻² d⁻¹ from the estuary was estimated using **Eq. 4.2**:

$$TE_{DIC} = (\rho DIC_{AZE} Q)/S \quad (4.2)$$

Where DIC_{AZE} is the apparent zero end member of DIC in mmol kg⁻¹, ρ is the density of the water in kg m⁻³ at this site, Q is the average riverine flow during the sampling period in m³ d⁻¹ and S is the surface area of the estuary in m². DIC_{AZE} was determined using DIC and salinity data from the longitudinal and time series surveys. For most sites, The DIC_{AZE} was the y-intercept of the DIC vs. salinity plot when DIC values for salinities above 20 were considered. Above a salinity of 20, the estuaries appeared to act more conservatively. The intercept was determined with a linear regression. In several cases, there was insufficient data to calculate the DIC_{AZE}, as freshwater inputs were too low to produce a salinity gradient in the sampled extent of the estuary. In these low flow conditions, fluvial DIC input and CO₂ flux were considered, but DIC production within the estuary could not be determined.

Using TE_{DIC} and FI_{DIC} we can estimate DIC flux within the estuary (EF_{DIC}) in $mmol\ m^{-2}\ d^{-1}$ using **Eq. 4.3**:

$$EF_{DIC} = TE_{DIC} + F_{CO_2} - FI_{DIC} \quad (4.3)$$

where F_{CO_2} is the atmospheric flux of CO_2 . This calculation assumes that the pCO_2 within the estuary was at steady state, or that the average fluxes across the water-air interface were equal to average CO_2 production or consumption. The term TE_{DIC} relies on river flow and assumes steady state between water input (Q) and output to the ocean. In the case of closed-mouth estuaries, there is no such steady state, meaning that calculation of TE_{DIC} is not possible. Likewise, EF_{DIC} , which relies on TE_{DIC} cannot be determined.

The components of the alkalinity budget were determined in the same way as DIC with the **Eq. 4.1-4.3** being adapted for TA measurements. The TA apparent zero endmember (TA_{AZE}) was calculated in the same way as DIC_{AZE} , using measurements of TA in samples with salinity >20 . The TA budget thus included these terms analogous to those used in the DIC budget: fluvial input of TA (FI_{TA}), total export of TA to the ocean (TE_{TA}) and TA flux within the estuary (EF_{TA}). The only difference between the DIC and TA budgets was the calculation of EF_{TA} compared to EF_{DIC} , as F_{CO_2} does not affect EF_{TA} as it does EF_{DIC} (**Eq. 4.4**).

$$EF_{TA} = TE_{TA} - FI_{TA} \quad (4.4)$$

The terms EF_{TA} and EF_{DIC} provide a means to interpret carbon transformation within each estuary and determine the relative importance of anaerobic and aerobic processes. The term EF_{DIC} is a measure of the net DIC flux occurring within the estuary as a product of aerobic and anaerobic processes as well as air-water fluxes. Contrasting this, EF_{TA} is representative of alkalinity producing processes only, and in the current study is a measure of the importance of anaerobic respiration.

4.4.7 DIC sources

The $\delta^{13}\text{C}_{\text{DIC}}$ of the fluvial DIC input influences the $\delta^{13}\text{C}_{\text{DIC}}$ observed in the estuary and exported to the ocean, but does not give an indication of the $\delta^{13}\text{C}_{\text{DIC}}$ resulting from processes occurring within the estuary ($\delta^{13}\text{C}_{\text{Est}}$). Several studies use $\delta^{13}\text{C}$ and DIC mass balances to calculate the $\delta^{13}\text{C}$ of the processes occurring in sediment (Hu and Burdige 2007) or to calculate the proportion of DIC added via a specific pathway (mangroves) (Miyajima et al. 2009). Our approach considered the input of DIC from marine and riverine sources, and determined the $\delta^{13}\text{C}_{\text{DIC}}$ of DIC unaccounted for by the conservative mixing model. To calculate $\delta^{13}\text{C}_{\text{Est}}$ for a single sample 'x' of estuarine water, **Eq. 4.5** was used:

$$\delta^{13}\text{C}_{\text{Est}} = (\delta^{13}\text{C}_x \text{DIC}_x - \delta^{13}\text{C}_{\text{CMM}} \text{DIC}_{\text{CMM}}) / (\text{DIC}_x - \text{DIC}_{\text{CMM}}) \quad (4.5)$$

where $\delta^{13}\text{C}_x$ and $\delta^{13}\text{C}_{\text{CMM}}$ are the actual and conservative mixing model $\delta^{13}\text{C}_{\text{DIC}}$ values (‰), respectively, of a single sample, and DIC_x and DIC_{CMM} are the actual and conservative mixing model DIC concentrations (mM), respectively, of a single sample. The values of $\delta^{13}\text{C}_{\text{Est}}$ in each sample were only used when the magnitude of the term $(\text{DIC}_x - \text{DIC}_{\text{CMM}})$ was >0.1 mM, which was arbitrarily chosen based on the observation that when the magnitude of this term was <0.1 mM, values of $\delta^{13}\text{C}_{\text{Est}}$ tended to be unrealistically high due to the term being the denominator in **Eq. 4.5** and amplifying any error present.

The values of $\delta^{13}\text{C}_x$ and DIC_x were the measured values obtained from each sample 'x', whereas DIC_{CMM} and $\delta^{13}\text{C}_{\text{CMM}}$ were calculated according to **Eq. 4.6** and **Eq. 4.7** (Miyajima et al. 2009):

$$\text{DIC}_{\text{CMM}} = (\text{S}_x \text{DIC}_m + (\text{S}_m - \text{S}_x) \text{DIC}_r) / \text{S}_m \quad (4.6)$$

$$\delta^{13}\text{C}_{\text{CMM}} = (\text{S}_x \text{DIC}_m \delta^{13}\text{C}_m + (\text{S}_m - \text{S}_x) \text{DIC}_r \delta^{13}\text{C}_r) / \text{S}_m \text{DIC}_{\text{CMM}} \quad (4.7)$$

Where S_x and S_m are the salinity values of a sample and the marine endmember respectively, DIC_m and DIC_r are the DIC concentrations of the marine and riverine endmembers respectively and $\delta^{13}\text{C}_m$ and $\delta^{13}\text{C}_r$ are the $\delta^{13}\text{C}_{\text{DIC}}$ values of the marine and riverine endmembers respectively. These equations assume that the salinity of the riverine endmember is zero. Mixing plots of DIC_{CMM} vs. salinity are always linear whereas conservative mixing of $\delta^{13}\text{C}_{\text{DIC}}$ is only linear if the $\delta^{13}\text{C}_{\text{DIC}}$ of the river is equal to the $\delta^{13}\text{C}_{\text{DIC}}$ of seawater (unlikely), or if the DIC in the river is equal to the DIC in seawater, which is possible considering the large range of DIC values found in fresh water.

4.4.8 Calculation of TP loading

Effective total phosphorus (TP) loads for each estuary were calculated from river flow (ML d^{-1}) and TP concentration (mg L^{-1}) data downloaded from the Victoria Department of Environment and Primary Industries website (<http://data.water.vic.gov.au/monitoring.htm>). Effective TP loads per unit area of the receiving estuaries ($\text{g m}^{-2} \text{yr}^{-1}$) for the period 1990-2013 were calculated using a flow stratified Kendall's ratio estimator (Kendall et al. 1983) implemented in Excel with a VBA-coded algorithm (Tan et al. 2005).

4.5 Results

4.5.1 Fluvial inputs

The fluvial inputs varied considerably between estuaries, both in terms of flow (0-70200 $\text{m}^3 \text{d}^{-1}$) and in terms of concentrations of DIC (0-8.6 mmol L^{-1}) and TA (006-8.7

mmol L⁻¹) (**Table 4.2**). The fluvial concentrations of DIC and TA at Wingan River were consistently low over all three sampling periods (0-0.21 and 0.06-0.14 mmol L⁻¹ for DIC and TA respectively) and were the lowest out of all the rivers entering the eight estuaries. The Moyne River had the highest DIC (5.8-8.6 mmol L⁻¹) concentrations during all three samplings periods, which was accompanied with a relatively high TA. The Curdies River and the Kororoit Creek had fluvial DIC and TA concentrations which were well above average seawater concentrations (average seawater: ~2.1 and ~2.3 mmol L⁻¹ respectively). The Bass River and the Werribee River had concentrations of TA and DIC which were slightly elevated with regard to seawater, except during campaign 1, when river flows were much higher. River flows varied considerably, and were generally the highest during campaign 1 (20400 – 702000 m³ d⁻¹) and the lowest during campaign 3 (0-35800 m³ d⁻¹).

Table 4.2: Riverine DIC concentrations, TA concentrations and average river flow at the field sites during each campaign

Impact	Site	Fluvial DIC (mmol L ⁻¹)	Fluvial TA (mmol L ⁻¹)	Fluvial inflow (m ³ d ⁻¹)
<i>Campaign 1</i>				
Low	A	0.36	0.45	219160
	Wi	0	0.10	93401
Moderate	M	5.8	5.2	38866
	T	1.6	0.86	66342
High	B	1.3	1.1	701961
	C	4.8	4	378244
	K	2.6	3.3	20402
	We	1.7	1.5	211823
<i>Campaign 2</i>				
Low	A	0.91	0.41	91391
	Wi	0.21	0.06	83081
Moderate	M	8.6	7.1	7607
	T	1.7	0.87	35627
High	B	2.9	2.9	10110
	C	5	5.2	16828

	K	7.9	6.1	3730
	We	2.6	3.9	73087
<hr/>				
	<i>Campaign 3</i>			
Low	A	1	1.2	35806
	Wi	0.12	0.14	5815
Moderate	M	7.8	7.1	4172
	T	1.3	1	8476
High	B	2.8	3.3	7539
	C	4.4	5.2	558
	K	4.5	8.7	5629
	We	3.3	3.6	0

4.5.2 Carbon budget

Components of the inorganic carbon budget considered include FI_{DIC} , TE_{DIC} , F_{CO_2} and EF_{DIC} (**Table 4.3**). FI_{DIC} varied considerably between estuaries, being dependant on river discharge and the DIC of the freshwater endmember. The FI_{DIC} is clearly the highest in Bass estuary during campaign 1. Flooding during this sampling period meant that the river flow was ~100 times higher than the same river during campaign 3. The high river input coupled with a relatively high DIC (1.3 mM) meant that ~4890 mmol m⁻² d⁻¹ of DIC was exported as TA and CO₂. This flood event also precluded collection of data with any spatial or temporal variation as the estuary was highly flushed making a complete inorganic carbon budget difficult to determine. For this site and period, EF_{DIC} was assumed to be equal to F_{CO_2} , as all longitudinal samples were essentially the same as the riverine endmember with regard to salinity, DIC and TA.

Table 4.3: Carbon budget of the eight estuaries. Included is fluvial DIC input (FI_{DIC}), total ocean export of DIC (TE_{DIC}), atmospheric flux of CO₂ (F_{CO_2}) and estuarine flux of DIC (EF_{DIC}). Negative CO₂ fluxes represent a flux of CO₂ into the estuary from the atmosphere. Note: In several estuaries, the estuary mouth is closed and in these cases, TE_{DIC} and EF_{DIC} are not present. *The Bass estuary was in flood during campaign 1, so

there was no variation in TA or DIC along the estuarine gradient. In this case, TE_{DIC} was assumed to be equal to FI_{DIC} .

Impact	Site	FIDIC (mmol m ⁻² day ⁻¹)	TEDIC (mmol m ⁻² day ⁻¹)	FCO ₂ (mmol m ⁻² day ⁻¹)	EFDIC (mmol m ⁻² day ⁻¹)
<i>Campaign 1</i>					
Low	A	91	-	502	-
	Wi	0	34	5	39
Moderate	M	169	146	0	-23
	T	289	190	16	-83
High	B	4894	*4894	59	59
	C	535	-	23	-
	K	324	451	15	142
	We	526	973	63	510
<i>Campaign 2</i>					
Low	A	97	-	95	-
	Wi	14	14	41	1
Moderate	M	49	26	-3	-26
	T	169	211	38	80
High	B	157	196	34	73
	C	25	-	-17	-
	K	179	285	38	144
	We	284	406	25	147
<i>Campaign 3</i>					
Low	A	43	-	178	-
	Wi	1	2	77	78
Moderate	M	24	0	0	-24
	T	31	72	181	222
High	B	115	213	28	126
	C	1	-	-10	-
	K	154	125	66	37
	We	0	0	77	77

Curdies and Aire had either completely or nearly closed estuary mouths during each of the three sampling periods. In these cases, the TE_{DIC} is assumed to be nil, as water is not being exported to the ocean in high amounts. The limitation of this inorganic carbon budget approach in estuaries with closed mouths suggests that only FI_{DIC} and F_{CO_2} should

be considered and therefore we excluded EF_{DIC} from the budget and subsequent estuary comparisons. Fluvial input of DIC and TA was very dependent on river flow and at every site, the greatest flow during early spring was accompanied with a higher fluvial DIC input (**Table 4.3**). One inconsistency to this was the FI_{DIC} at Kororoit Creek which showed a higher DIC input during summer compared to autumn despite a lower flow, which was driven by the much higher DIC concentration measured in the freshwater endmember during the summer sampling period.

When comparing carbon fluxes between sites (**Table 4.3**), there was considerable variation in all components of the carbon budget. Fluvial input of DIC ranged between $4894 \text{ mmol m}^{-2} \text{ d}^{-1}$ at Bass during the flood on campaign 1 and close to $0 \text{ mmol m}^{-2} \text{ d}^{-1}$ during low flow conditions in campaign 3 at Wingan, Werribee and Curdies. Fluvial input of DIC was negligible at Wingan during campaign 1 due to the low concentration of DIC in the river water. With regard to pCO_2 fluxes, the estuaries ranged between sources and sinks of CO_2 , with fluxes out of the estuary as high as $502 \text{ mmol m}^{-2} \text{ d}^{-1}$ from the Aire in campaign 1, and as high as $17 \text{ mmol m}^{-2} \text{ d}^{-1}$ into the estuary at Curdies during campaign 2. EF_{DIC} ranged between $-83 \text{ mmol m}^{-2} \text{ d}^{-1}$ in Tarra during campaign 1 and $510 \text{ mmol m}^{-2} \text{ d}^{-1}$ in Werribee during campaign 1, representing both net autotrophic and net heterotrophic conditions respectively.

The TA exports varied considerably between estuaries and campaigns (**Table 4.4**). The Bass estuary was observed to export the most TA ($3807 \text{ mmol m}^{-2} \text{ d}^{-1}$) and this occurred during the flood event on campaign 1 and was comprised completely of FI_{TA} . The values of EF_{TA} varied from $-31 \text{ mmol m}^{-2} \text{ d}^{-1}$ at the Kororoit estuary during campaign 3, to $273 \text{ mmol m}^{-2} \text{ d}^{-1}$ at the Werribee estuary during campaign 1. In many estuaries, FI_{TA} was greater than EF_{TA} indicating that much of the TA being exported is either from catchments or from riverine processes.

Table 4.4: Alkalinity budget of the eight estuaries. Included is fluvial TA input (FI_{TA}), total ocean export of TA (TE_{TA}) and estuarine flux of TA (EF_{TA}). Note: In several estuaries, the estuary mouth is closed and in these cases, TE_{TA} and EF_{TA} are not present.

*The Bass estuary was in flood during campaign 1, so there was no variation in TA or DIC along the estuarine gradient. In this case, TE_{TA} was assumed to be equal to FI_{TA} .

Impact	Site	FI_{TA} (mmol m ⁻² d ⁻¹)	TE_{TA} (mmol m ⁻² d ⁻¹)	EF_{TA} (mmol m ⁻² d ⁻¹)
<i>Campaign 1</i>				
Low	A	113	-	-
	Wi	8	24	17
Moderate	M	151	186	36
	T	160	257	98
High	B	3807	*3807	0
	C	442	-	-
	K	410	592	182
	We	455	728	273
<i>Campaign 2</i>				
Low	A	44	-	-
	Wi	4	13	9
Moderate	M	40	38	-2
	T	87	122	35
High	B	157	180	23
	C	26	-	-
	K	138	310	172
	We	418	414	-4
<i>Campaign 3</i>				
Low	A	49	-	-
	Wi	1	0	0
Moderate	M	22	24	2
	T	25	40	15
High	B	132	202	69
	C	1	-	-
	K	295	264	-31
	We	0	0	0

4.5.3 Mixing plots

Mixing plots of DIC, TA and $\delta^{13}\text{C}_{\text{DIC}}$ (**Appendix 4B**) were produced from a combination of time series measurements and longitudinal measurements. Conservative mixing patterns of DIC and TA depend on the DIC and TA concentration of the freshwater inputs and are linearly dependant on salinity. When the concentrations of these species are higher in the freshwater than seawater, the concentration is expected to decrease as salinity increases, as the two sources of water mix. When the concentration of DIC and TA is lower in the freshwater inputs, the concentration given by the conservative mixing model increases as the proportion of seawater in the sample increases. The conservative mixing line for DIC and TA is always linear, with its range extending to both the freshwater and the seawater endmembers. The measured concentrations of DIC, TA and $\delta^{13}\text{C}_{\text{DIC}}$ often differed from the conservative mixing line (**Appendix 4B**). For several data sets (Bass during campaign 1, Moyne during campaign 1 and 3) there were limited points along the salinity gradient, so mixing plots lack sufficient completeness to observe any non-conservative behaviour occurring. In some cases, (TA sample from Bass during campaign 1 and $\delta^{13}\text{C}_{\text{DIC}}$ sample from Wingan during campaign 2) endmember samples were not available, so conservative mixing lines are not present.

The $\delta^{13}\text{C}_{\text{DIC}}$ plots always showed a lower value in the freshwater endmembers, which was generally from -10 to -13 but ranged from -8.2 to -17.0 compared to the seawater endmembers, which were generally between 0 and 2 and ranged from -2.4 to 2.3. The hyperbolic conservative mixing lines follow **Eq. 4.7**. It is evident that for some sites where riverine DIC concentration is close to seawater DIC concentration, the $\delta^{13}\text{C}_{\text{DIC}}$ mixing plots are approaching linearity. For most sites, $\delta^{13}\text{C}_{\text{DIC}}$ mixes non-conservatively, with most data in the mixing plots being of lower values than the conservative mixing line.

4.5.4 Estuarine changes in DIC and $\delta^{13}\text{C}_{\text{DIC}}$

Because $\delta^{13}\text{C}_{\text{Est}}$ is representative of the $\delta^{13}\text{C}_{\text{DIC}}$ of the net processes affecting DIC within the estuary (and accounts for DIC inputs from the river and the ocean), it can provide a means to determine how estuarine processes are affecting $\delta^{13}\text{C}_{\text{DIC}}$. The plots in **Fig. 4.3** show plots of $\delta^{13}\text{C}_{\text{Est}}$ and ΔDIC along the salinity gradient and can be used to determine the major changes in DIC and $\delta^{13}\text{C}_{\text{Est}}$ within the estuary. In several instances, such as at the Aire and Curdies estuaries and at the Moyne estuary during campaign 3, there was insufficient data across a salinity gradient, so time series plots of DIC and $\delta^{13}\text{C}_{\text{Est}}$ were produced which indicate changes in these measurements over a diurnal cycle (**Fig. 4.4**). As expected, based on the mixing plots, the values of ΔDIC in most estuaries are most often positive, although both positive and negative values were common.

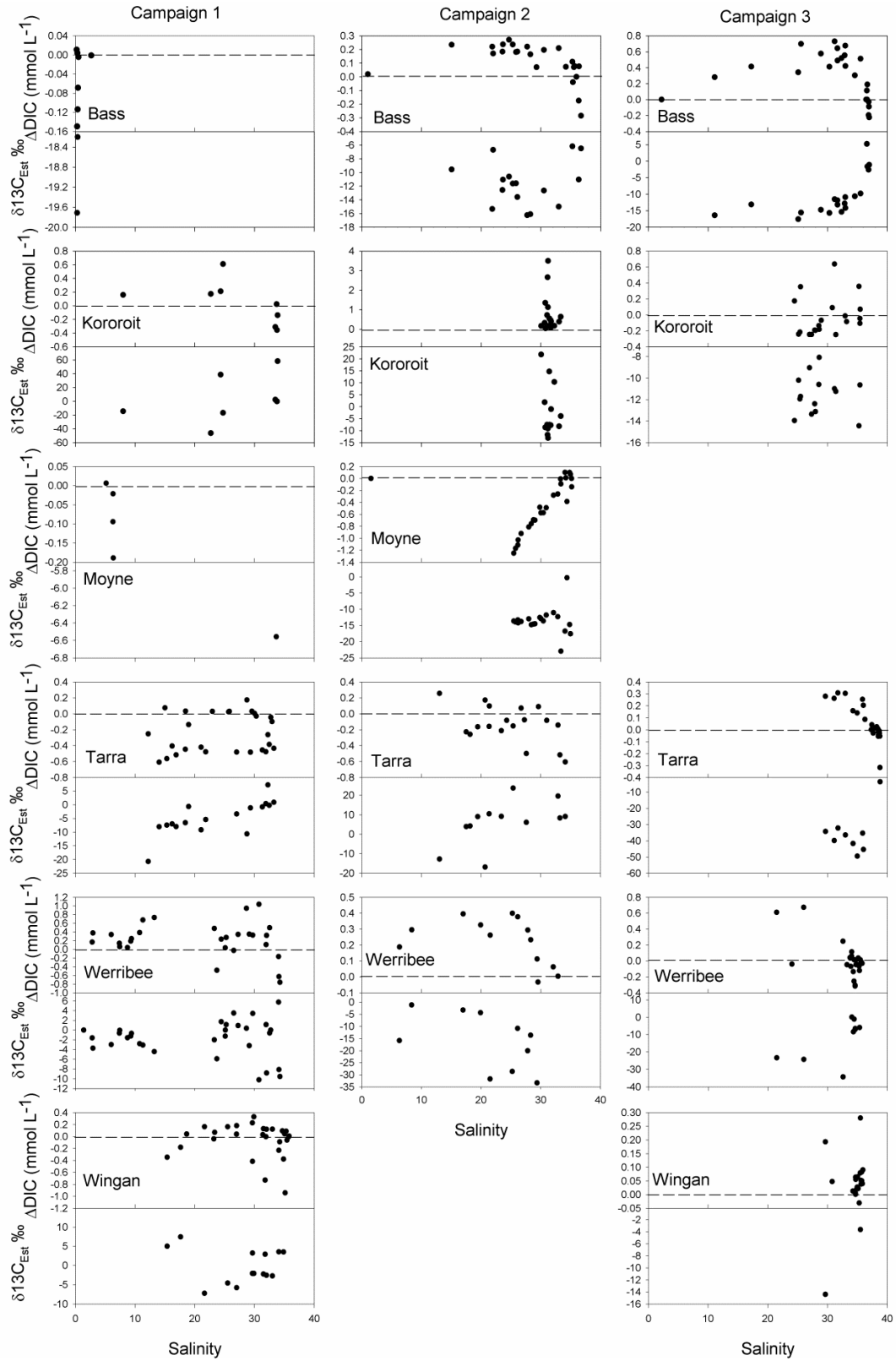


Figure 4.3: Plots of calculated ΔDIC (deviation from conservative mixing) and $\delta^{13}\text{C}_{\text{Est}}$ vs. salinity for sites with sufficient mixing data. Above and below the dashed line represents production and consumption of DIC respectively.

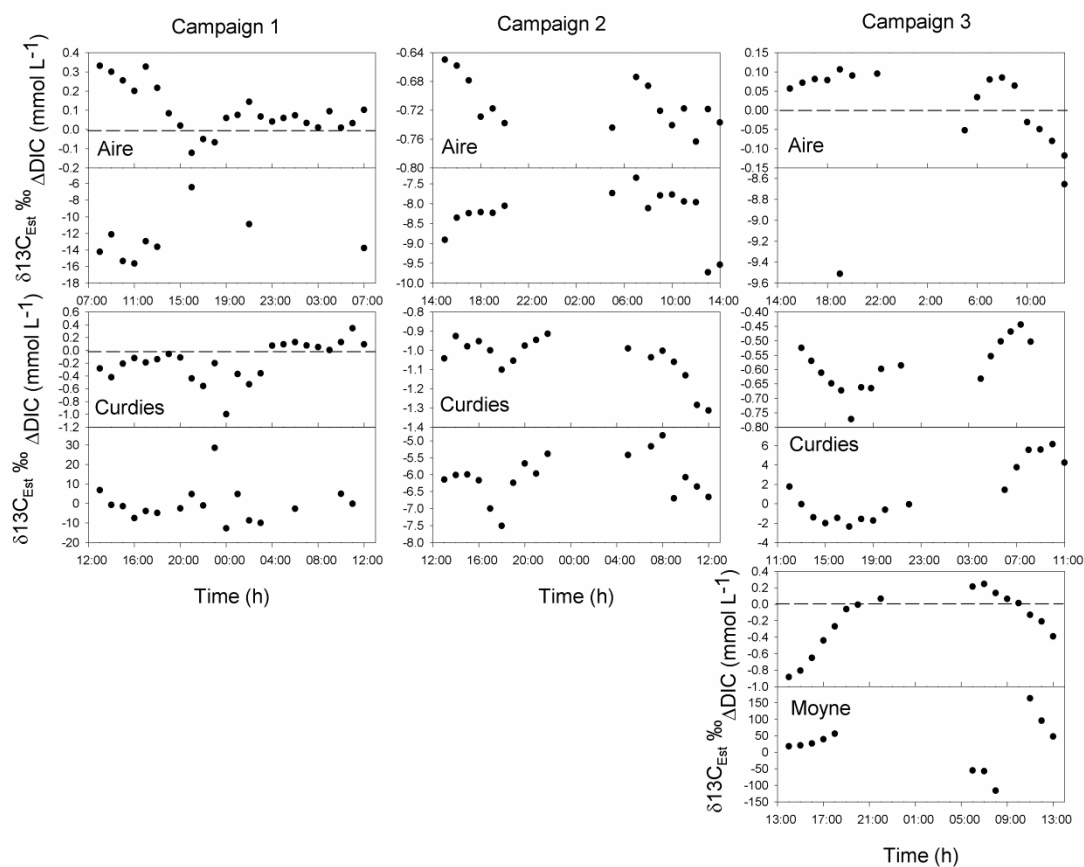


Figure 4.4: Plots of calculated ΔDIC and $\delta^{13}\text{C}_{\text{Est}}$ vs. time for sites where diurnal effects were the dominant factors affecting carbon dynamics. Above and below the dashed line represents production and consumption of DIC respectively.

4.6 Discussion

4.6.1 Fluvial inputs of inorganic carbon

The total fluvial input of DIC and TA was highly influenced by river flow and in most cases, fluvial input of these species accounted for the majority of total export (**Table 4.2**). This is unsurprising considering the high DIC and TA concentrations in some of the freshwater samples (up to 8.6 mM and 7.1 mM for DIC and TA respectively). These high

values may reflect the high rate of organic matter breakdown and denitrification in the river as well as the catchment geology which may contain significant quantities of carbonate and silicate bearing soils and rocks, which contribute DIC upon erosion. Negative $\delta^{13}\text{C}_{\text{DIC}}$ values for freshwater samples are typical, as a substantial amount of DIC within rivers is presumed to be produced from the breakdown of terrestrial C3 derived organic carbon which has a $\delta^{13}\text{C}$ of approximately -28‰ (O'leary 1988). Freshwater $\delta^{13}\text{C}_{\text{DIC}}$ is expected to have a value somewhere between the $\delta^{13}\text{C}$ of mineral carbonate (~0‰) and biogenic carbon (~-28‰), with typical freshwater $\delta^{13}\text{C}_{\text{DIC}}$ values usually being close to -12‰ (Spiker 1980). The freshwater samples observed at our sites ranged from -17‰ at the Wingan to -8.5‰ at the Kororoit. This large range in freshwater $\delta^{13}\text{C}_{\text{DIC}}$ may reflect the relative contributions of carbonate dissolution and organic matter breakdown in the catchment as well as rates of atmospheric exchange of CO_2 and photosynthesis, which tend to result in more positive $\delta^{13}\text{C}_{\text{DIC}}$ values. The catchment of the Wingan River in particular is heavily forested, and the low fluvial TA ($<0.15 \text{ mmol L}^{-1}$), DIC ($<0.21 \text{ mmol L}^{-1}$) and $\delta^{13}\text{C}_{\text{DIC}}$ (~-17‰) indicate that DIC contributions from eroded terrestrial minerals are low in comparison to the freshwater endmembers of the other sites.

4.6.2 Estuarine fluxes of CO_2

The flux of CO_2 is typically high in estuaries with highly impacted catchments as shown by the highly supersaturated pCO_2 seen in many impacted European, North American and Asian estuaries (Frankignoulle et al. 1996; Frankignoulle et al. 1998; Cai et al. 1999; Raymond et al. 2000; Frankignoulle and Borges 2001; Wang and Cai 2004; Zhai et al. 2005; Borges et al. 2006). It is also common for some estuaries to exhibit undersaturated pCO_2 spatially and seasonally as a result of intense photosynthesis due to abundant nutrients from terrestrial runoff (Boehme et al. 1998; Raymond et al. 2000). Of

the estuaries surveyed in this work, there are examples of both sinks and sources of CO₂ to the atmosphere (**Table 4.3**). The flux of CO₂ from the Aire was consistently the highest (up to 502 mmol m⁻² d⁻¹ during campaign 1), this being a reflection of the high pCO₂ (>3000 µatm) which was maintained throughout the sampling periods during each campaign. The reason for the high pCO₂ was evidently the closed estuary mouth, which prevented flushing by seawater and created a lagoon with low salinity and relatively unbuffered high pCO₂ water. The closed estuary mouth, and low kinetic energy of the system may have favoured deposition of terrestrial organic matter, leading to intense microbial respiration. The Bass, Kororoit, Tarra, Werribee and Wangan estuaries were also sources of CO₂ during each campaign, and fluxes were generally higher during campaign 1. The generally higher fluxes of CO₂ during campaign 1 were due to the higher river flows during this time, which increased the extent of the high pCO₂ freshwater in the estuary and may have exported greater amounts of organic carbon to the estuary. The Curdies and Moyne estuaries acted as net sinks of CO₂ during campaign 2, with CO₂ fluxes of -17 mmol m⁻² d⁻¹ at the Curdies and -3 mmol m⁻² d⁻¹ at the Moyne. The Moyne did not act as a strong sink or source during campaign 1 and 3 whereas the Curdies acted as a source of CO₂ in campaign 1 (23 mmol m⁻² d⁻¹) and a sink in campaign 3 (-10 mmol m⁻² d⁻¹). In these two estuaries, the pCO₂ was most often undersaturated within the surface water reflecting a high rate of carbon fixation by primary producers. Measurements of O₂ in these two estuaries were nearly always supersaturated, and only dropped below 100% saturation during night time (data not shown). During each campaign, there were extensive beds of seagrass and macroalgae at the Moyne, and macroalgae at the Curdies, which were presumed to be the main contributors to the low pCO₂ condition via photosynthesis. Despite both these systems being autotrophic, there were significant differences in estuary flushing. Where the Moyne estuary was well

flushed and subject to tidal flows, the estuary mouth of Curdies was either partially or completely closed during each campaign. Typically, $p\text{CO}_2$ and O_2 showed diurnal changes, with higher $p\text{CO}_2$ levels occurring at night, when photosynthesis was not occurring. The $p\text{CO}_2$ and O_2 at the Werribee estuary showed strong diurnal changes up to $1300 \mu\text{atm}$ for $\Delta p\text{CO}_2$ and 96% for ΔO_2 saturation during each campaign (data not shown) indicating high rates of photosynthesis and respiration resulting from the high availability of nutrients and labile organic matter. The observation of high variability in respiration within the Werribee estuary is common in highly anthropogenically impacted waterways as they tend to have elevated carbon loadings and at times, intense primary production (Nixon 1995) due to nutrient inputs.

4.6.3 Non-conservative behaviour in DIC, TA and $\delta^{13}\text{C}_{\text{DIC}}$

The non-conservative behaviour of DIC that was observed in the mixing plots (**Appendix 4B**) can be a result of several processes. Increases in DIC can occur due to aerobic and anaerobic respiration (sulfate reduction), atmospheric influx of CO_2 into the estuary, and carbonate dissolution. Photosynthesis, flux of CO_2 to the atmosphere and carbonate precipitation are processes that consume inorganic carbon, leading to lower than conservative DIC values. Respiration and photosynthesis can both occur along an estuarine gradient leading to production and consumption of DIC respectively as well as either undersaturation or supersaturation of $p\text{CO}_2$. Respiration and photosynthesis are both likely to occur in estuaries, due to the high availability of labile organic carbon and inorganic nutrients.

Non-conservative behaviour in TA may be due to anaerobic alkalinity production, which leads to increases in TA, or carbonate dissolution/precipitation, which leads to

decreases or increases in TA respectively. These processes also affect DIC as they involve the production or removal of inorganic carbon. The oxidation of reduced sulfides, which are a product of sulfate reduction can also cause consumption of TA, but not DIC, unless the decrease in pH associated with this reaction facilitates higher CO₂ fluxes to the atmosphere.

Non-conservative behaviour of $\delta^{13}\text{C}_{\text{DIC}}$ may be due to several processes (Miyajima et al. 2009). In estuaries, the $\delta^{13}\text{C}_{\text{DIC}}$ is a result of the mixing of seawater, which typically has a $\delta^{13}\text{C}_{\text{DIC}}$ of around 2‰, and river water, with a $\delta^{13}\text{C}_{\text{DIC}}$ of ~-12‰ as well as physical and biological processes occurring within the estuary. Processes that add carbon directly to the DIC pool, such as organic matter degradation, tend to decrease $\delta^{13}\text{C}_{\text{DIC}}$ towards a value equal to the $\delta^{13}\text{C}$ of the organic matter source. Likewise, carbonate dissolution increases $\delta^{13}\text{C}_{\text{DIC}}$, towards the $\delta^{13}\text{C}_{\text{DIC}}$ of the carbonate (typically around 0‰). Processes involving the removal of DIC from the system are associated with kinetic isotope fractionation, for instance CO₂ efflux into the atmosphere, carbonate precipitation and photosynthesis lead to more positive $\delta^{13}\text{C}_{\text{DIC}}$ values. Isotopic exchange of dissolved CO₂ with atmospheric CO₂ forces $\delta^{13}\text{C}_{\text{DIC}}$ to equilibrium values (0‰), so will generally increase the $\delta^{13}\text{C}_{\text{DIC}}$ in rivers and estuaries.

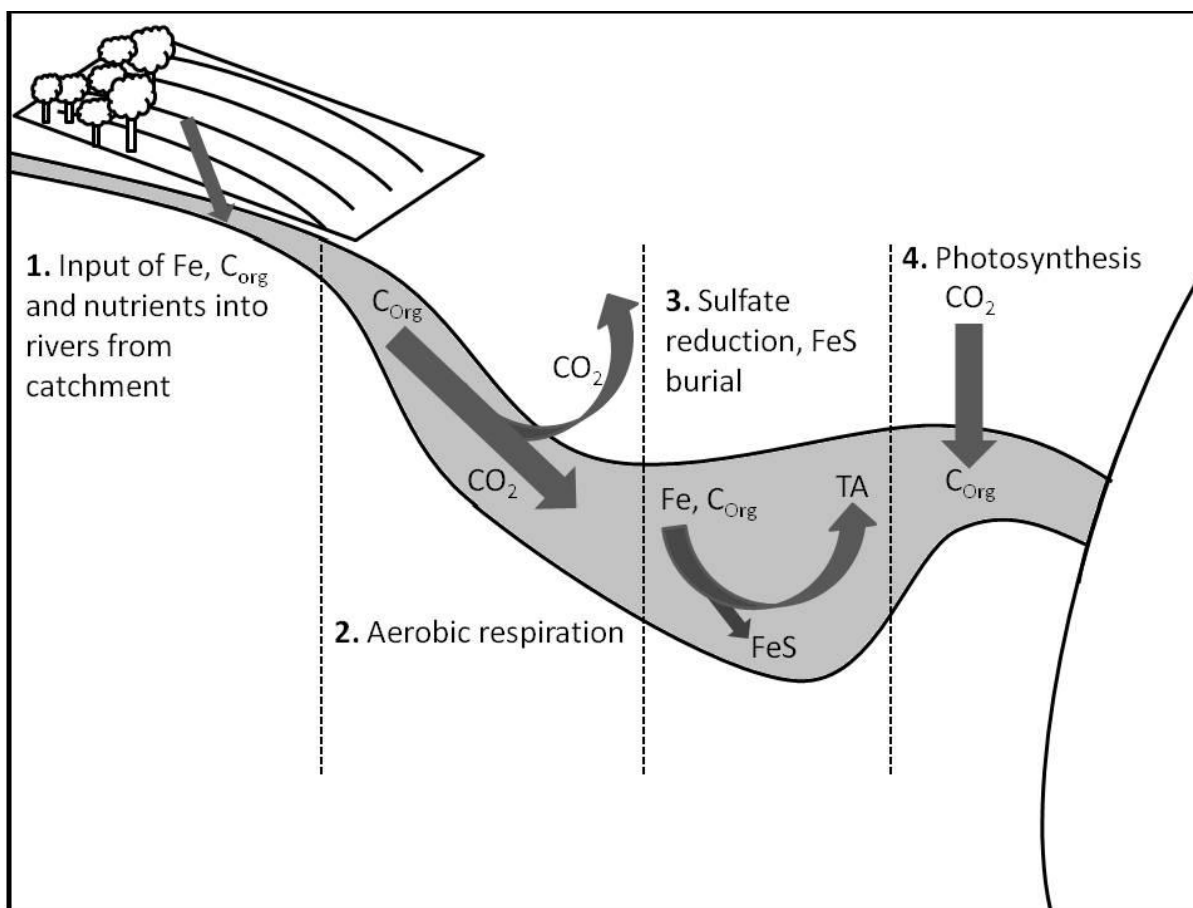


Figure 4.5: Schematic diagram of the dominant modes of carbon transformation occurring in estuaries: 1. Inputs of terrestrial materials, Fe, organic carbon and inorganic nutrients, 2. Aerobic respiration and corresponding CO₂ production, 3. Sulfate reduction, associated FeS burial and TA production, 4. Photosynthesis.

The dominant modes of carbon transformation we observed at the eight estuaries are represented by the processes 2-4 in **Fig. 4.5** and are presented in **Table 4.5** for each sampling campaign. Within well flushed estuaries, carbonate dissolution and carbonate precipitation are probably too slow to have an observable influence on $\delta^{13}\text{C}_{\text{DIC}}$, TA and DIC values (Miyajima et al. 2009) and previous work (Faber et al. submitted, chapter 3) indicates that carbonate dissolution in intertidal mudflats is negligible (contributing ~0.2% of total DIC export) when advection from intertidal zones is driven by tidal pumping. Within the Curdies and the Aire estuaries, carbonate dissolution or precipitation may have

an influence due to the long residence time of water within the system, but this effect could not be observed in these estuaries due to the lack of data points within the mixing zone, and the extent of the sampling periods (24 h) which were presumably too short to observe carbonate dissolution or precipitation in significant quantities. The lack of mixing in these systems due to their isolation from tidal influences and their considerable stratification meant that our sampling regime was not suited to investigation of carbonate dissolution or precipitation in these two systems.

The main factors influencing $\delta^{13}\text{C}_{\text{DIC}}$ can be investigated using the $\delta^{13}\text{C}_{\text{Est}}$ plots which provide an estimate of how $\delta^{13}\text{C}_{\text{DIC}}$ changes along a salinity gradient (**Fig. 4.3**) or over a diurnal cycle (**Fig. 4.4**). Plots showing both a production of DIC and low $\delta^{13}\text{C}_{\text{Est}}$ values indicate that respiration is occurring, driving the $\delta^{13}\text{C}_{\text{DIC}}$ to a value closer to the $\delta^{13}\text{C}$ of the organic matter source. On the other hand, consumption of DIC and an increase in $\delta^{13}\text{C}_{\text{Est}}$ would indicate that photosynthesis is occurring. Because the $\delta^{13}\text{C}_{\text{Est}}$ value represents the $\delta^{13}\text{C}$ of the added/removed fraction of DIC, it can be representative of numerous processes occurring simultaneously, for instance respiration, as well as loss of DIC as a CO_2 flux to the atmosphere. For the purposes of this study, we use the ranges in $\delta^{13}\text{C}_{\text{Est}}$ observed as an indicator of the dominant carbon transformation rather than identification of organic matter sources (**Table 4.5**). This is because we have not considered the changes in $\delta^{13}\text{C}$ due to the effect of CO_2 fluxes across the water-air interface towards isotopic equilibrium with the atmosphere and our small data sets and poorly constrained values of gas transfer velocities precluded this type of analysis.

The categorisation of the dominant mode of carbon transformation (**Table 4.5**) was conducted by comparing EF_{DIC} , EF_{TA} , FCO_2 and interpretations of conservative mixing plots. The modes identified are aerobic respiration, anaerobic respiration (sulfate reduction and FeS burial) and photosynthesis, which are represented by processes 2-4

respectively in **Fig. 4.5**. Positive values of EF_{DIC} represent a net gain of DIC and positive values of EF_{TA} are interpreted as the production of TA by anaerobic respiration. To determine whether aerobic or anaerobic processes dominate within an estuary, the magnitudes of EF_{DIC} and EF_{TA} were compared. When EF_{TA} was less than 10% of EF_{DIC} , aerobic respiration was labelled as the dominant process. When $EF_{TA} \geq EF_{DIC}$ then anaerobic respiration dominated. In many instances, both aerobic and anaerobic respiration processes were important carbon transformation processes. In some cases, the values of EF_{DIC} and EF_{TA} were deemed to be inappropriate (discussed below) to determine the dominant mode of carbon transformation, so mixing plots were inspected to determine if production or consumption of TA or DIC were likely. The ranges of $\delta^{13}C_{Est}$ from **Figs. 4.3 and 4.4** were used to support the categorisation because carbon transformations are expected to change $\delta^{13}C$ in a predictable way. The use of $\delta^{13}C_{Est}$ values also allowed us to postulate the presence of processes such as methane oxidation, and decreased isotopic fractionation due to intense photosynthesis that led to uncharacteristically low $\delta^{13}C_{Est}$ values.

Site	Dominant mode of carbon transformation	CO ₂ source/sink	$\delta^{13}\text{C}_{\text{est}}$ range (‰)	Possible processes causing $\delta^{13}\text{C}_{\text{est}}$ values
<i>Campaign 1</i>				
A	Aerobic respiration	source	-15.6—6.4	Organic matter breakdown, rapid CO ₂ efflux
B	Aerobic respiration	source	-19.7—18.7	Organic matter breakdown
C	*Photosynthesis/Aerobic respiration	*source	-12.7—28.5	Photosynthesis and respiration by macroalgae
K	Anaerobic respiration	source	-46.3—58.2	Unclear
M	Conservative	-	-6.6	Unclear, poorly constrained
T	*Anaerobic/Aerobic respiration	source	-10.7	Organic matter breakdown.
We	Anaerobic/Aerobic respiration	source	-27.6—1.2	Terrestrial organic matter breakdown
Wi	Anaerobic/Aerobic respiration	source	-7.2—7.4	Photosynthesis and organic matter breakdown
<i>Campaign 2</i>				
A	Aerobic respiration	source	-9.7—7.3	Organic matter breakdown, rapid CO ₂ efflux
B	Anaerobic/Aerobic respiration	source	-16.2—6.2	Organic matter breakdown
C	Photosynthesis	sink	-7.5—4.8	Photosynthesis/Decreased isotopic fractionation of dissolving CO ₂
K	Anaerobic respiration	source	-13.1—21.8	Unclear
M	Photosynthesis	sink	-16.8—11.1	Unclear, poorly constrained
T	Anaerobic/Aerobic respiration	source	-16.8—23.6	Unclear
We	Aerobic respiration	source	-33.3—1.1	Respiration of organic matter, methane oxidation?
Wi	Aerobic respiration	source	-	-
<i>Campaign 3</i>				
A	Aerobic respiration	source	-23.9—4.4	Organic matter breakdown, rapid CO ₂ efflux
B	Anaerobic/Aerobic respiration	source	-17.6—5.2	Organic matter breakdown
C	Photosynthesis	sink	-2.4—6.1	Photosynthesis/Decreased isotopic fractionation of dissolving CO ₂

K	Anaerobic/Aerobic respiration	source	-14.4—8.1	Organic matter breakdown
M	*Conservative/Photosynthesis	-	-	Unclear, poorly constrained
T	Aerobic respiration	source	-49.4—3.6	Respiration of organic matter, methane oxidation?
We	* Anaerobic/Aerobic respiration	source	-34.3—0.1	Respiration of organic matter, methane oxidation?
Wi	Aerobic respiration	source	-14.4—3.6	Photosynthesis and organic matter breakdown

*conflicting interpretation between budgets and conservative mixing plot are discussed in the text.

Table 4.5: Estuarine carbon transformations in each estuary, during each campaign. Dominant modes of carbon transformation are based on interpretation of FCO_2 , EF_{TA} , EF_{DIC} and conservative mixing plots. Also included is the direction of CO_2 fluxes (source vs. sink), ranges of $\delta^{13}C_{est}$ observed and an explanation of the possible processes causing these $\delta^{13}C_{est}$ values. Note: Positive $\delta^{13}C_{est}$ values may represent addition of DIC with a high $\delta^{13}C$, or loss of DIC with low $\delta^{13}C$.

Aerobic respiration was clearly the dominant mode of carbon transformation at the Aire estuary and it was nearly always the strongest source of CO₂ to the atmosphere (up to 502 mmol m⁻² d⁻¹). The high degree of stratification, and the lack of mixing data in for DIC, TA and $\delta^{13}\text{C}_{\text{DIC}}$ means that interpretation of the Aire's carbon dynamics beyond the general label of “heterotrophic” is difficult. In our categorisation of carbon transformation modes, we make no distinction between aerobic respiration and anaerobic respiration immediately followed by oxidation of reduced substances (such as sulfide). At the Aire, it is likely that anaerobic processes dominated in the sediments due to low DO in the bottom waters (which were as low as 13% during campaign 3, data not shown). Although sulfide didn't appear to be in the surface water, judging by odour, the deep, stratified water column likely meant that free sulfide was able to oxidise before it could diffuse to the surface. Higher than expected values of $\delta^{13}\text{C}_{\text{Est}}$ (up to -4.4‰; **Table 4.5**) in a system that is probably degrading mostly terrestrially organic matter (due to isolation from the ocean, and limited aquatic vegetation) indicates that the high pCO₂ flux to the atmosphere may be driving isotopic equilibrium of the surface water with the atmosphere. One other possibility for the low $\delta^{13}\text{C}_{\text{Est}}$ values is carbon dissolution resulting from the acidity produced by the high concentrations of pCO₂ or H₂S, but we have no evidence to support this hypothesis.

The Bass, Kororoit, Tarra and Werribee estuaries showed highly non-conservative behaviour in $\delta^{13}\text{C}_{\text{DIC}}$, DIC and TA and these systems usually had high rates of DIC and TA production within the estuary (**Table 4.3, Table 4.4**), except during no flow (Werribee, campaign 3) or during very high flow (Bass, campaign 1). The Bass was always a source of CO₂ to the atmosphere and produced TA, except when in flood during campaign 1. At the Bass during campaign 1 and 2, organic matter was respired mostly aerobically whereas during campaign 3, anaerobic respiration was more important to

carbon fluxes. The Kororoit estuary was very reactive considering the high ΔDIC values (**Fig.4.3**) and the fact that the estuary is relatively small (<3 km long). Mixing plots for campaigns 1 and 2 show very non-conservative behaviour in DIC and TA concentrations, and anaerobic respiration dominated carbon dynamics in these campaigns (**Table 4.5**). The Kororoit was a large producer of alkalinity compared to most other estuaries during campaign 1 and 2. In campaign 3 however, the Kororoit appeared to be aerobically respiring organic carbon and EF_{TA} values suggest that alkalinity consumption was occurring. The reason for uncharacteristically high $\delta^{13}\text{C}_{\text{Est}}$ values at Kororoit estuary (up to 58.2‰ during campaign 1 and 21.8‰ during campaign 2) is unclear. The more explicable $\delta^{13}\text{C}_{\text{Est}}$ values during campaign 3 (-14.4—8.1‰) are expected as a result of organic matter respiration.

The Tarra produced TA during each campaign but the dominant mode of carbon transformation was aerobic respiration. Our data is conflicting in that the EF_{DIC} value for campaign 1 is negative, suggesting that DIC removal processes were important. This was unlikely the case in this estuary due to consistently supersaturated pCO_2 , and upon inspection of the mixing plots we have determined the EF_{DIC} value to be unreliable because the freshwater endmember was unrealistically high and was not a representative endmember of the water we were sampling downstream. Aerobic respiration was the dominant process at the Tarra during campaign 2, but high $\delta^{13}\text{C}_{\text{Est}}$ values (up to 23.6‰) suggest that photosynthesis was the dominant process affecting DIC in some samples. This was probably as a result of water being imported into the estuary from the adjacent embayment, which was heavily vegetated with seagrass. Being a tide dominated estuary, the import of chemically different water from far outside the estuary mouth is likely an important dynamic in data sets from this site. Another explanation of the high $\delta^{13}\text{C}_{\text{Est}}$ at the Tarra during campaign 2 is that fast efflux of CO_2 to the atmosphere increased the

value of $\delta^{13}\text{C}$ towards isotopic equilibrium with the atmosphere. The very low $\delta^{13}\text{C}_{\text{Est}}$ values (-49.4--3.6‰) calculated from the Tarra estuary during campaign 3, coupled with DIC production (up to 0.3 mmol L^{-1}) suggest that methane oxidation is occurring in the estuary, although we lack methane measurements to support this. Similarly, there are $\delta^{13}\text{C}_{\text{Est}}$ values of below -30‰ at the Werribee during campaign 2 and 3 suggesting methane oxidation. The observation of very low $\delta^{13}\text{C}_{\text{Est}}$ values corresponds with low $\delta^{13}\text{C}_{\text{DIC}}$ that is expected when methane with a $\delta^{13}\text{C}$ of ~-72--43‰ (Schubert et al. 2011) is oxidised. Low $\delta^{13}\text{C}_{\text{DIC}}$ values have been observed in sediment DIC profiles where methane oxidation is occurring (Schubert et al. 2011) and precipitated carbonate that has been formed as a product of methane oxidation (Valentine 2002). Due to the high spatial and temporal variability of methane in estuaries owing to tidal pumping of sediment porewater (Deborde et al. 2010), high resolution time series and longitudinal data coupled with our method of using $\delta^{13}\text{C}_{\text{Est}}$ may provide future researchers an opportunity to examine the overall importance of methane oxidation in carbon budgets, although that is beyond the scope of this study.

The Moyne during campaign 2, showed higher than conservative values for $\delta^{13}\text{C}_{\text{DIC}}$ in the mixing plot and was identified as a carbon sink as a result of photosynthesis. The higher than conservative values of $\delta^{13}\text{C}_{\text{DIC}}$ at Moyne during campaign 2 coincided with a consumption of DIC indicated by a less than conservative concentration of DIC in the mixing plot. This is supported by the observation of subsaturated pCO_2 (as low as $140 \text{ } \mu\text{atm}$) and supersaturated DO (as high as 150%) for much of the sampling period (data not shown). The dominant modes of carbon transformation were difficult to determine at the Moyne, campaigns 1 and 3, because our data was poorly constrained due to a lack of data points within the mixing zone of the estuary, low river flow and high flushing rates. In campaign 3, we speculate that

photosynthesis was the dominant process due to the negative value of EF_{DIC} , and the presence of extensive macroalgae and seagrass communities, which would undertake high rates of photosynthesis.

The Curdies estuary was similar to the Moyne during campaign 2, in that photosynthesis was the dominant process in campaigns 2 and 3 (**Table 4.5**). Measurements of DO (data not shown) were often supersaturated, confirming the presence of intense photosynthesis. However, within surface water at this site, there was an uncharacteristic decrease in $\delta^{13}C_{DIC}$ during campaign 2 and 3, indicated by $\delta^{13}C_{Est}$ values ranging from -7.5—-4.8 during campaign 2 and -2.4—-6.1 during campaign 3 (**Table 4.5**). The values of $\delta^{13}C_{Est}$ for the Moyne during campaign 2 are a similar anomaly and have a range of -16.8—-11.1 (**Table 4.5**). Our explanation of these values are as follows: Intense photosynthesis which leads to $pH > 9$ can cause rapid invasion of atmospheric CO_2 and accompanying this, decreased photosynthetic isotopic fractionation due to CO_2 limitation can lead to a decrease in the $\delta^{13}C_{DIC}$ of the DIC pool (Herczeg and Fairbanks 1987). Our data suggest that this occurred in Curdies during campaign 2 and 3 and Moyne during campaign 2 where the rapid consumption of DIC due to intense photosynthesis was associated with a decrease, instead of an increase, in $\delta^{13}C_{DIC}$. Low pCO_2 in the water column as well as stratification due to lack of tidal flushing and current may have been responsible for decreased isotopic fractionation at the Curdies. This explanation is supported by observations of large amounts of gas bubbles being emitted from areas of macroalgae (*Ulva* species) when disturbed, which were presumed to be oxygen, considering the DO was as high as ~230% saturation. The large, shallow lake upstream of the sampling sites at the Moyne may have had similar processes occurring but these could not be observed due to lack of data points in this area. Despite the dominance of photosynthesis at the Curdies, there were zones of intense respiration observed during

campaign 2 and 3. DO as low as 45% was observed in uncharacteristically deep (~5 m) and stratified water, accompanied with the release of large amounts of hydrogen sulfide, which were observed anecdotally during sampling. We postulate that the high spatial heterogeneity of dominant carbon transformation modes at the Curdies is a result of low mixing, and eutrophication as a result of intense photosynthesis.

4.6.4 Carbon budget components comparison

The total export of DIC (TE_{DIC}) differed considerably between sites as well as campaigns (**Table 4.3**). Because TE_{DIC} includes FI_{DIC} , very high TE_{DIC} values may be as a result of high fluvial DIC inputs, high estuarine DIC fluxes, or a combination of both. The Bass estuary during campaign 1 has an extremely high TE_{DIC} despite low EF_{DIC} due to a very high riverine flow rate as well as high DIC concentrations within the exported water. During this sampling period, the Bass exported the greatest amount of DIC ($4894 \text{ mmol m}^{-2} \text{ d}^{-1}$) out of any of the estuaries. Positive and negative values of EF_{DIC} were calculated for each of the estuaries, indicating a variety of trophic states (net heterotrophic and net autotrophic). Werribee showed the highest EF_{DIC} that we measured, during campaign 1 which was also reflected in the highly non-conservative behaviour in the DIC mixing plots (**Appendix 4B**), however, at the Werribee, no river flow during campaign 3 meant that EF_{DIC} was equal to FCO_2 and was $77 \text{ mmol m}^{-2} \text{ d}^{-1}$. This is a limitation of our method used to calculate DIC and TA budgets in that application of **Eqs. 4.2 and 4.3** assumes that estuary production of DIC is partly proportional to river flow. At the Aire and Curdies, the lack of EF_{DIC} and EF_{TA} values is due to the estuary mouths being closed. However, it is likely that there is DIC storage within the Aire estuary until the estuary mouth opens seasonally, as it was obviously heterotrophic. Conversely, the Curdies estuary appeared to be autotrophic (based on mixing plots and CO_2 fluxes) and acted as a sink for atmospheric CO_2 in campaigns 2 and 3. Due to the high metabolic heterogeneity,

low amounts of mixing, and high amounts of stratification at the Curdies, our sampling regime only allows for a basic understanding of carbon dynamics in this estuary. In these estuaries with closed mouths, seasonal or intermittent openings of the estuary mouth can be expected to change the carbon dynamics considerably.

In most cases, FI_{DIC} dominated DIC export from the estuaries, with most exceptions during campaign 3, indicating that riverine DIC inputs are substantially more important to the carbon budget than DIC fluxes within these estuaries. In many cases, CO_2 fluxes to the atmosphere contributed most to EF_{DIC} . High CO_2 fluxes are generally expected of estuarine systems due to terrestrial organic matter input, and have been observed in many studies (Frankignoulle et al. 1998). Low CO_2 fluxes relative to advected DIC fluxes have been observed by other studies (Raymond et al. 1997), and our data set has examples of this as well (**Table 4.3**).

In general, highly impacted estuaries had higher values of EF_{DIC} , due to increased organic carbon loading. Wangan had low values of EF_{DIC} during campaigns 1 and 2 (39 and 1 $mmol\ m^{-2}\ d^{-1}$ respectively) but during campaign 3, FCO_2 was 77 $mmol\ m^{-2}\ d^{-1}$ and was higher than both FI_{DIC} and TE_{DIC} . Carbon budgets of the closed Curdies and Aire estuaries were not used for this land use gradient comparison.

4.6.5 The effect of catchment impact on carbon dynamics and alkalinity export

In this study, we used mean total phosphorous (TP) effective annual loading for 1990-2012 as a component in determining land use impact (**Appendix 4A**), as TP loading data was available for each of the field sites. TP has been shown to be highly correlated with total suspended solids (TSS) in agricultural catchments (Ekholm et al. 2000), due to

the fact that much of the P is in particulate form, and concentrations of these substances reflect erosion within the catchment. As Fe is predominantly in particulate form in rivers, inputs are related to TSS (Martin and Meybeck 1979) and thus TP. Because more intensive anthropogenic land use in the catchment leads to increased TSS input (Alongi and Mckinnon 2005), TP can be considered as a proxy for anthropogenic impacts on the catchment.

In pristine estuaries such as Wangan, the near-conservative mixing behaviour of DIC and relatively low primary production, are evidently a result of low carbon loading and low nutrient availability. Contrasting this, the more impacted estuaries generally showed non-conservative behaviour of DIC and at times had high rates of photosynthesis. The highly impacted estuaries Kororoit and Werribee tended to exhibit higher rates of anaerobic respiration due to the high availability of organic carbon in these estuaries. The Werribee in particular also showed strong diurnal changes in $p\text{CO}_2$ and O_2 (data not shown) indicating that the competing processes of respiration and photosynthesis are both occurring at high rates due to the availability of inorganic nutrients. Across the field campaigns, the highly impacted estuaries Werribee, Kororoit (and to a lesser extent Bass and Tarra) showed more variation in EF_{DIC} suggesting that these systems may be more temporally dynamic with regard to carbon transformation than less impacted estuaries. In **Fig. 4.6** we compare EF_{TA} with relative catchment impact levels (**Table 1**) as well as the mean effective TP loading from 1990-2013. We use this long term average because we hypothesise that these estuaries may extensively recycle Fe when previously buried FeS is resuspended and reoxidised, and in these sites, year to year average river discharge can change dramatically.

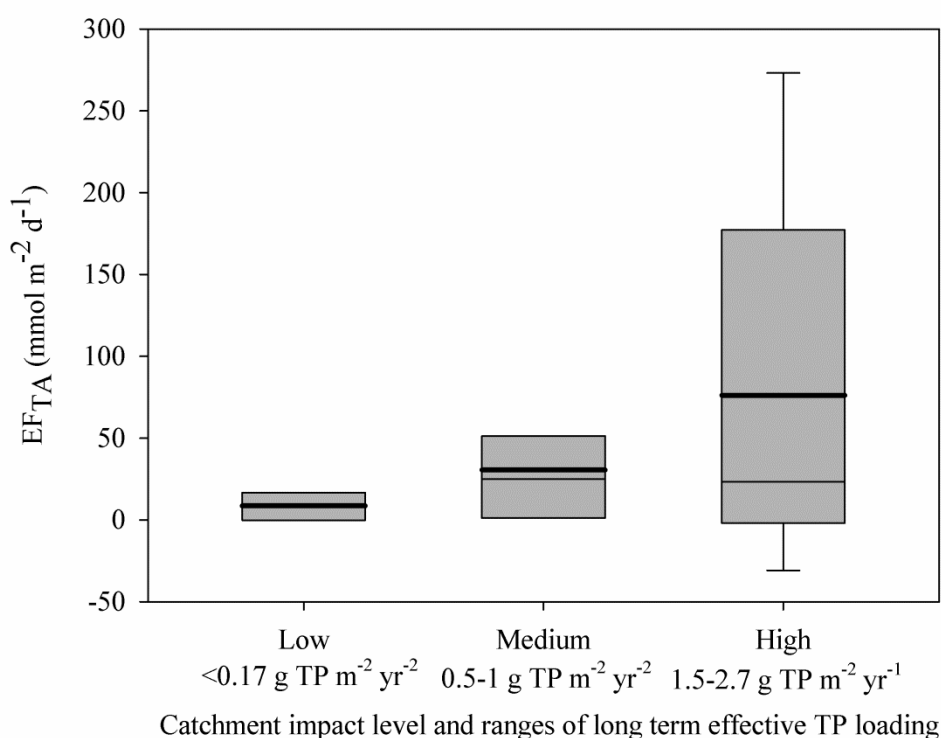


Figure 4.6: Estuary fluxes of TA vs. catchment impact level and the ranges of long term TP loading from 1990-2013. Median and mean values are represented by the plain and bold lines respectively on each box. n=3, 6 and 9 for low, moderate and high catchment impacts respectively.

In general, the highly impacted estuaries Bass, Kororoit and Werribee showed highly non-conservative behaviour with regard to TA (**Appendix 4B**) and were more likely to have anaerobic respiration contributing most to EF_{DIC} (**Table 4.5**). In many cases, EF_{TA} values were higher in more highly impacted estuaries (**Fig. 4.6**), for instance Werribee (-4-273 mmol m⁻² d⁻¹), Kororoit (-31-182 mmol m⁻² d⁻¹) and Bass (0-69 mmol m⁻² d⁻¹) compared to the least impacted Wingan (0-17 mmol m⁻² d⁻¹) (**Table 4.4**). The moderately impacted estuaries Moyne and Tarra had EF_{TA} values of -2-36 mmol m⁻² d⁻¹ and 15-98 mmol m⁻² d⁻¹ respectively.

The generally high EF_{TA} at impacted sites is probably due to the higher loadings of Fe in these estuaries, which allows net alkalinity production through FeS burial (Process 3, **Figure 4.5**). Interestingly, the highly impacted estuaries have a much greater range in EF_{TA} , and have examples of more extreme TA production as well as consumption. The negative values of EF_{TA} at the Kororoit during campaign 3 and at the Werribee during campaign 2 suggest that alkalinity consumption due to reduced sulfur oxidation is occurring. We hypothesise that this is because there is a large amounts of FeS within the sediment of the highly impacted estuaries due to higher long-term rates of FeS burial, which may be reoxidised if conditions permit, intermittently consuming alkalinity. Another recent study (Faber et al. submitted, Chapter 3) suggested that Fe recycling may be responsible for allowing high instantaneous TA fluxes from tidal flats which led to an overestimate of yearly TA exports when extrapolated. Our evidence of high variability in TA fluxes from highly impacted estuaries emphasises the need for regular sampling in these systems to observe their full ranges of metabolic activity. The mixing behaviours of Aire and Curdies are difficult to consider and compare due to the closed mouth of these estuaries, so could not be included in this comparison.

4.6.6 Future avenues of research

The concept of 'blue carbon' is used to describe organic carbon stores in coastal ecosystems. Vegetated habitats such as seagrass, mangroves and salt marsh are significant blue carbon sinks, which store large amounts of organic material in their sediments for long periods. Recently, discussion has surrounded the security of these habitats in the face of destruction and rising sea levels (Hopkinson et al. 2012). Although the loss of these habitats has been recognised to release large amounts of inorganic carbon upon organic matter mineralisation (Fourqurean et al. 2012), the concurrent oxidation of reduced sulfur

and corresponding acid production within these sediments has not been investigated. Hu and Cai (2011) briefly mentioned this phenomenon and the uncertainties due to limited studies and the lack of well constrained estimates on reduced sulfur burial rates in vegetated habitats. In terms of global carbon budgets, we suggest consideration of the effects of acid production (or alkalinity consumption) associated with the destruction of vegetated coastal habitats in order to better understand how vegetated habitat destruction may influence the global carbon budget. Another possibility is that rising sea levels may resuspend sediments or increase inputs of oxidised Fe through erosion, influencing global alkalinity budgets.

With regard to investigation into estuary carbon dynamics, well constrained estimates of gas transfer velocities and inclusion of a term into **Eq. 4.5** to account for the effect of progression of ^{13}C towards atmospheric isotopic equilibrium on $\delta^{13}\text{C}_{\text{Est}}$, could allow this methodology to be used to identify sources of organic carbon being respired with consideration to spatial and temporal dimensions.

4.7 Conclusion

Because estuaries are highly reactive zones and intermediates between terrestrial and marine systems, their relevance to the global carbon cycle is important. This study aimed to describe how anthropogenic land use in river catchments influences inorganic carbon export and found that estuaries with highly impacted catchments tend to behave differently in terms of inorganic carbon and alkalinity production. Work done by other authors has shown that anaerobic alkalinity production in coastal oceans may be an important component of global alkalinity fluxes, which control CO_2 uptake by oceans, and our previous work has indicated that the strength of the land-ocean link is important

to alkalinity exports from intertidal systems. Therefore, this study, although limited, increases understanding of how human influences are likely to alter the global carbon cycle under different land use regimes. The work towards identifying dominant modes of carbon transformation using $\delta^{13}\text{C}_{\text{Est}}$ provided useful insight into carbon dynamics of the more complex situations and allowed speculation on other processes occurring.

4.8 Acknowledgements

The authors acknowledge Erinn Richmond for help in field work and Fiona Warry for calculating total phosphorous loading data.

4.9 References

- Allan, D., D. Erickson, and J. Fay. 1997. The influence of catchment land use on stream integrity across multiple spatial scales. *Freshwater Biology* **37**: 149-161.
- Almgren, T., D. Dyrssen, and S. Fonselius. 1983. Determination of alkalinity and total carbonate., p. 99-123. *In* K. Grasshoff, M. Ehrhardt and K. Kremling [eds.], *Methods of seawater analysis*. Springer-Verlag, Chemie.
- Alongi, D., and A. Mckinnon. 2005. The cycling and fate of terrestrially-derived sediments and nutrients in the coastal zone of the Great Barrier Reef shelf. *Marine Pollution Bulletin* **51**: 239-252.
- Bauer, J. E., W.-J. Cai, P. A. Raymond, T. S. Bianchi, C. S. Hopkinson, and P. A. Regnier. 2013. The changing carbon cycle of the coastal ocean. *Nature* **504**: 61-70.
- Berner, R. A., M. R. Scott, and C. Thomlinson. 1970. Carbonate alkalinity in the pore waters of anoxic marine sediments. *Limnology and Oceanography*: 544-549.
- Boehme, S., C. Sabine, and C. Reimers. 1998. CO₂ fluxes from a coastal transect: a time-series approach. *Marine Chemistry* **63**: 49-67.
- Borges, A., L. S. Schiettecatte, G. Abril, B. Delille, and F. Gazeau. 2006. Carbon dioxide in European coastal waters. *Estuarine, Coastal and Shelf Science* **70**: 375-387.
- Boyle, E., J. Edmond, and E. Sholkovitz. 1977. The mechanism of iron removal in estuaries. *Geochimica et Cosmochimica Acta* **41**: 1313-1324.
- Cai, W., L. Pomeroy, M. Moran, and Y. Wang. 1999. Oxygen and carbon dioxide mass balance for the estuarine-intertidal marsh complex of five rivers in the southeastern US. *Limnology and Oceanography* **44**: 639-649.

- Canfield, D. E. and others 1993. Pathways of organic carbon oxidation in three continental margin sediments. *Marine Geology* **113**: 27-40.
- Chen, C.-T. A. 2002. Shelf-vs. dissolution-generated alkalinity above the chemical lysocline. *Deep Sea Research Part II: Topical Studies in Oceanography* **49**: 5365-5375.
- Dauer, D. M., J. A. Ranasinghe, and S. B. Weisberg. 2000. Relationships between benthic community condition, water quality, sediment quality, nutrient loads, and land use patterns in Chesapeake Bay. *Estuaries* **23**: 80-96.
- Deborde, J. and others 2010. Methane sources, sinks and fluxes in a temperate tidal Lagoon: The Arcachon lagoon (SW France). *Estuarine, Coastal and Shelf Science* **89**: 256-266.
- Dickson, A. G., J. D. Afghan, and G. C. Anderson. 2003. Reference materials for oceanic CO₂ analysis: a method for the certification of total alkalinity. *Marine Chemistry* **80**: 185-197.
- Dunne, T. 1979. Sediment yield and land use in tropical catchments. *Journal of Hydrology* **42**: 281-300.
- Ekholm, P. and others 2000. Relationship between catchment characteristics and nutrient concentrations in an agricultural river system. *Water Research* **34**: 3709-3716.
- Faber, P., A. Kessler, J. Bull, I. McKelvie, F. Meysman, and P. Cook. 2012. The role of alkalinity generation in controlling the fluxes of CO₂ during exposure and inundation on tidal flats. *Biogeosciences* **9**: 4087-4097.
- Fourqurean, J. W. and others 2012. Seagrass ecosystems as a globally significant carbon stock. *Nature Geoscience* **5**: 505-509.

- Frankignoulle, M. and others 1998. Carbon dioxide emission from European estuaries. *Science* **282**: 434.
- Frankignoulle, M., and A. Borges. 2001. Direct and indirect pCO₂ measurements in a wide range of pCO₂ and salinity values (the Scheldt estuary). *Aquatic Geochemistry* **7**: 267-273.
- Frankignoulle, M., I. Bourge, and R. Wollast. 1996. Atmospheric CO₂ fluxes in a highly polluted estuary (the Scheldt). *Limnology and Oceanography* **41**: 365-369.
- Gazeau, F. and others 2005. Net ecosystem metabolism in a micro-tidal estuary (Randers Fjord, Denmark): evaluation of methods. *Marine Ecology Progress Series* **301**: 23-41.
- Haese, R. R. 2000. The reactivity of iron, p. 233-261. *Marine geochemistry*. Springer.
- Hammond, D., P. Giordani, W. Berelson, and R. Poletti. 1999. Diagenesis of carbon and nutrients and benthic exchange in sediments of the Northern Adriatic Sea. *Marine Chemistry* **66**: 53-79.
- Herczeg, A. L., and R. G. Fairbanks. 1987. Anomalous carbon isotope fractionation between atmospheric CO₂ and dissolved inorganic carbon induced by intense photosynthesis. *Geochimica et Cosmochimica Acta* **51**: 895-899.
- Hopkinson, C. S., W.-J. Cai, and X. Hu. 2012. Carbon sequestration in wetland dominated coastal systems—a global sink of rapidly diminishing magnitude. *Current Opinion in Environmental Sustainability* **4**: 186-194.
- Hopkinson, C. S., and J. J. Vallino. 1995. The relationships among man's activities in watersheds and estuaries: a model of runoff effects on patterns of estuarine community metabolism. *Estuaries* **18**: 598-621.

- Howarth, R. W., J. R. Fruci, and D. Sherman. 1991. Inputs of sediment and carbon to an estuarine ecosystem: Influence of land use. *Ecological Applications* **27**: 27-39.
- Hu, X., and D. J. Burdige. 2007. Enriched stable carbon isotopes in the pore waters of carbonate sediments dominated by seagrasses: Evidence for coupled carbonate dissolution and reprecipitation. *Geochimica et Cosmochimica Acta* **71**: 129-144,
- Hu, X., and W. J. Cai. 2011. An assessment of ocean margin anaerobic processes on oceanic alkalinity budget. *Global Biogeochemical Cycles* **25**: 1-11.
- Jordan, T. E., J. C. Cornwell, W. R. Boynton, and J. T. Anderson. 2008. Changes in phosphorus biogeochemistry along an estuarine salinity gradient: The iron conveyor belt. *Limnology and Oceanography* **53**: 172-184.
- Kaul, L. W., and P. N. Froelich. 1984. Modeling estuarine nutrient geochemistry in a simple system. *Geochimica et Cosmochimica Acta* **48**: 1417-1433.
- Kendall, A., A. Stuart, and J. K. Ord. 1983. *Advanced theory of statistics*, 4 ed. Griffin.
- Martens, C. S., and M. B. Goldhaber. 1978. Early diagenesis in transitional sedimentary environments of the White Oak River Estuary, North Carolina. *Limnol. Oceanogr* **23**: 428-441.
- Martin, J.-M., and M. Meybeck. 1979. Elemental mass-balance of material carried by major world rivers. *Marine Chemistry* **7**: 173-206.
- Middelburg, J. and others 1996. Organic matter mineralization in intertidal sediments along an estuarine gradient. *Marine Ecology Progress Series*. Oldendorf **132**: 157-168.
- Miyajima, T., Y. Tsuboi, Y. Tanaka, and I. Koike. 2009. Export of inorganic carbon from two Southeast Asian mangrove forests to adjacent estuaries as estimated by the

- stable isotope composition of dissolved inorganic carbon. *Journal of Geophysical Research* **114**: G01024.
- Neil, D. T., A. R. Orpin, P. V. Ridd, and B. Yu. 2002. Sediment yield and impacts from river catchments to the Great Barrier Reef lagoon: a review. *Marine and Freshwater Research* **53**: 733-752.
- Nixon, S. 1995. Coastal marine eutrophication: a definition, social causes, and future concerns. *Ophelia* **41**: 199-219,
- O'leary, M. H. 1988. Carbon isotopes in photosynthesis. *Bioscience* **38**: 328-336.
- Rabouille, C., F. T. Mackenzie, and L. M. Ver. 2001. Influence of the human perturbation on carbon, nitrogen, and oxygen biogeochemical cycles in the global coastal ocean. *Geochimica et Cosmochimica Acta* **65**: 3615-3641.
- Raymond, P., J. Bauer, and J. Cole. 2000. Atmospheric CO₂ evasion, dissolved inorganic carbon production, and net heterotrophy in the York River estuary. *Limnology and Oceanography* **45**: 1707-1717.
- Raymond, P., N. Caraco, and J. Cole. 1997. Carbon dioxide concentration and atmospheric flux in the Hudson River. *Estuaries and Coasts* **20**: 381-390.
- Raymond, P., and J. Cole. 2001. Gas exchange in rivers and estuaries: Choosing a gas transfer velocity. *Estuaries and Coasts* **24**: 312-317.
- Reeburgh, W. 1983. Rates of biogeochemical processes in anoxic sediments. *Annual Review of Earth and Planetary Sciences* **11**: 269-298.
- Regnier, P. and others 2013. Anthropogenic perturbation of the carbon fluxes from land to ocean. *Nature Geoscience*.

Schubert, C. J., F. Vazquez, T. Lösekann-Behrens, K. Knittel, M. Tonolla, and A. Boetius.

2011. Evidence for anaerobic oxidation of methane in sediments of a freshwater system (Lago di Cadagno). *FEMS Microbiology Ecology* **76**: 26-38.

Smith, S., and J. Hollibaugh. 1993. Coastal metabolism and the oceanic organic carbon balance. *Reviews of Geophysics* **31**: 75-89.

Spiker, E. 1980. The behavior of C-14 and C-13 in estuarine water; effects of in situ CO₂ (sub 2) production and atmospheric change. *Radiocarbon* **22**: 647-654.

Tan, K.-S., D. Fox, and T. Etchells. 2005. Generator for uncertainty measures and load estimates using alternative formulae. Australian Centre for Environmetrics, University of Melbourne.

Thomas, H. and others 2009. Enhanced ocean carbon storage from anaerobic alkalinity generation in coastal sediments. *Biogeosciences* **6**: 267-274.

Valentine, D. L. 2002. Biogeochemistry and microbial ecology of methane oxidation in anoxic environments: a review. *Antonie van Leeuwenhoek* **81**: 271-282.

Wang, Z., and W. Cai. 2004. Carbon dioxide degassing and inorganic carbon export from a marsh-dominated estuary (the Duplin River): A marsh CO₂ pump. *Limnology and Oceanography* **49**: 341-354.

Wanninkhof, R. 1992. Relationship between wind speed and gas exchange. *Journal of Geophysical Research* **97**: 7373–7382.

Zeebe, R., and D. Wolf-Gladrow. 2001. CO₂ in seawater: Equilibrium, kinetics, isotopes, Chapter. Elsevier Science.

Zhai, W., M. Dai, W. Cai, Y. Wang, and Z. Wang. 2005. High partial pressure of CO₂ and its maintaining mechanism in a subtropical estuary: the Pearl River estuary, China. *Marine Chemistry* **93**: 21-32.

4.10 Appendices

4.10.1 Appendix 4A Estuary selection

The eight study estuaries were selected from a group of twenty-seven potential estuaries distributed along the Victoria coast. The criteria used to select these eight estuaries were based on multivariate patterns in catchment land use characteristics and the extent of nutrient loading occurring in the receiving estuary. The location of each estuary in ordination space and the magnitude of nutrient loading were considered in tandem to define a qualitative gradient of potential environmental degradation.

Briefly, areal proportions of major land use characteristics within the river catchment of each estuary were obtained from the National Environmental Stream Attributes database (v1.1; <http://www.ga.gov.au/metadata-gateway/metadata/record/73045/>). Land use definitions allowed individual grid cells to be defined as multiple categories; therefore, the percentage land use data were not constrained to sum to 100%. Catchments were defined as all areas upstream of the final river segment terminating at the head of the estuary. A total of $n = 13$ catchment land use categories and $n = 4$ human population variables (Table A1) were available for each catchment. Data were normalized for each variable and principal components analysis (PCA) used to examine the multivariate structure of the dataset. Initial examination of the data indicated the presence of multicollinearity among some of the variables (e.g., $r_s > 0.70$); therefore, one of each of the highly correlated variables was removed and the reduced dataset of $n = 7$ land use characteristics and $n = 1$ population variable (Table A1) was used in this analysis.

Phosphorus was selected as the focal nutrient for the consideration of nutrient loading as a forcing variable on estuary biogeochemistry. Total phosphorus (TP) loads for each estuary were calculated from river flow (ML/d) and TP concentration (mg/l) data

downloaded from the Victoria Department of Environment and Primary Industries website (<http://data.water.vic.gov.au/monitoring.htm>). Long term average (1990-2012) annual TP loads per unit area of the receiving estuaries ($\text{Mg/km}^2/\text{yr}$) were calculated using a flow stratified Kendall's ratio estimator (Kendall et al. 1983) implemented in Excel with a VBA-coded algorithm (Tan et al. 2005). These loads were corrected for hydrological loading regime and P-specific nutrient retention dynamics (Kirchner and Dillon 1975; Seitzinger et al. 2002) to generate best estimates of 'effective' (i.e., retained) TP loading to each estuary.

Results from the principal components analysis indicated the presence of two dominant gradients in the various land uses comprising the catchments of the analysed estuaries (Fig A1a). The first gradient describes a transition from estuaries with river catchments dominated by intact tracts of forest that experience very little human population pressure to those with highly modified, agricultural catchments that experience extensive low-population pressure. Most of the estuaries included in this analysis fell along this primary gradient. The second gradient described a trend toward increased urbanization among several catchments. These catchments had increased areas dedicated to urban land uses, more extensive alteration of the hydrology of the river itself (e.g., impoundments), and increased high intensity animal and plant agriculture. Scaling estuary points by mean effective annual TP load (Fig A1b) indicates that loading generally increases along the forested–agriculture gradient and also along the undeveloped–urbanized gradient.

Based on these results, we selected 8 estuaries that described the full range of potential land use and nutrient loading conditions available in Victoria. Six estuaries that experienced substantially different nutrient loads were specifically selected to fall along the forested–agriculture gradient: Wingan River and Aire River (predominantly forested; low nutrient loads), Moyne River and Tarra River (intermediate-to-highly agricultural;

intermediate nutrient loads), Curdies River and Bass River (highly agricultural; high nutrient loads). Two estuaries (Kororoit Creek and Werribee River) were selected to represent systems with highly modified, urbanized catchments that experience intermediate-to-high nutrient loads.

Works Cited

Kendall, A., A. Stuart, and J. K. Ord. 1983. Advanced theory of statistics, 4 ed. Griffin.

Kirchner, W. B., and P. J. Dillon. 1975. An empirical method of estimating the retention of phosphorus in lakes. *Water Resources Research* **11**: 182-183.

Seitzinger, S. P. and others 2002. Nitrogen retention in rivers: model development and application to watersheds in the northeastern USA. *Biogeochemistry* **57**: 199-237.

Tan, K.-S., D. Fox, and T. Etchells. 2005. Generator for uncertainty measures and load estimates using alternative formulae. Australian Centre for Environmetrics, University of Melbourne.

Table A1. Table of river catchment land use and population characteristics considered in multivariate analysis of 27 estuaries in Victoria, Australia. Variables included in the final principal components analysis are shown (PCA; Yes – included, No – excluded) with codes used for plotting variable loading vectors in Figure A1a & b.

Data type	Variable description	PCA	Figure A1 code
Land use characteristics	Proportion of catchment that is modified land (i.e. not conservation)	Yes	Modified
	Proportion of catchment that is irrigated land	No	-
	Proportion of catchment that is used for aquaculture	No	-
	Proportion of catchment that is used for intensive animal production	Yes	Animal_Prod
	Proportion of catchment that is used for intensive plant production	Yes	Plant_Prod
	Proportion of catchment with landuses where herb/pesticides are likely to be used	No	
	Proportion of catchment with landuses where fertilizer is likely to be used	Yes	Fertilizer
	Proportion of catchment that is used for forestry	Yes	Forested
	Proportion of catchment that is used for mining	No	-
	Proportion of catchment that is urban	Yes	Urbanized
	Proportion of catchment that is used for irrigation supply/drainage	No	-
	Proportion of catchment that is an artificial impoundment	Yes	Impoundment
	Proportion of catchment that is a road	No	-
Population variables	Proportion of catchment with population density > 1 person/km ²	Yes	Pouplation_Prop_1
	Proportion of catchment with population density > 10 people/km ²	No	-
	Catchment average population density	No	-
	Catchment maximum population density	No	-

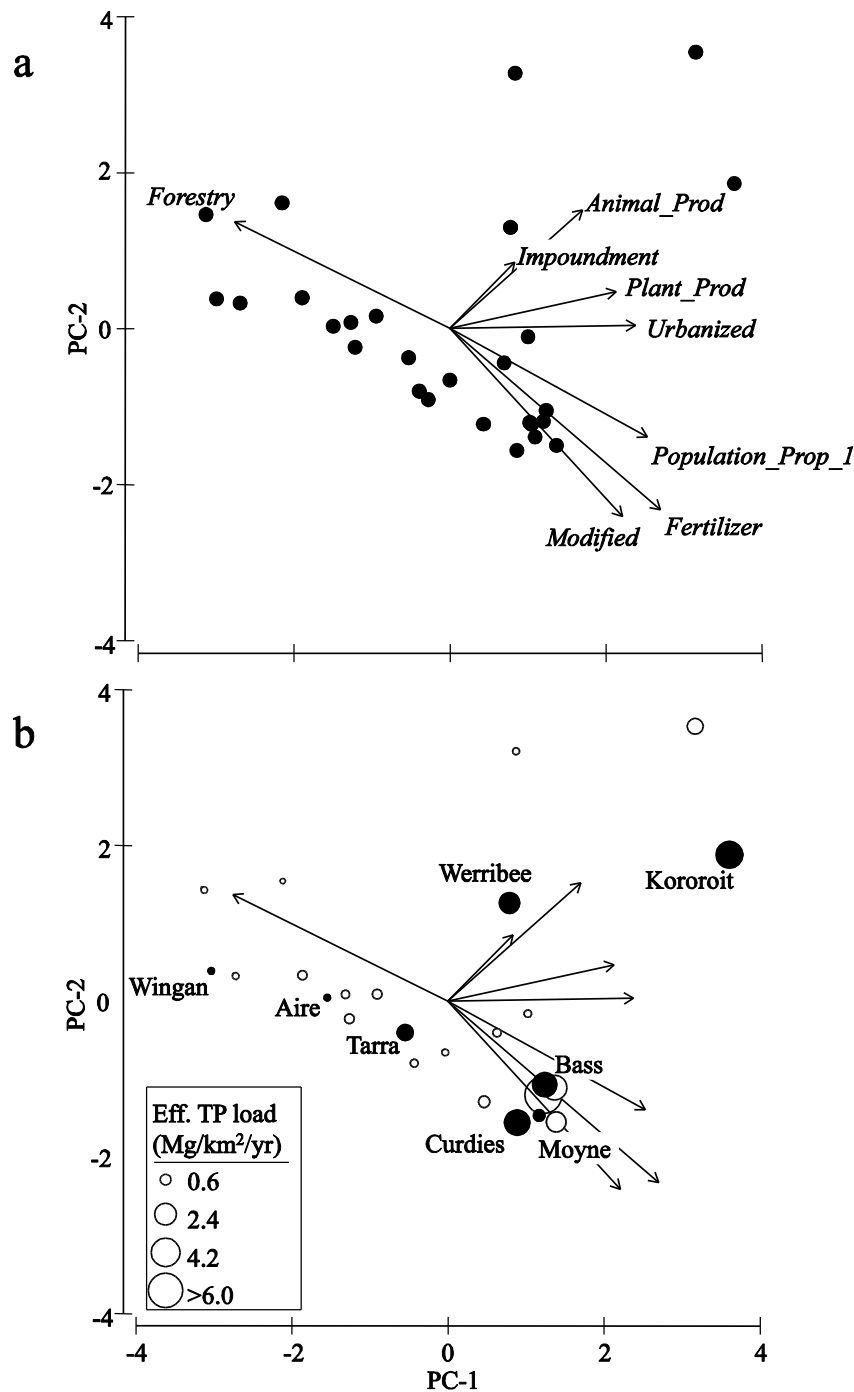
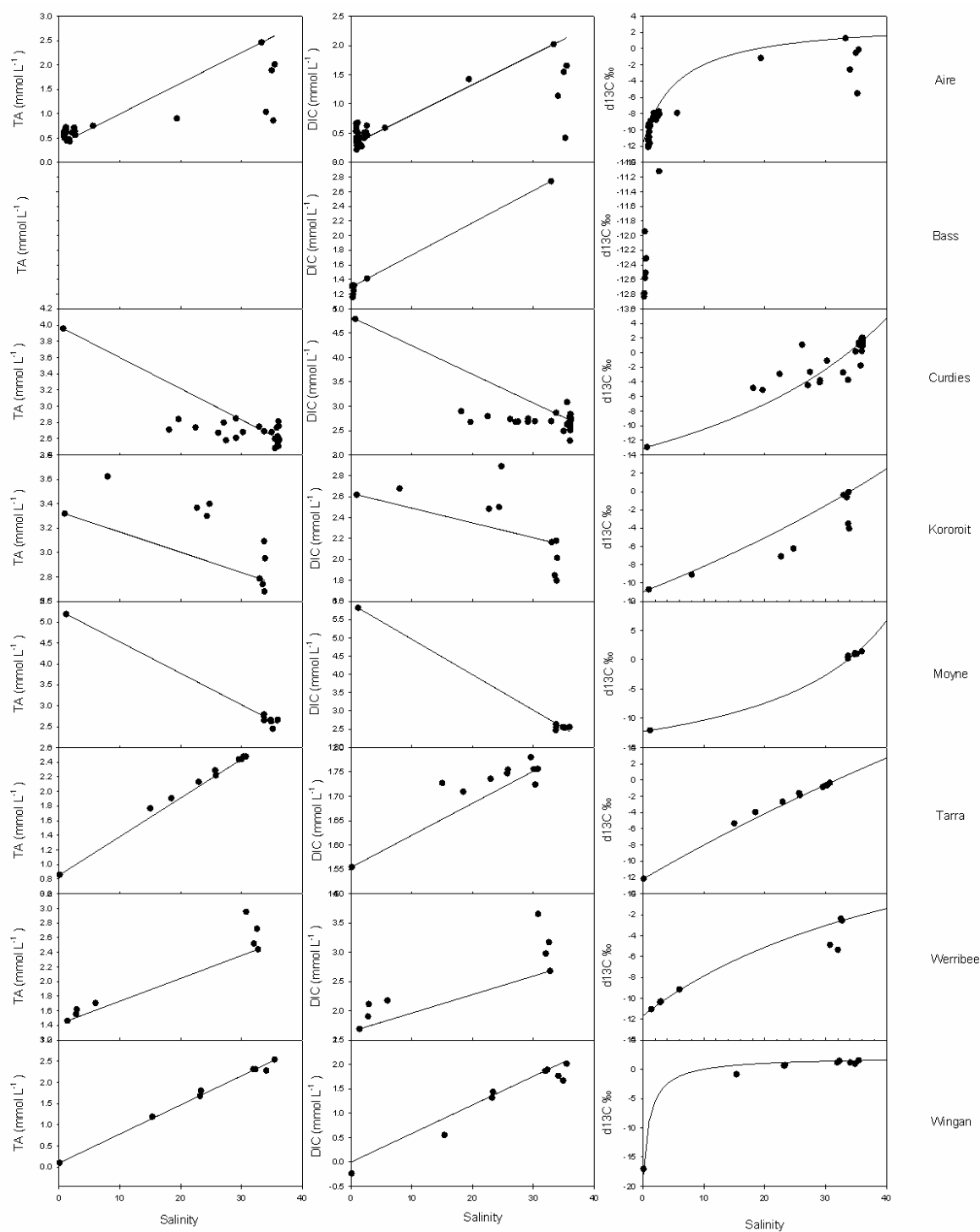
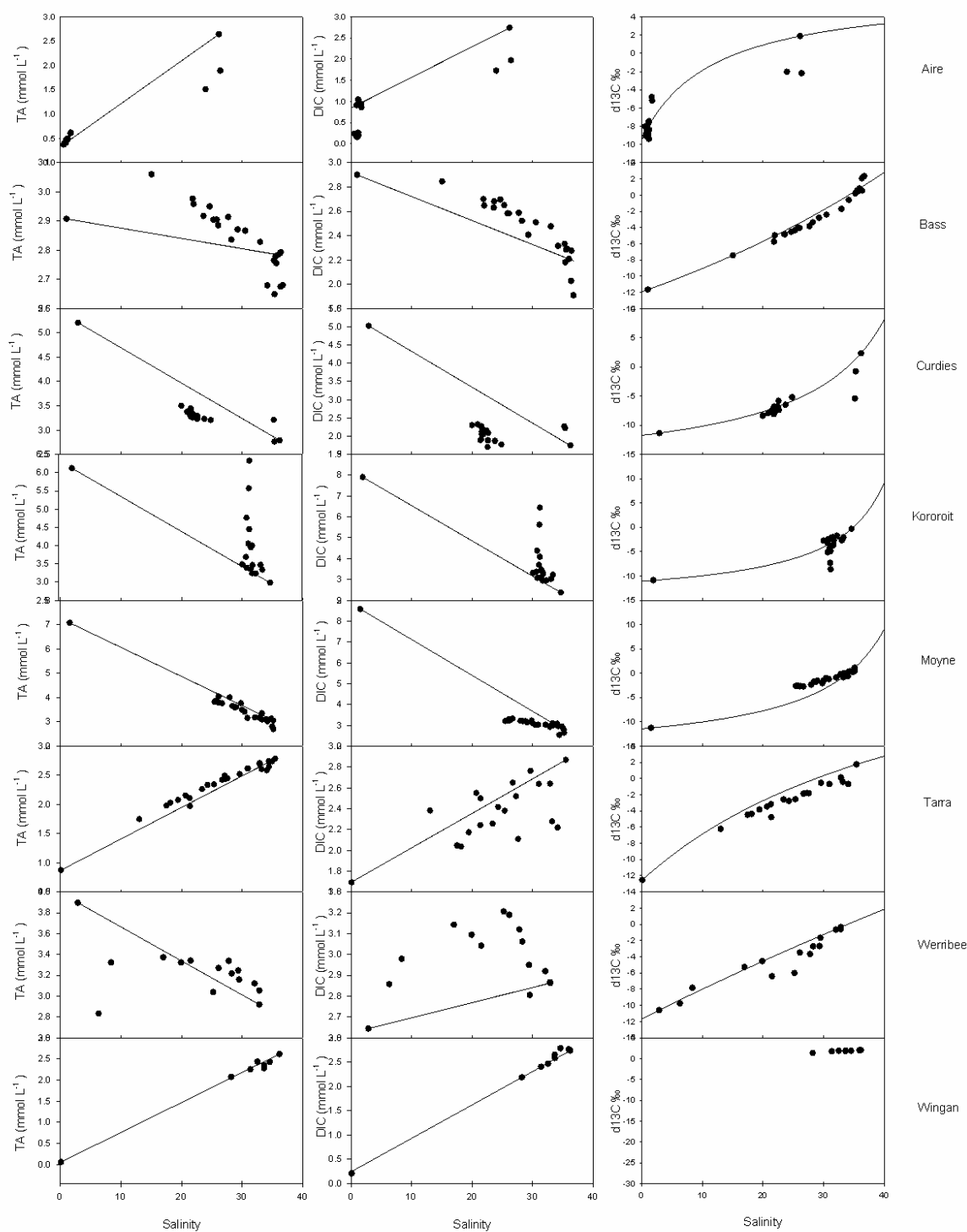


Figure A1: Ordination of 27 estuaries in Victoria, Australia based on principal components analysis of catchment land use ($n = 7$) and population ($n = 1$) characteristics. Upper panel a) shows the location of individual estuaries (solid circles) in ordination space and variable loading vectors on principal components 1 (PC-1, x-axis) and 2 (PC-2, y-axis). Lower panel b) ordination is replotted (with variable loading vectors retained but identifiers excluded for clarity) with estuaries size-coded by mean annual effective total

phosphorus load (TP load) from 1990-2012; estuaries selected for inclusion in this study are filled and labelled; other estuaries are depicted as empty circles.

4.10.2 Appendix 4B: Mixing plots





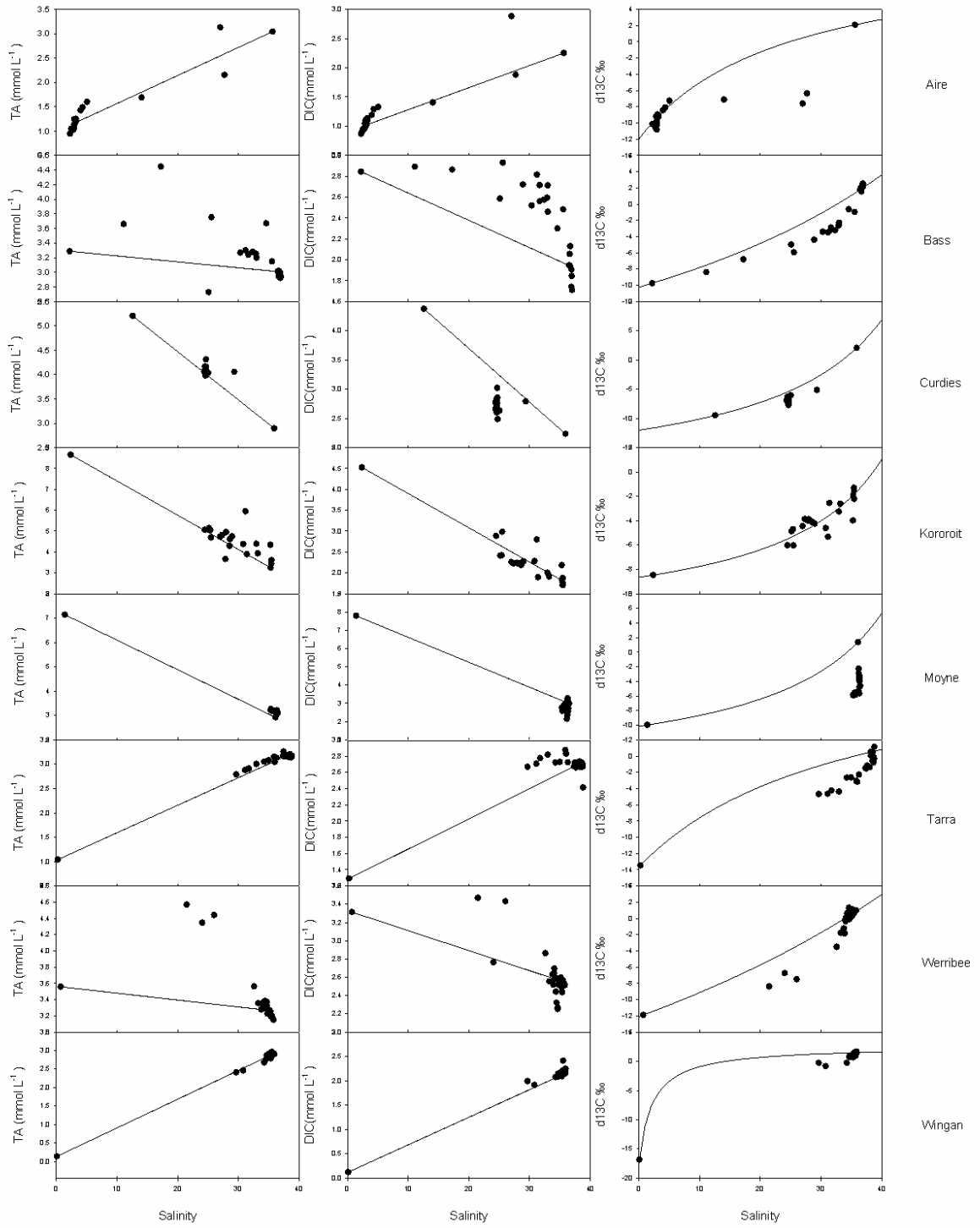


Figure A2: Mixing plots of TA, DIC and $\delta^{13}\text{C}_{\text{DIC}}$ for field sites from campaign 1 (top), 2 (middle) and 3 (bottom). The hyperbolic solid lines are expected concentrations given conservative mixing. The scale on salinity is 0-40 for each plot.

5. Discussion and concluding remarks

5.1 Research questions

As described in the introduction, the aims of this thesis can be summarised using several general research questions:

1. Does alkalinity generation within tidal flat sediments control the relative export of inorganic carbon to the atmosphere and to coastal waters?
2. Do differing degrees of terrestrial inputs influence the dominant modes of carbon export from tidal flats?
3. Do differing regimes of anthropogenic land use in river catchments control inorganic carbon and alkalinity production in estuaries?

Three approaches to data collection were taken to address these research questions:

1. Observational data: in situ measurements, including time series measurements of DIC, TA, pCO₂, nutrients and water quality parameters such as salinity, temperature, %DO and pH as well as measurements from draining porewater.
2. Experimental data: Core incubations for TA and DIC fluxes.
3. Computer modelling data: Employing a computer model to determine fluxes of substances across the sediment-water interface. Experimental variables were changed to determine the effects on fluxes.

5.2 Chapter summaries

5.2.1 Chapter 2 summary

Chapter 2 ties together field observations by Cook et al. (2004), laboratory core incubations and computer modelling to determine the presence of a discrepancy between inundated and exposed fluxes of inorganic carbon from intertidal mudflats. This research is relevant to studies of benthic metabolism on intertidal mudflats, which often only consider CO₂ during exposure (Middelburg et al. 1996; Migné et al. 2005) or DIC flux during inundation (Cai et al. 1999). The use of a computer model provided an opportunity to probe inorganic fluxes under different conditions, without the need for repeated core incubations or field observations, both of which are logistically complicated and time consuming.

The field observations, core incubations and computer modelling of inorganic carbon fluxes clearly showed that fluxes of DIC during inundation were greater than CO₂ during exposure (**Fig 5.1**).

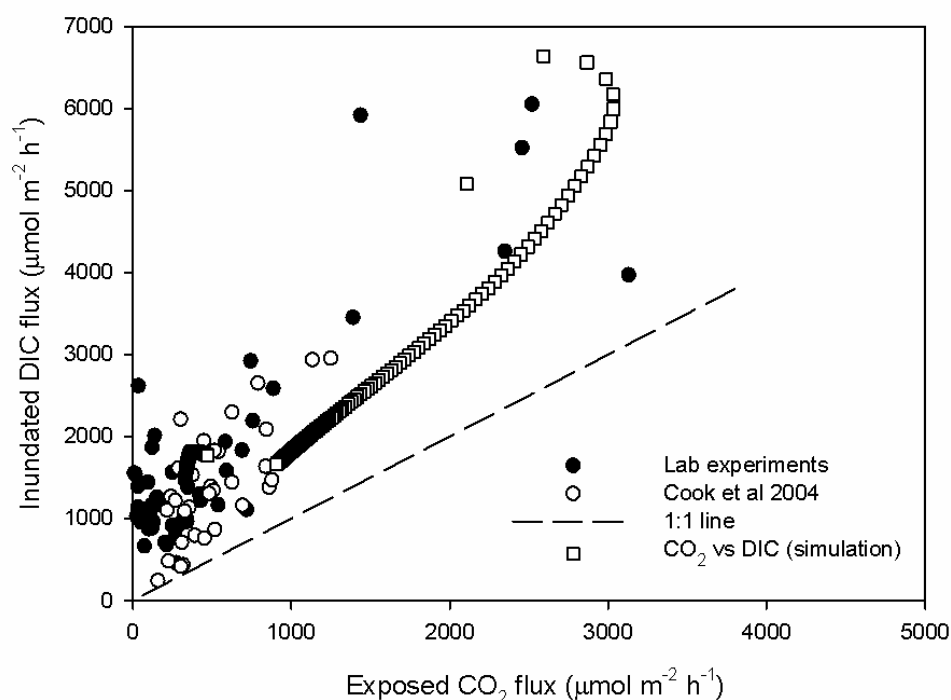


Figure 5.1: Fluxes of dissolved inorganic carbon (DIC) versus exposed CO₂ fluxes for two experimental data sets, and a model simulation.

The computer model indicated that this discrepancy was due to the net production of alkalinity within the sediment due to anaerobic processes. Due to its involvement in reduced sulfur burial, and thus net alkalinity production, Fe was investigated as a driver in the discrepancy and it was found that higher Fe concentrations caused a greater DIC flux during inundation and a lower CO₂ flux during exposure.

5.2.2 Chapter 3 summary

Chapter 3 investigates the dominant modes of carbon export in two inlets, Watson Inlet (WI) and Chinaman Inlet (CI) with extensive intertidal zones. WI receives water and terrestrially sourced substances from a highly impacted creek so has a greater terrestrial influence. The differences in TA, DIC, DOC and POC export between these two inlets

was investigated using time series measurements, which enabled us to determine net exports of substances by considering fluxes out of and into the inlet due to the tidal cycle, over the course of 24 hr. These advective exports are summarised in **Fig. 5.2**. Sediment porewater measurements were taken, along with ^{222}Rn in the porewater and during the time series, to determine the contribution of porewater exchange to substance export. The source of DIC was determined by considering $\delta^{13}\text{C}$ values and comparing them with known organic carbon sources within the inlets which included mangroves, and benthic carbon (seagrass and microphytobenthos).

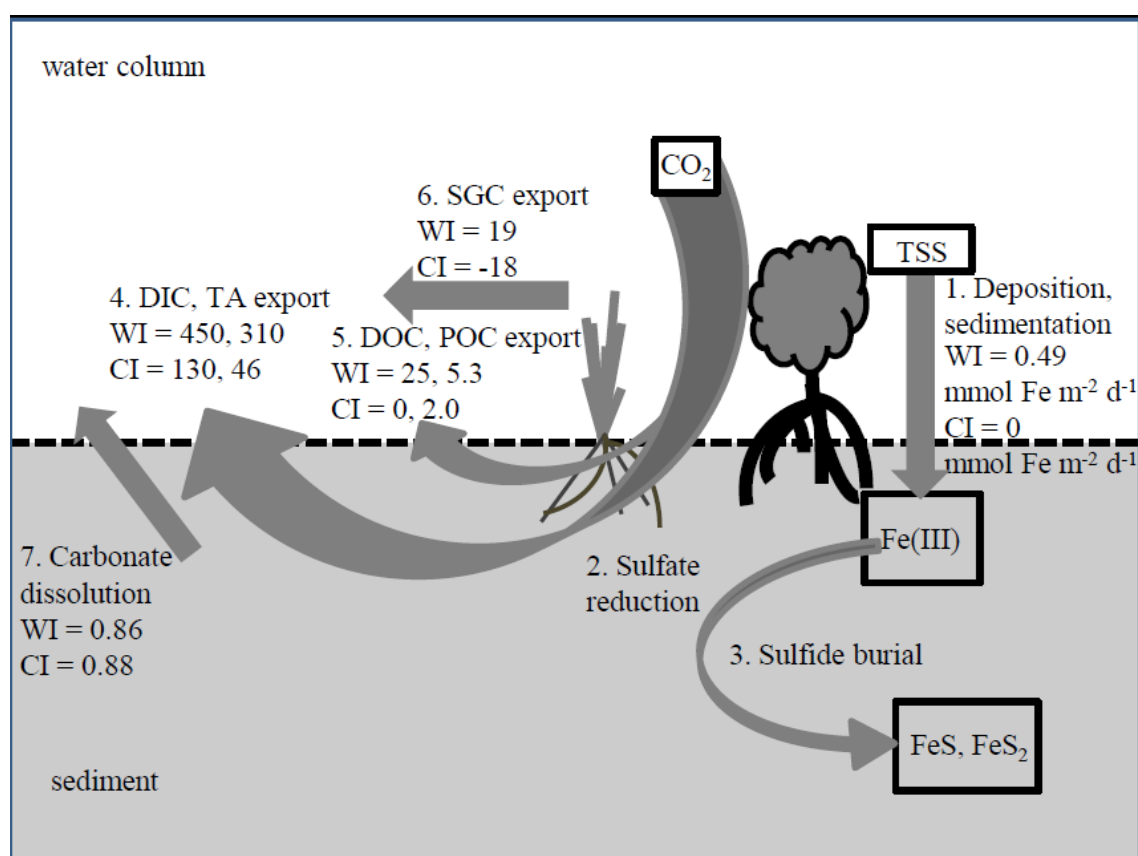


Figure 5.2: Conceptual diagram of the components of carbon export from the intertidal zones of the Watson Inlet (WI) and Chinaman Inlet (CI). The dashed line represents the sediment water interface. Processes 1-3 represent inputs of Fe, sulfate reduction and FeS/FeS_2 burial. The large arrow represents the carbon pump, taking in CO_2 from the

atmosphere and releasing it as 4. DIC, 5. DOC and “micro” POC and 6. seagrass POC.

Also included is carbonate dissolution (7). Units are $\text{mmol C m}^{-2} \text{ d}^{-1}$ for carbon, $\text{mmol TA m}^{-2} \text{ d}^{-1}$ for TA and $\text{mmol Fe m}^{-2} \text{ d}^{-1}$ for Fe.

It was found that alkalinity export differed between the inlets, with WI exporting much more alkalinity. Porewater exchange was significant to the export of inorganic carbon in both sites. Export of DIC was calculated to be 91 to 99% of total carbon export, with DOC and POC making up smaller fractions. Carbonate dissolution was a minor process, only contributing ~0.2% to the total carbon export at both sites. The contributions of mangrove organic matter to the DIC export was calculated at 88-93% in WI and 32-59% in CI.

The finding that WI exported more alkalinity than CI has relevance to studies of carbon dynamics in intertidal zones, as the strength of land-sea interactions controls Fe input. Coastal oceans and estuaries receive particularly high Fe inputs due to flocculation and settling of suspended Fe containing particles (Boyle et al. 1977; Martin and Meybeck 1979; Haese 2000) because Fe is derived from the weathering of rock in catchments, and loadings are related to the extent of anthropogenic impact in the catchment known (Dauer et al. 2000; Neil et al. 2002; Alongi and Mckinnon 2005). This finding relates to Chapter 2 which examines the effect of Fe on alkalinity flux from the sediment.

Because of recent work investigating the “missing mangrove carbon sink” (Bouillon et al. 2008a; Maher et al. 2013), this study may provide useful insight into carbon export from mangrove systems, as a carbon budget, including DIC sources was determined.

5.2.3 Chapter 4 summary

Chapter 4 investigates the dominant modes of inorganic carbon export from eight Southern Australian estuaries during three seasons; spring, summer and autumn, labelled as campaign 1-3 respectively. The investigation utilised two sampling regimes: a time series regime, which attempted to collect data during a variety of tidal conditions and under different diurnal effects; and a longitudinal regime, which aimed to get samples throughout the mixing zone of the estuary.

The estuaries represented a gradient of catchment impacts (high, moderate, low) and it was hypothesised that increasing impact would change how carbon exported. One common theme of the work in this thesis was the link of Fe with alkalinity flux and this chapter investigates that link by relating Fe fluxes from estuaries with alkalinity fluxes.

For much of the analysis, the data from the two sampling regimes were pooled as they both provided similar information regarding mixing and could both be used to detect non-conservative behaviour in DIC, $\delta^{13}\text{C}$ and TA. The data was used to calculate budgets during each campaign and the dominant modes of carbon transformation were identified, where possible. Carbon budgets varied considerably between sites and campaigns, and some estuaries displayed more than one dominant process during different campaigns. The fluxes of TA within the estuary (EF_{TA}) show a much higher mean and more variability in highly impacted estuaries (**Fig. 5.3**). The high variability in EF_{TA} in the highly impact estuaries suggests that FeS oxidation is occurring in these estuaries during certain periods.

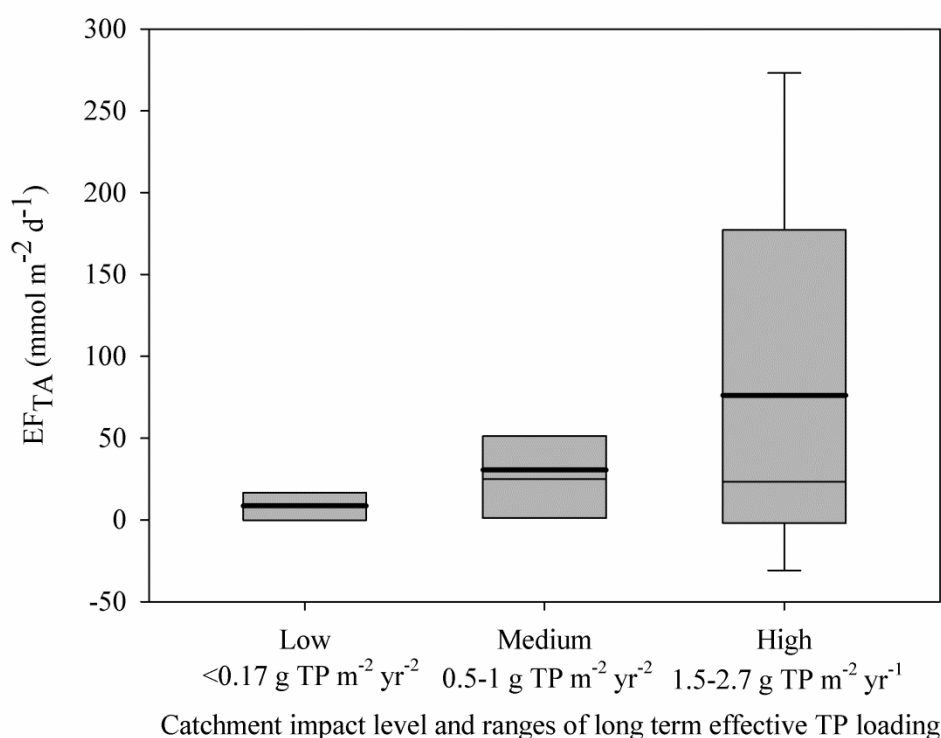


Figure 5.3: Estuary fluxes of TA vs. catchment impact level and the ranges of long term TP loading from 1990-2013. Median and mean values are represented by the plain and bold lines respectively on each box. $n=3$, 6 and 9 for low, moderate and high catchment impacts respectively.

Our use of $\delta^{13}\text{C}$ in this study provided useful insight into the processes affecting DIC flux. We were also able to speculate about other processes important to a comprehensive understanding of estuarine carbon dynamics such as methane oxidation.

5.3 Implications of present research

The findings of chapters 2 and 3 have important implications for research on intertidal flats. Chapter 2 describes the importance of considering inundated and exposed inorganic carbon fluxes in studies of mudflat metabolism due to differences in inundated and exposed fluxes.

Chapter 3 emphasises the importance of considering porewater exchange in budgets of carbon in intertidal systems. The large difference between core incubations, which measure diffusive fluxes, and in situ measurements further illustrate the importance of considering advective fluxes in intertidal systems if accurate system budgets are to be obtained. Using TA as a tracer to estimate porewater export agreed well with estimates from Rn^{222} measurements, which are more commonly used, and the estimates of porewater export from the inlets were similar to values found by another Australian study (Gleeson et al. 2013). A major finding in the paper is the strong discrepancy between extrapolated alkalinity exports and the inputs of Fe required to produce it. This indicates high temporal variability in alkalinity exports due to sulfate reduction and may be driven by tide heights, extreme weather events or changes in sediment fauna behaviour.

The estuaries investigated in this study are small and contribute very little to the global alkalinity budget, however the findings are important in terms of how anthropogenic land use in catchments affect alkalinity exports. Hu and Cai (2011) pointed out the importance of considering the role of internal recycling of sulfur and metal species when determining net alkalinity gain, arguing that only permanent loss of reduced sulfur and metal (for instance pyrite burial) results in net alkalinity production. The observation of high seasonal variability in more impacted estuaries emphasises this point, and we observed that although the more highly impacted estuaries export more alkalinity, they are also subject to extreme variation in alkalinity export, including periods where alkalinity consumption is occurring due to oxidation of reduced sulfur species. Because of the observed variability in TA fluxes, no attempt was made to extrapolate the data to yearly fluxes. The variability in alkalinity flux may have consequences for shellfish which rely on supersaturated carbonate to build shells because during periods of intense sulfide oxidation, the produced acid may drive carbonate dissolution. Because estuaries are

environmentally and economically important for shellfish, a greater understanding of how anthropogenic changes in catchments affects alkalinity dynamics (and therefore carbonate saturation) is relevant.

5.4 Future research

The research encompassed by these studies aims to address the questions posed in the start of this chapter. Each chapter, and this thesis as a whole has something to offer future studies involving carbon budgets, mudflat metabolism and terrestrial influences on inorganic carbon export. Chapter 2 shows that studies of metabolism and the formulation of carbon budgets in coastal areas may be highly dependent on the availability of oxidized Fe which provides a means for inorganic carbon to be exported as alkalinity. Although I further analysed the link between Fe and alkalinity export in Chapter 3, I think that the conclusions made in this paper provide important information to future studies, especially those investigating benthic metabolism in intertidal areas and anthropogenic contributions to global carbon and alkalinity budgets.

In Chapter 3, we identified the need for further observational studies aiming to capture the reduction/oxidation cycling of Fe which may consist of periods of alkalinity production followed by rapid consumption during resuspension events. Because the oxidation of reduced sulfur produces acid, it can contribute towards carbonate dissolution. The link between sulfide oxidation and carbonate dissolution may be one possible avenue of research, especially with regard to seasonal variation in these two processes. A recent study showed that alkalinity release due to carbonate dissolution can vary dramatically between seasons (Rao et al. 2014), with other processes such as sulfate reduction also contributing towards alkalinity production.

Chapter 4 provides a preliminary study into the effects of land use on how carbon is exported. The major findings of this study indicate that studies across land use gradients are one area where further research would be beneficial to our understanding of estuarine carbon dynamics and how these are influenced by anthropogenic activities. Comparing the dynamics of TA export with measured Fe inputs to estuaries is one possible avenue for future research. The findings of our research indicate that high sampling rates on the scale of weeks or even days may be important to fully understand alkalinity dynamics in highly impacted estuaries. I suggest based on this study, that more tightly constrained carbon isotope data and modelling could provide researchers with the ability to determine a variety of processes occurring along an estuarine gradient, which are otherwise difficult to determine.

5.5 References

- Alongi, D., and A. Mckinnon. 2005. The cycling and fate of terrestrially-derived sediments and nutrients in the coastal zone of the Great Barrier Reef shelf. *Marine Pollution Bulletin* **51**: 239-252.
- Bouillon, S. and others 2008. Mangrove production and carbon sinks: a revision of global budget estimates. *Global Biogeochemical Cycles* **22**: GB2013.
- Boyle, E., J. Edmond, and E. Sholkovitz. 1977. The mechanism of iron removal in estuaries. *Geochimica et Cosmochimica Acta* **41**: 1313-1324.
- Cai, W., L. Pomeroy, M. Moran, and Y. Wang. 1999. Oxygen and carbon dioxide mass balance for the estuarine-intertidal marsh complex of five rivers in the southeastern US. *Limnology and Oceanography* **44**: 639-649.
- Cook, P., E. Butler, and B. Eyre. 2004. Carbon and nitrogen cycling on intertidal mudflats of a temperate Australian estuary I. Benthic metabolism. *Marine Ecology Progress Series* **280**: 25-38.
- Dauer, D. M., J. A. Ranasinghe, and S. B. Weisberg. 2000. Relationships between benthic community condition, water quality, sediment quality, nutrient loads, and land use patterns in Chesapeake Bay. *Estuaries* **23**: 80-96.
- Haese, R. R. 2000. The reactivity of iron, p. 233-261. *Marine geochemistry*. Springer.
- Hu, X., and W. J. Cai. 2011. An assessment of ocean margin anaerobic processes on oceanic alkalinity budget. *Global Biogeochemical Cycles* **25**: GB3003.
- Maher, D., I. Santos, L. Golsby-Smith, J. Gleeson, and B. Eyre. 2013. Groundwater-derived dissolved inorganic and organic carbon exports from a mangrove tidal creek: The missing mangrove carbon sink? *Limnol. Oceanogr* **58**: 475-488.
- Martin, J.-M., and M. Meybeck. 1979. Elemental mass-balance of material carried by major world rivers. *Marine Chemistry* **7**: 173-206.

- Middelburg, J. and others 1996. Organic matter mineralization in intertidal sediments along an estuarine gradient. *Marine Ecology Progress Series*. Oldendorf **132**: 157-168.
- Migné, A., D. Davoult, J. J. Bourrand, and G. Boucher. 2005. Benthic primary production, respiration and remineralisation: in situ measurements in the soft-bottom Abra alba community of the western English Channel (North Brittany). *Journal of Sea Research* **53**: 223-229.
- Neil, D. T., A. R. Orpin, P. V. Ridd, and B. Yu. 2002. Sediment yield and impacts from river catchments to the Great Barrier Reef lagoon: a review. *Marine and Freshwater Research* **53**: 733-752.
- Rao, A. M. F., S. Y. Malkin, F. Montserrat, and F. J. R. Meysman. 2014. Alkalinity production in intertidal sands intensified by lugworm bioirrigation. *Estuarine, Coastal and Shelf Science* **148**: 36-47.

